ERRATA

Page	Line	
46	14	for "oven" read 'hot-plate'
51	26	for "sodium" read 'sodium oxide'
76	17	for "solubility" read 'rate of solution'
144	11	for "was" read 'may be'
144	15	for "assuming that the" read 'assuming that (1) the heat of reaction is of $C + O_2$ and (2) the'
158		after appendix heading add '(The heat of reaction of carbon with $NaVO_3$ was not available)'

THE DISSOLUTION OF CARBON-CONTAINING OXIDE REFRACTORIES IN MELTS

A Thesis submitted for the degree of

DOCTOR OF PHILOSOPHY

in the

University of London

by

HAN KYOU PARK, M.PHIL., D.I.C.

Department of Chemical Engineering and Chemical Technology

Imperial College of Science and Technology

London SW7

May 1976

ABSTRACT

The dissolution behaviour of carbon-containing magnesia compared to the corresponding unfilled porous magnesia and to single crystal was studied in melts under forced convection, simulating the conditions in oxygen steelmaking.

The technique employed was capable of following both the rate of oxidation of carbon in carbon-containing magnesia in contact with simple melts and also the accompanying corrosion of magnesia. This consisted in simultaneously analysing the evolved CO/CO_2 gases by gas chromatography and magnesia dissolved in the melt by atomic absorption spectroscopy. The melts chosen in ascending order of melting point were metavanadate, tetraborate and disilicate of sodium. The first was easily reduced by carbon.

The study revealed that the carbon reduced the rate of corrosion of magnesia in borate and silicate melts. The opposite occured in sodium metavanadate, when, exceptionally, only CO_2 was evolved. In the rather more inert borate and silicate melts the oxidation of carbon was most dependent on temperature. As an example, at 952°C in borate melt a carbon content of approximate 3.2 weight % was required to reduce the rate of 32% porous magnesia as low as that of single crystal, whilst about 12.5 weight % of carbon was required in silicate melt at 1,350°C. However when the carbon was oxidised vigorously by vanadate at 750°C, the carbon enhanced the corrosion rate of magnesia for which three possible reasons are given. The general conclusion, indicating the dependence of corrosion rate of magnesia on the oxidation rate of carbon is in good agreement with the author's earlier work on carbon-containing alumina under melts.

The rate determining process for magnesia corrosion in these melts was found to be again the commonly encountered transport control. One of

a number of pieces of evidence supporting transport control was the dependence of corrosion rate on the rate of stirring as predicted by mass transfer theory. Unlike the thick boundary layer formed on alumina it appears from electron microprobe measurements that during the corrosion of magnesia the layer is possibly only a few microns thick. For this reason and the absence of solubility data, diffusion coefficients of 'magnesia' in the melts could not be calculated, but are displayed for 'alumina'.

To my parents and my wife, Yung Joo

ACKNOWLEDGEMENTS

The author wishes to express his deep gratitude to Mr. L.R. Barrett, for his continued advice, guidance and encouragement at all stages of the investigation. The author is grateful to Emeritus Professor J. White of the University of Sheffield, for valuable suggestions. The author is also grateful to Dr. M. Cable of the University of Sheffield, for helpful discussions.

The author would like to thank:-

Dr. D.L. Trimm and Dr. J.A. Busby (now at Johnson Matthey Company Limited) for their advice in constructing the gas chromatograph.

Dr. M. Streat for the use of atomic absorption spectrophotometer.

The Analytical Services Laboratory staff for chemical analyses and especially to Mr. P.R. Monk for the EPMA.

The Glass Workshop staff for the use of their ceramic machining tools.

Mr. R. Harris and the workshop staff for their help in constructing apparatus.

Mr. L. Moulder for the preparation of the photographs.

Miss S. Tolley for the typing.

The author is indebted to the Hancock Bequest for some financial assistance and the British Council for the award of fees.

Finally, the author would like to thank his family especially to his wife, Yung Joo, and his parents Mr. and Mrs. B. Park (Kim) for their unlimited support.

CONTENTS

	PAGE NO.
ABSTRACT	2
ACKNOWLEDGEMENTS	5
LIST OF CONTENTS	6
UNITS USED, SI UNITS AND CONVERSION FACTORS	7
CHAPTER 1 : INTRODUCTION	8
CHAPTER 2 : CURRENT UNDERSTANDING OF SLAG ATTACK ON CARBON-CONTAINING OXIDE REFRACTORIES	10
CHAPTER 3 : PREPARATION OF MATERIALS	22
CHAPTER 4 : EXPERIMENTAL WORK	31
CHAPTER 5 : OXIDATION OF CARBON UNDER MELTS	53
CHAPTER 6 : STUDIES OF REFRACTORY - MELT INTERFACES BY ELECTRON MICROPROBE ANALYSER	74
CHAPTER 7 : DISCUSSION OF RESULTS	110
SUMMARY	157
APPENDIX	158
REFERENCES	160

Units used*: SI units and conversion factors

Name of quantity	Unit used	SI Unit	Conversion
Length	inch	metre (m)	1 inch = 0.0254 m
	Angstrom (Å)		1 Å = 10^{-10} m
Pressure, Stress	ton/in^2	newton (N)/m^2	1 ton/in^2 = 15.444 MN/m^2
Kinematic viscosity	cm^2/s (stokes)	m^2/s	1 stokes = 10^{-4} m^2/s
Dynamic viscosity	gm/cm/s (poise)	Ns/m^2	1 poise = 0.1 Ns/m^2
Energy	calorie	joule (J)	1 calorie = 4.184 J

* The units used in the text other than multiples and submultiples of SI units are displayed.

CHAPTER 1

INTRODUCTION

Greater need and efficiency in the production of steel has promoted the basic oxygen - blown process to the leading position in steelmaking over the last 15 years. For example, world steel output by the process has increased to 41% in 1971 from 5% in 1961 (15). At present, almost 60% of the steel produced in the United Kingdom is produced by the process and this is scheduled to rise to 75% by the end of the decade (90). This change of process in steelmaking where at least half of all refractories used has been consumed, has brought about the change of kind of refractories used for linings in steelmaking vessels.

Refractories currently favoured for linings in basic oxygen steelmaking converters are magnesite or dolomite refractories containing up to 4% of carbon formulated from pitch, even though steelmaking is a decarburization process. This is because carbon deposited in the pores of refractories has been shown to improve the corrosion resistance of the refractories to slag attack.

Much effort has therefore been made to assess the value of carbon in refractories when attacked by slags. As a result, several views have been put forward that would explain the role of carbon. However, the work hitherto reported in the literature has been mainly of a practical nature such as the observation of sectioned corroded refractories, lacking in evidence for improvement. The present research was, therefore, undertaken in order to understand the problem of slag attack on carbon-containing oxide refractories by a quantitative approach.

The rate of corrosion of refractories in slags is a complex subject. However, since quantitative studies were carried out by numerous workers at Imperial College (64)(74)(32)(83)(38)(2)(39)(41) while valuable contributions were made by Flood (35), Cooper and Kingery (21)(22),

Hlavac (47) and others, much is known about the mechanism of corrosion. Also improved has been the technique for the measurement of rate. These available techniques were e.g., continuous weighing technique (84), intermittant weighing technique (64)(74)(32), rotating disc method (21) and flow tube method (38)(39)(41). For the present work, however, these techniques were all found to be inadequate. Thus the first technique involved the use of a balance which could not separate refractory corrosion from carbon oxidation, whilst the last three techniques involved the removal of adhered melt in an acid solution after the corrosion which was unsuitable owing to the solubility of magnesia. Therefore, experimental work was carried out by analysing magnesia dissolved in the melt by atomic absorption spectroscopy by withdrawing small samples during the run and the CO/CO_2 gases evolved by gas chromatography.

CHAPTER 2

CURRENT UNDERSTANDING OF SLAG ATTACK ON CARBON - CONTAINING OXIDE REFRACTORIES

2.1. Practical carbon - bearing basic refractories

2.2. Effect of carbon on slag attack

- 2.2.1. Reduction of iron oxide to metallic iron
- 2.2.2. Non-wetting characteristics of carbon
- 2.2.3. Reduction of MgO
- 2.2.4. Other possible effects

2.3. Residual carbon content

2.4. Structure of carbon formed in the pores

2.5. Oxidation of carbon in basic refractories

CHAPTER 2

CURRENT UNDERSTANDING OF SLAG ATTACK ON CARBON - CONTAINING OXIDE REFRACTORIES

2.1. Practical carbon - bearing basic refractories

Prior to a discussion on problems of slag attack on carbon - containing refractories, it is thought desirable to give a brief description of industrial refractories.

The types of refractory currently used for basic oxygen steel-making converters are pitch-bonded, tempered and pitch-impregnated. These are made from the various types of grains of periclase, magnesite and dolomite.

Pitch-bonded bricks are produced by pressing blended suitably-sized refractory raw materials with hot pitch. These are either cooled for storage or tempered commonly at 450 - 600^{o}F to improve several brick properties, i.e. to increase low temperature hot strength - this increase reduces possible failure of the lining during burn - in, and to improve resistance to hydration. Thus, pitch in the brick is utilized in three ways:-

1) initially it provides bond for the brick to be handled
2) it helps protect from hydration
3) it deposits carbon after the heat treatment.

Pitch-impregnated bricks are produced by impregnating molten pitch into the open pores of pre-sintered brick using a vacuum - pressure technique. This technique is basically similar to the method used in the present work. The detail is described in section 3.2.2.

On carbonization, carbon is merely formulated in the pores as a type of filler in bricks manufactured by the procedure described above. No evidence was reported (53) that the carbon does bond with refractory grains.

2.2. Effect of carbon on slag attack

Robinson (80) reported that if the carbon is present in the brick slag penetration is a matter of millimetres compared with centimetres if carbon is absent. Figure 2.1. shows the chemical composition of the two types of brick taken from converters after service. This clearly illustrates the significant effect of carbon in the brick in decreasing the depth of penetration of iron oxides, lime and silica into the brick. As a result, it is often noticed (53) that carbon-containing bricks normally wear with uniformity whilst non-carbon-containing bricks wear in an unpredictable manner with sudden loss of an appreciable thickness of bricks.

Kappmeyer and Hubble (53) stated that refractories containing carbon exhibited 2 to 3 times as much resistance to slag attack as refractories without carbon. It is now apparent that the improvement in corrosion resistance is achieved by the carbon deposited from pitch in the pores on carbonization, as it reduces slag penetration into the pores. However, there are several views proposed in the literature on what way slag penetration is inhibited.

2.2.1. Reduction of iron oxide to metallic iron

Chesters (16) proposed as a possible mechanism that the carbon reduces ferric oxide (or calcium ferrite) to FeO or even metallic iron which is virtually non-corrosive to magnesia and lime. White (101) also agreed that the carbon would stop iron oxide attacking the brick for a similar reason provided that enough carbon is retained in the brick. In fact, Herron, Beechan and Padfield (43) concluded that the round metallic particles found at the base of the decarburized zone were evidence of the reduction of iron oxide by the carbon and thus assumed this to be the major mechanism of carbon removal.

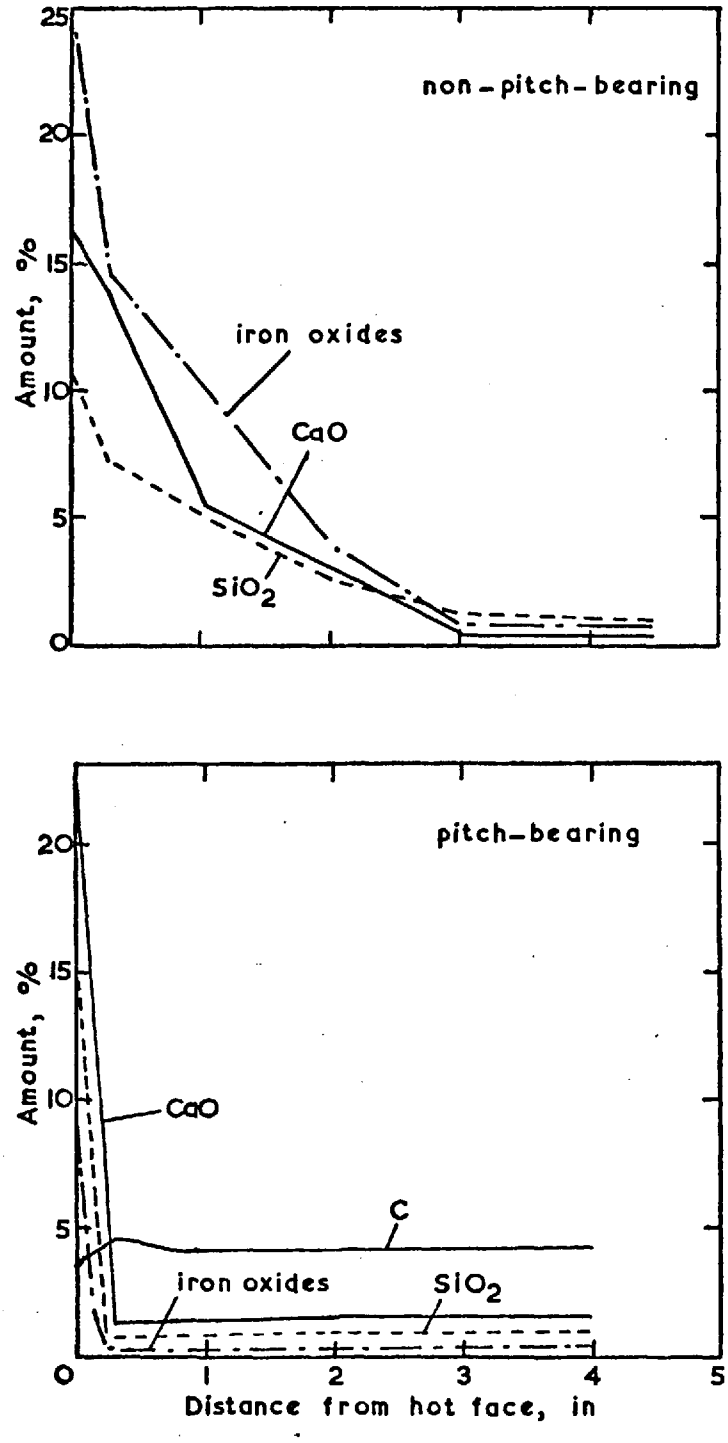

Figure 2.1. Comparison of chemical compositions of periclase brick used with and without pitch (after Kappmeyer and Hubble).

Later, Barthel (4) proposed from his microscopic examination of worn carbon-bearing refractories that the reduction of penetrated metal ions and solidification of the remaining oxide liquid results in reduced slag attack, if the ratio of $CaO/(P_2O_5 + SiO_2)$ in the slag is high. If the ratio is low, then the effect of carbon is largely of a physical nature, i.e. due to the non-wetting characteristics of carbon.

Recently, however, Webster and Jackson (99) pointed out that the amount of FeO that can be reduced by carbon is limited to about 6 times the weight of carbon present in the brick. It does suggest that although this mechanism may operate to some extent, the possibility is restricted to the residual carbon content.

2.2.2. Non-wetting characteristics of carbon

As is well known, the contact angle (θ) measures the wetting characteristics of a solid by a liquid. If θ is smaller than 90^o, it could be said that a refractory is wetted by slag. Comeforo and Hursh (19) showed that the rate of penetration of liquid into a refractory is more dependent on the contact angle between refractory and slag than the pore size in the refractory. In consequence, if θ approaches zero the rate of corrosion would be faster due to rapid penetration into the pores. On the other hand, if θ is larger than 90^o the wetting is said not to occur. Towers (91) appreciated that a higher contact angle and a higher interfacial energy essentially combine to reduce the corrosion of a refractory.

As carbon shows a large contact angle with a liquid, several workers proposed that the reduced slag penetration into the pores of a brick is due to the non-wetting characteristics of carbon. Barthel (5) proposed that the carbon inhibited further slag penetration due to this reason. Herron, Beechan and Padfield (43) also concluded that the carbon prevents slag penetration due to lack of wetting from their

microscopic examination of the test samples subjected to a slag. These authors varied the amount of residual carbon in the basic refractories and observed that the penetration of slag stopped immediately where more than 3 weight % of carbon was present, but the penetration occured when the carbon content fell below 3 weight % in the specimens. Webster and Jackson (99) also reported that slag penetration was observed only as far as the carbon residue.

2.2.3. Reduction of MgO

Robinson (80) proposed that the presssure of carbon monoxide gas generated by the oxidation of carbon within the brick may delay the entry of the liquid. Supporting this speculation was the work by Pickering and Batchelor (72) who demonstrated experimentally the fundamental incompatibility of the carbon and magnesia in the lining at steel making temperature of 1,600°C. These authors detected the weight losses of carbon-containing magnesia above 1,400°C, due to direct reduction of magnesia by carbon, which was accompanied by strength losses. This fact convinced them that carbon could be lost in this way from the composite carbon/magnesia refractories and vapour pressure arising from the reaction may help to inhibit slag penetration. On the other hand, it is suggested that a self-destructive process due to the strength losses could be encountered if operating temperatures were raised or pressures lowered.

In view of the fact that reaction products are magnesium and carbon monoxide, the oxidation of magnesium vapour and the deposition of magnesia can be considered. In fact, many authors (72) (57) (10) observed the formation of dense magnesia layer external to the carbon-containing magnesia under isothermal laboratory conditions. This observation lead Brezny and Landy (10) in particular to conclude that this so-called 'protective layer' would retard the refractory consumption by slag attack. However, Carniglia (13) pointed out that although the MgO - C reaction is not insignificant, the reaction is limited

to a very narrow zone near the hot face and is less rapid than might be inferred from laboratory tests under isothermal heating, because there exist large changes in product gas pressures and the large temperature gradient in the linings of the converter during each heat. In service, it is also postulated that the dense magnesia layer should not form except under certain circumstances as the average recession rate of carbon-bearing refractories (0.03 - 0.06 in/heat) is greater than the growth rate of dense magnesia (0.005 in/heat) and the oxidation rate of carbon (0.005 - 0.02 in/heat) by the magnesia. These inferences lead him to conclude that oxidizing agents such as Fe_2O_3, CO_2 and O_2 appear to cause the majority of carbon recession at steelmaking temperature.

2.2.4. Other possible effects

As long as carbon is retained in the pores, the carbon would physically resist slag entry by blocking the pores. When it happens, the addition of carbon would show the reverse effect of porosity. This observation was made by the author (69) from an earlier work on the corrosion resistance of carbon - containing alumina in sodium tetraborate melt below 1,000°C at which the carbon was nearly inert to magnesia and melt. The study has shown that the porous alumina specimen became denser (less porous) by the addition of carbon, i.e. 3.7 weight % of carbon by pitch to 29% porous alumina made it act like 20% porous alumina under slag attack.

Carbon being a good thermal conductor, another possibility is that the addition of carbon improves the spalling resistance. However, it was considered (99) that the improvement would probably be quite small as the increase of thermal conductivity of impregnated magnesite refractories after coking amounted to only 5% (58).

The improvement of hot strength of refractory by the impregnation is another aspect that could be considered as a possibility. Kappmeyer

and Hubble (53) reported that the strength of the carbon-bearing brick was about 50% higher at the higher temperatures than non-carbon-bearing brick. They attributed this to the inhibiting effect of carbon on movement of any liquids formed within the brick. Webster and Jackson (99) were of the opinion that although the carbon itself is unlikely to increase the hot strength since it is not continuous, it is possible that the impurity element Fe_2O_3 is reduced to FeO which formed a solid solution with periclase and thus the formation of low melting calcium ferrite was prevented. They reported this consideration was confirmed by experiment when the strength of a fired magnesite dolomite brick containing an amount of calcium ferrite was more than doubled when tested in a reducing atmosphere at 1,400°C.

2.3. Residual carbon content

From the foregoing discussions, it can be seen that carbon was clearly beneficial in refractories with respect to corrosion resistance by one or a combination of the several possibilities considered which operate to some degree. Then the question arises as to the matter of an optimum residual carbon content for maximising the refractory life. Indeed, this was a subject of study by several workers. For example, Herron, Beechan and Padfield (43) reported that the 3 weight % of retained carbon is required to minimize the slag penetration. Further addition did not help to inhibit further slag penetration. Hubble (49) also reported that the brick containing a higher residual carbon content (up to about 4%), obtained from higher softening point pitches has shown better corrosion resistance. However, Spencer (90) stated that approximately 2% are adequate to provide two desirable features: a very narrow decarburized zone and prevention of slag penetration. Trials of further addition up to 4% by the use of high softening point pitches have failed to improve service performance.

Another noteworthy finding observed by Kappmeyer and Hubble (53) was that the refractories containing up to 12% carbon have shown disappointing results when the source of carbon was by other than pitch, i.e. carbon or graphite additions and precoking of grains coated with pitch, etc., to yield higher residual carbon content. In this connection, however, an earlier research by the author (69) indicated that carbon deposited from resin performed better than carbon from pitch at same residual carbon content. Further trial (103) confirmed the above conclusion. A possible reason offered lay in the different physical states of the two impregnants during carbonization. In detail, the pitch liquifies before it is decomposed to leave a carbon residue whereas the resin polymerizes before it is carbonized without passing through a liquid phase. Considering these two forms of carbon, carbon from resin may feasibly be distributed over the entire surface of the interior, whereas pitch may accumulate at preferred positions in its liquid state before carbonization.

2.4. Structure of carbon formed in the pores

The mode of occurrence of carbon particles in a brick depends mainly upon the manner in which the pitch is introduced into the brick (53). For example, the pitch-impregnated brick contains large continuous particles deposited in large pores of the brick. On the other hand, the tempered brick contains fine particles randomly located in the matrix. In either case, the shape, size and degree of continuity of carbon particles is directly related to the structure of pores. The carbon exists as a type of filler as mentioned in the section 2.1. However, the study by Gilbert and Batchelor (37) on carbon-containing basic bricks with scanning electron microscopy has shown that there is a tendency for pitch coke to form coatings on the pore walls (pitch-impregnated brick) or on the refractory grains (tempered brick).

The work by Herron and Runk (44) indicated that the carbon uniformly distributed as fine particles performed better than the carbon poorly distributed as coarse particles with respect to slag infiltration. Also observed by them was that, when the carbon was distributed as fine particles, not so much carbon (less than 3% by weight) was required to minimize slag penetration.

In view of the fact that the hot face of the brick is exposed to high temperature for a relatively short period of time, significant graphitization of residual carbon has not been observed. As would be expected, Kappmeyer and Hubble (53) found that the degree of crystallinity of the carbon from a used lining was equivalent to that of pitch coked to 1,650^{o}C, which is far removed from that of graphite.

2.5. Oxidation of carbon in basic refractories

The oxidation of carbon during service can be divided into three main categories; first the oxidation by oxide slag, secondly the oxidation by air between heats when the vessel atmosphere becomes oxidizing and thirdly the oxidation by oxide constituents in basic refractories. As the relevant literature on the oxidation of carbon by air and slag will be reviewed in detail in Chapter 5, attention will be paid, in this section, to the oxidation of carbon with particular reference to the refractory texture.

The ignition temperature of carbon depends upon such process variables as the sources of carbon, conditions of preparation and thermal history. For example, Ephraim (30) stated that the ignition temperature of wood charcoal prepared at low temperature was 300^{o}C whereas soot from hydrocarbon oils or some graphitic gas carbons was 371^{o}C. When the soot was heated at 910^{o}C for three hours, the ignition temperature was raised to 476^{o}C. For pure graphite, Riley (79) has given threshold oxidation

temperatures of 520°C to 560°C at which sample loses approximately 1 percent of its weight for 24 hours. The temperature at which residual carbon (formed from pitch after coking at 1,000°C) oxidizes in magnesite and dolomite brick was studied by Palin and Richardson (68). The temperature quoted was of the order of 800°C for dolomite but varied between 400°C and 700°C for different magnesites. The apparent difference in the temperature was attributed to the formation of calcium carbonate in dolomite as carbon oxidizes, which decomposes at about 800°C. The formation of carbonate was confirmed by detecting the majority of reaction product, CO_2, evolved above 900°C which was assumed to have originated from carbonate rather than carbon because, in the presence of carbon, CO has a greater stability than CO_2 at this temperature.

The rate of oxidation of carbon in brick by air is an important parameter affecting the life of carbon. This was earlier studied by Barrett, Ford and Green (3) who concluded that the diffusion of the reacting gases through the brick was the rate controlling process. The conclusion was recently confirmed by Nacamu and Batchelor (66) who studied the rate of carbon oxidation as a function of brick texture. These workers observed that the rate of oxidation was increased with increasing apparent porosity while little effect was seen from pore size distribution or air permeability. This lead them to conclude that the rate of carbon oxidation was dependent on the volume of space available for diffusion and not on the nature of the diffusion path.

As mentioned in the section 2.2.3., the oxidation of carbon by magnesia can occur at steel making temperature. The reactivity between graphite and magnesia was studied by Komarek, Coucoulas and Klinger (55) who concluded that the desorption of CO from the graphite surface was the rate controlling process of the reaction, obeying a linear rate law on the basis that the measured activation energy, 60 Kcal/mol, was similar to the value for the gasification of graphite by CO_2. From their study

of the MgO - C reaction in pitch-impregnated brick, Leonard and Herron (57) cited the similarity of the activation energy obtained, 63 Kcal/mol, for the reaction to that found by Komarek et al. (55) and suggested that the rate controlling process was the surface reaction. However, this interpretation is in conflict with the conclusion drawn by Carniglia (13) that the rate limiting process is the diffusion of the reaction products Mg and CO gases out of the pore-channels of the brick. For experimental evidence, he reported that the weight loss of small specimens of coked pitch-impregnated brick was 10.5 mg/min in a rapidly flowing Ar atmosphere whereas the weight loss of an identical specimen was 0.13 mg/min when shielded from a flowing Ar atmosphere.

As a result of the oxidation of carbon by various oxidizing agents mentioned at the beginning of the section, it is usual to reveal a decarburized zone ranging from 2 mm to 10 mm thick at the hot face in the carbon-containing brick after service. Then slag penetration would be inevitable within this zone and accordingly corrode at a faster rate. Thus, the importance of oxidation of carbon in carbon-containing brick was appreciated by Carr, Evans, Leonard and Richardson (14) who suggested the oxidation of carbon could well be the rate determining factor. Similarly, Ohba, Ikenoue and Nishikawa (67) also suggested that the wear rate is determined by the forming rate of the decarburized zone.

CHAPTER 3

PREPARATION OF MATERIALS

3.1. Materials used

3.1.1. Melts

3.1.2. MgO

3.1.3. Pitch

3.1.4. Crucibles

3.2. Preparation of the specimens

3.2.1. Production of sintered magnesia

3.2.2. Pitch impregnation

3.2.3. Carbonization

3.2.4. Surface area measurement

CHAPTER 3

PREPARATION OF MATERIALS

3.1. Materials used

3.1.1. Melts

General purpose reagent (GPR) grade of fused sodium tetraborate and sodium metavandate, supplied by Hopkin and Williams were used for melts below 1,000°C. Joseph Crosfield and Sons 'Pyramid' brand sodium disilicate was used above 1,300°C. All powdered reagents were dried in an oven at 120°C before being weighed into the crucible. Semi-quantitative X-ray fluorecense analysis impurities are listed in table 3.1. together with that of MgO. The analysis was done by the Analytical Services Laboratory of Imperial College.

Table 3.1.

	Impurity												
	Mg	Al	K	Ca	Zn	Ti	As	Mn	Ni	Zr	Fe	S	Cl
$NaVO_3$	O	O	O	O	O	-	-	-	-	-	-	X	X
$Na_2B_4O_7$	O	O	O	O	-	O	O	-	-	-	-	X	X
Na_2O2SiO_2	X	O	X	O	O	O	-	O	O	O	X	X	X
MgO	Δ	-	-	O	O	O	-	O	O	O	X	X	-

Key, Δ ; Major > 95%
X ; Minor 0.5 - 0.05%
O ; Trace < 0.05%
- ; not detected

The impurities of most concern were those likely to interfere with Mg determination by the atomic absorption spectrometer as will be discussed in section 4.4.2. An equally important impurity was Mg, if present in appreciable quantity, which could affect the dissolution rate of MgO. Mg present in minor quantity was not considered to be a serious matter in the analysis by the atomic absorption spectrophotometer because blank reagents containing the same amount of magnesium were added to the standard solutions used for calibration.

Normally melts were used several times in a prior investigation (69) for economy, whilst ensuring that the concentration of dissolved refractory was well below the saturation concentration. In the present investigation, a fresh melt was always used for every experiment to minimize introduction of error considering that the melt is analysed for an increase of magnesium concentration as will be described in section 4.1.

3.1.2. MgO

Single crystals of magnesia procured for an earlier research were used. The specimens were prepared to a suitable size by sectioning with a sharp knife-edge along the cleavage of the crystal. For the production of sintered porous magnesia specimens, fused magnesia powder of 99.9% purity supplied by Super Refractories Limited was used. The reduction of particle size was necessary for the production of green pellets to provide enough strength to be handled. The impurity content of the powder ground in an agate mortar, is also tabulated in the table 3.1.

3.1.3. Pitch

Lean tar pitch, a by-product of distillation of coal, supplied by the British Carbonization Research Association was used as a source of carbon. The suppliers elementary analysis of the pitch was approximately

C = 92.4%, H = 4.5%, N = 1.0%, the balance being mainly oxygen and some sulphur. The following properties of the pitch which relate the amount of carbon residue after carbonization were also provided by the supplier,

Softening point	81.5 °C
Coking value	55.2 %
Toluene insoluble value	34.6 %
Quinoline insoluble value	4.2 %

To deposit a small amount of carbon residue in the pores of refractories, the pitch was diluted with a lean tar heavy distillate. This of course lowered the viscosity of the pitch and softening point by about 2°C with 1 part of distillate in 100 parts of the pitch.

3.1.4. Crucibles

Due to the lack of any alternative other than platinum to contain the melts at elevated temperatures, a Pt 20% Rh crucible was used even though the crucible was not recommended by the manufacturer to be used in a reducing atmosphere. The crucible was 10 cm long and 5 cm in diameter and contained 200 gms of the powdered melt. It was always supported by a closely fitting fully sintered alumina crucible in order to protect the furnace tube wall in the event of leakage.

3.2. Preparation of the specimens

3.2.1. Production of sintered magnesia

It was intended to produce sintered magnesia specimens of around 30% porosity for the corrosion experiments so as to highlight the effect of carbon deposited in the pores when the specimen is subjected to slags. Also by having specimens with more porosity than refractories normally used in the steel-making industry, specimens with more carbon content could be prepared. This is because the quantity of pitch retained after impregnation of the specimen is directly related to the porosity of the

specimen.

Powder from the bottle was ground in an agate mortar for two hours open to the atmosphere to reduce the particle size. Freshly ground powders were always mixed with a bulk of previously ground powder and moulded as such. This of course contained moisture amounting to 0.4 weight % which acted as a binder. Green specimens of about 1.9 cm in diameter and 0.4 cm in width, each weighing approximately 2.5 gm were prepared by pressing at 7.8 tons/in^2 in a hardened silver steel lined stainless steel mould.

After drying, five green specimens at a time were contained in a close fitting fully sintered magnesia crucible and sintered in a commercial platinum wire wound furnace at 1,450^{o}C for an hour. A mercury balance as previously used by Hill (46) in his sintering studies was employed to measure the densities of sintered specimens from which the porosities were calculated. The average porosity of the specimens was 32% and specimens with 32% ± 1% were accepted for the corrosion test.

A hole of about 0.3 cm in diameter was drilled in all specimens with a diamond profile grinding wheel to be accommodated on to the platinum stirrer that will be described in section 4.2.1.

3.2.2. Pitch impregnation

In order to introduce the pitch into the pores of sintered magnesia specimens, the specimens were immersed in molten pitch contained in a Buchner flask near its boiling point. Vacuum by a rotary pump was applied for 30 minutes before the air was admitted to allow molten pitch to penetrate through the open pores of magnesia specimens. Then the molten pitch with the specimens was poured through a sieve to collect the pitch-containing MgO specimens. Molten hot pitch adhering to the surface of specimens was cleaned off with a tissue to minimize adhered pitch on the surface of specimens.

3.2.3. Carbonization

The purpose of carbonization was to remove the pitch volatiles and to decompose the pitch so that thermally stable carbon is deposited in the pores of magnesia which would not undergo any structural change itself during the corrosion experiment. The chosen temperature for carbonization was 1,400°C bearing in mind that most of the corrosion experiments would be carried out up to 1,400°C. Also above this temperature there would be reduction of magnesia by carbon that will result in significant microstructural change as reported by Pickering and Batchelor (72).

The pitch impregnated specimens contained in a specially machined graphite crucible were carbonized in a molybdenum tape-wound tube furnace. The specimens were kept at 1,400°C in the uniform hot zone of the furnace for 30 minutes in an atmosphere of flowing oxygen-free nitrogen. The molybdenum furnace used adopted the annulus system for providing an atmosphere of flowing mixed gas (10% hydrogen and 90% nitrogen) to protect the molybdenum tape from oxidation. The furnace temperature was manually set at 1,400°C during the carbonization with a suitable furnace current predetermined by a blank run. The temperature was measured by a Pt 5% Rh/Pt 20% Rh thermocouple.

After the carbonization, carbon adhering around the specimens was removed by rubbing with a knife-edge and then the weight increase was noted. To increase the quantity of carbon in magnesia, carbonized specimens were impregnated and carbonized again.

3.2.4. Surface area measurement

The geometrical surface area of specimens shaped circular (porous polycrystals) or squared (single crystals) was measured with a micrometer screw gauge. The curved area of flat parts of the specimens shaped half circular was measured by counting the area pressed on a graph paper as previously used by Reed (74).

The measurements were carried out with each specimen before and after the corrosion testing as the area of the corroded specimen was reduced. The area during the run was obtained by plotting the original area and final area as a function of time, assuming that the area changes linearly. An effort was made without much success to get an insight into the area change within the pores with a scanning electron micrographs. These are reproduced in figure 3.1.

Figure 3.1. Scanning electron micrographs of porous magnesia corroded in $Na_2B_4O_7$ at 900°C

(Left to Right)

(a) 32% porous sintered magnesia

X 420 X 8,400

(b) Corroded magnesia under natural convection at 900°C

X 405 X 8,100

(c) Corroded magnesia under forced convection at 900°C

X 780 X 7,800

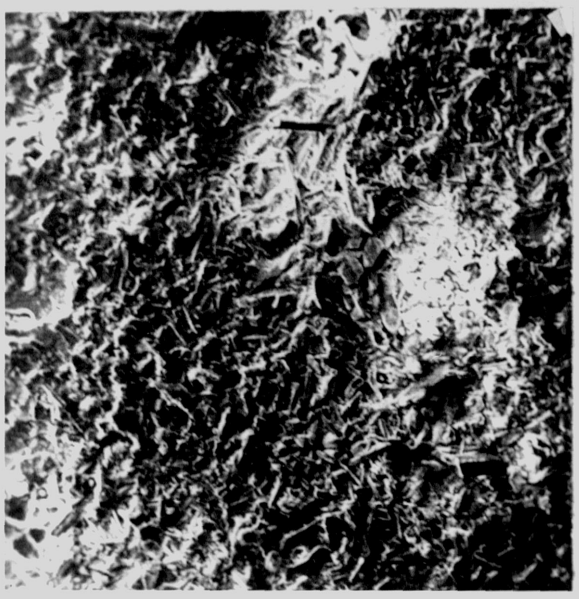

CHAPTER 4

EXPERIMENTAL WORK

4.1. Plan of the work

4.2. Apparatus for corrosion testing

- 4.2.1. Platinum stirrer
- 4.2.2. Sampling of the melt
- 4.2.3. Furnace used

4.3. Experimental procedure

4.4. Analytical instruments used

- 4.4.1. Choice of instruments
- 4.4.2. Atomic absorption spectrophotometer
- 4.4.3. Gas chromatograph

CHAPTER 4

EXPERIMENTAL WORK

4.1. Plan of the work

The overall aim of experimental work was to determine the corrosion rate of magnesia and the oxidation rate of carbon in carbon-containing magnesia under melts.

Previously used static corrosion technique (64) which required removal of adhered melt was not suitable due to the solubility of magnesia in dilute acid solution. Continuous weighing technique (84) which required the use of balance was not suitable either, because the gas bubbles evolved due to oxidation of carbon yielded serious experimental error on reading of the balance. This called for the design of a totally different experimental technique.

The above two techniques involve an assessment of weight loss with a refractory testpiece and neglect melt composition change so long as concentration of refractory already dissolved does not affect subsequent corrosion. It was thought that magnesia corrosion could be followed by an analysis of melt composition change during the course of a corrosion experiment as long as the melt taken represents the whole.

Preliminary work was undertaken on these lines with stirring of melt. The mixing experiments with varying speed of stirring have shown that a small amount of the melt could represent the whole using an optimum speed. The results obtained and their discussion will be reported in section 7.1. Hence the work was planned to stir the melt with a platinum stirrer and procure small amounts of melt with the aid of platinum wire loops at controlled times. The representative melts were then analysed by atomic absorption spectrophotometer.

The oxidation rate of carbon in carbon-containing magnesia was followed by the gas chromatograph using a thermal conductivity type

detector. The use of a gas sampling valve enabled continuous analysis of the reaction products, CO/CO_2.

4.2. Apparatus for corrosion testing

4.2.1. Platinum stirrer

A conventional propeller-shaped stirrer was made by Johnson Matthey and Company Limited with Pt/20% Rh alloy. A photograph of the stirrer is shown in figure 4.1. The blade, 3.5 cm in diameter, was comprised of four sectors bent to an angle of 30^{o}. The top part of the shaft, 0.5 cm in diameter and 12 cm in length, was tapered to fit into a mullite extension tube. The connecting part of the inner wall of the mullite tube was machined to a taper to fit the shaft tightly. It was fixed in position with a Pt 20% Rh pin through pre-drilled holes. Avoidance of the use of adhesive enabled the stirrer to be used up to $1,400^{o}C$. No failure during the experimental runs was experienced, hence the connection has given satisfactory performance. A platinum rod, 0.2 cm in diameter and 1.3 cm in length, to accommodate a refractory specimen was welded on to the shaft, 1.5 cm clear of the blade. The specimen with the hole was pushed onto this rod, whilst sliding off the rod was avoided by bending the rod upwards using a pin to secure it.

4.2.2. Sampling of the melt

A loop of about 0.4 cm in diameter was made on one end of a Pt 20% Rh wire of 0.7 mm in diameter. A photograph of sampling loops after an experimental run can also be seen in figure 4.1. The other end of the wire, about 10 cm long, was tied on to the grooved end of a mullite extension tube through the holes drilled by an ultrasonic drill using SiC powder.

The amount of melt caught by immersing the loop into the melt depended upon the viscosity of the melt. But in most cases the loop

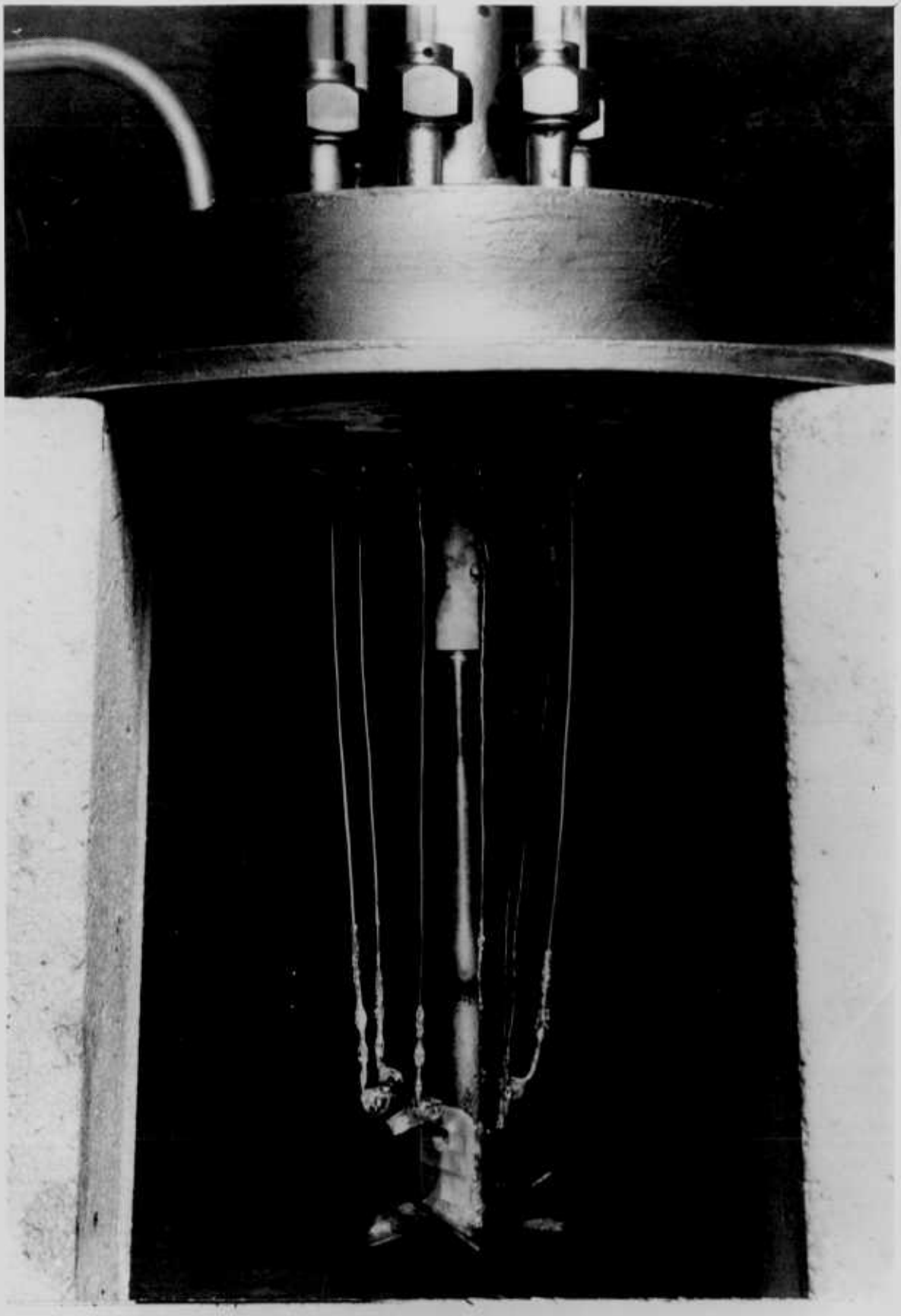

Figure 4.1. Furnace top arrangements.

was able to catch more than 0.02 gm which was the minimum quantity used for an analysis.

4.2.3. Furnace used

A vertical tube furnace was built with silicon carbide rods for heating elements. The furnace was suitable for continuous use up to 1,500°C with electrical power of 4.5 Kw. This furnace was chosen to be used for this study for its economy and easy operation in comparison with platinum and molybdenum wire wound furnaces previously used for higher temperature application. External features of the furnace can be seen in figure 4.2.

Twelve silicon carbide rods were used in a basket type arrangement around the impervious mullite tube of 75 x 65 mm. It had a uniform hot zone length of over 7 cm within ± 2.5°C at 1.040°C. The temperature of the furnace was controlled by Pt/13% Rh thermocouple connected to an on-off type automatic controller. A separate bare thermocouple was used to measure melt temperatures. To secure maximum service life of the rods, the furnace was operated continuously at 760°C even when it is not being used, to avoid cracking of rods due to further cooling of silica layer formed on the surface.

The top and bottom of the furnace tube were sealed by water cooled rubber 'O' rings { 15 } - the numbers refer to the corresponding numbers in figure 4.3. A mullite tube extension { 1 } for the platinum stirrer was introduced through a hole in the centre of the water cooled furnace top enclosure. A copper bearing { 3 }, imbedded in its housing on top of the enclosure, was fixed on to the tube to rotate the stirrer on its axis. The fixing and sealing of the bearing and the tube was done by placing a short length of tight fitting rubber tubing over it. The use of silicone grease on this joint enabled the ceramic tube to move freely without losing gas tightness.

Six sampling mullite tubes { 2 } were arranged to be introduced

Figure 4.2 Apparatus for the corrosion testing of carbon-containing refractories

Figure 4.3. Detailed views of corrosion testing furnace

1. Mullite tube extension for platinum stirrer
2. Mullite tube extension for platinum wire loop
3. Copper bearing
4. Gas outlet
5. Water cooled jacket
6. Pt 20% Rh wire loop
7. Pt 20% Rh stirrer
8. Mullite furnace tube
9. Silicon carbide rod heating elements
10. Recrystallized alumina supporting crucible
11. Pt 20% Rh crucible
12. Machined insulating brick support for crucible
13. Impervious alumina tube supporting No.10
14. Water cooled furnace bottom enclosure
15. Rubber 'O' ring
16. Water cooling
17. Gas inlet

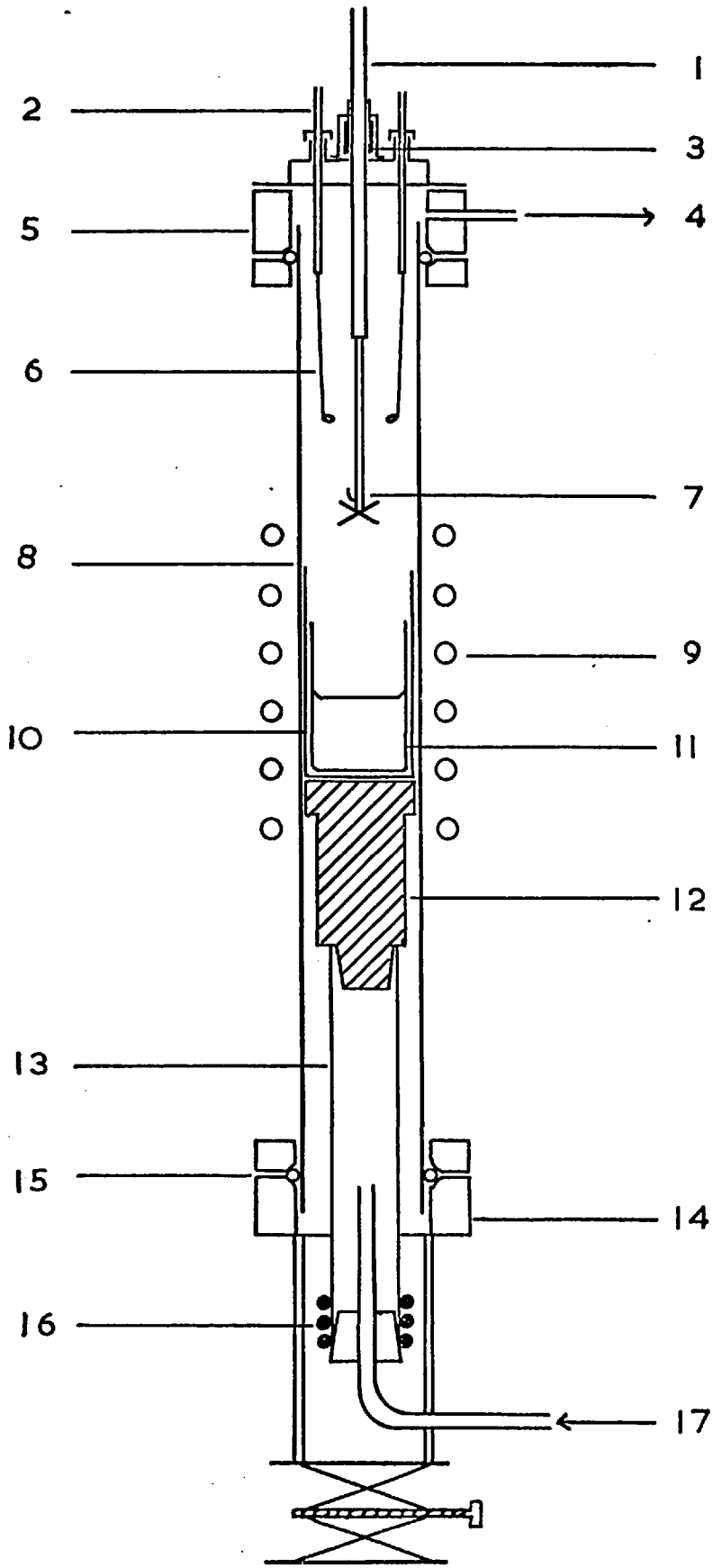
1
2
3
4
5
6
7
8
9
10
11
12
13
15
14
16
17

through 'O' ring seals, but normally one was used for the bare thermocouple to take the melt temperature. A good view of the arrangement can also be seen in the figure 4.1.

A machined insulating brick { 12 }, sitting on an alumina tube { 13 }, was used to support the crucibles. An inert atmosphere of O_2-free nitrogen gas was introduced from the bottom through the alumina tube. The bottom enclosure { 14 } sat on a laboratory jack with the aid of suitably machined ceramic tube in between. The use of the jack enabled the crucible to be placed in the predetermined hot zone.

4.3. Experimental procedure

Pre-weighed powdered slag contained in the platinum crucible was first melted in a Kanthal wire wound furnace. The hot crucible was then transferred into the silicon carbide rod furnace at around 800°C. This was carried out with each experimental run to avoid any thermal stress cracking of the furnace tube due to sudden immersion of cold crucible. The temperature of the furnace was then raised to a desired point in the course of 2 to 3 hours. Meanwhile, the furnace top enclosure containing the platinum stirrer and sampling loops was fitted on top of the furnace tube and de-gased with excess amount of O_2-free nitrogen. When the melt attained the desired temperature the inlet gas amount was adjusted and further left for up to an hour so that the melt temperature is stabilized. Usually when the gas chromatograph recorded less than 0.04% of oxygen, a run was commenced.

The platinum stirrer extension tube, now connected on to the shaft of the pre-warmed motor, was lowered down towards the melt in successive steps to avoid cracking of the specimen. The specimen was left just above the melt for up to 10 minutes to reach thermal equilibrium with the melt. As soon as the specimen was lowered into the pre-determined zone in the melt, stirring was commenced. During the immersion of the sampling loops into the melt, stirring was stopped for about ten seconds to avoid

any miscarriage of the sample melt while it was being released, i.e. due to tangling of the loop onto the stirrer.

When the experimental run terminated, the crucible was taken out of the furnace immediately and the melt was poured out while it was hot. Adhered melt onto the crucible wall, platinum stirrer and sampling loops was easily washed off in hot dilute HCl acid solution within a few hours. However, the sodium silicate melt took a few days to be leached away even in hot concentrated HCl acid. To avoid delaying the next run, an excess of sodium carbonate was added to the crucible and heated to around 950°C to fuse the remaining sodium silicate. After the evolution of CO_2, the compound was easily removed in hot running water. By this method, a clean crucible was ready for the next experimental run in about two to three hours.

4.4. Analytical instruments used

4.4.1. Choice of instruments

Choice of two analytical methods was required for the main part of the work: 1) a method for determining the concentration of magnesium in representative melts procured by the sample loops at varying times and 2) following reaction products in a gaseous form evolved during the experimental run. Choice of analytical instrument for the latter was relatively easy compared with the first because the gas chromatograph using solid absorbent for a column packing is known to separate the gases evolved, i.e. CO, CO_2 with a high degree of accuracy.

Choice of the best analytical method with accuracy for the determination of the magnesium concentration in melts was troublesome considering that all the melts used contain an excess amount of sodium and a fair amount of impurities as reported in the section 3.1.1. Also the analytical method chosen should be reproducible and not time consuming.

Three methods were under consideration, namely atomic absorption

spectroscopy (AAS) X-ray fluorescense and wet chemical analysis. Initial trial analysis was carried out with three analytical means; of these the analysis by XRF and chemical analysis were performed by the Analytical Services Laboratory, Department of Metallurgy and Material Science, Imperial College. The sample used for these analyses was $Na_2Si_2O_5$ glass containing MgO. $Na_2Si_2O_5$ was specially selected not only because major stress would be placed on this melt in the research but also because silicon is reported (28) to be one of the elements which interferes with Mg determination by atomic absorption spectroscopy.

The analytical procedure by wet chemical analysis is as follows: silica is first removed by hydrofluoric and perchloric acids, evaporating to fumes of $HClO_4$ twice. After diluting it with distilled water to make up 1% $HClO_4$, the assay is transferred to a mercury cathode separator to remove heavy metals present as impurities. There remain aluminium, calcium and magnesium. The aqueous layer is then extracted several times with a 5% solution of 8-hydroxyquinoline in chloroform to remove traces of heavy metals left from the mercury cathode separation and aluminium impurity. Finally calcium and sodium are removed by extracting further with the 5% 8-hydroxyquinoline solution in the chloroform at pH 10 with an addition of butyl cellosolve. Although the accuracy of analysis is reported to be within acceptable range, ± 3% to ± 5%, unfortunately the analysis was time consuming. The analysis of two samples in duplicate takes four days.

At the beginning of the research it was anticipated that atomic absorption spectrophotometer would not be a suitable instrument for Mg determination in the presence of excess sodium, because severe interference by sodium is expected. However, this was proved not to be so experimentally. This was performed by analysing sodium silicate melt containing a series of known quantities of magnesium. The powders were mixed and melted in platinum crucibles prior to the analysis. The results obtained are shown

below in comparison with the results obtained by X-ray fluorescence spectrophotometer.

Added amount of Mg (ppm)	Found by AAS (ppm)	XRF (ppm)
250	-	64
390	-	565
780	775	675
1,140	1,100	900
2,340	<1,900*	1,480

* small amount of the assay was spilt during the preparation

The above results on Mg determination indicate that not only is there no interference in the presence of 800 ppm sodium by AAS but also that analysis by AAS is superior to that of XRF. Further confirmation on effect of excess sodium was carried out by comparing standard solutions ranging from 0.5 - 4 ppm of Mg with and without sodium. There was an indication of somewhat increased noise level with the solutions containing sodium but no interference on absorbence was noticed. One of the sources of noise with the solutions containing sodium could be due to a few spurts introduced onto the flame as a result of sodium deposits on the wall of the burner. Hence these deposits were frequently removed.

From the experience described above, AAS was an automatic choice for its simplicity and accuracy, especially since the analysis was not time consuming compared with the wet chemical analysis and XRF for which a week was needed to analyse six samples.

4.4.2. Atomic absorption spectroscopy

As mentioned in the preceding section, analysis of increase of magnesium concentration in melt was carried out by using SP-90 Atomic Absorption Spectrophotometer, manufactured by Pye Unicam Limited, Cambridge.

The instrument requires the sample to be introduced in the form of an aqueous solution through the capillary tubing to the atomizer and the

cloud chamber where the solution is dispersed in the form of small droplets. This is then fed into an acetylene-air flame about 2,450°K with the fuel and oxidant mixture. At this temperature the solution becomes vaporized and the elements are dissociated into atoms. Most of the atoms are in the ground state level except a small proportion which are in an excited state, and are capable of absorbing characteristic radiation of the same element provided by a hollow cathode lamp. The absorption spectroscopy is based on the measurement of absorbed radiation by the atoms in the ground state. The amount of ground state atoms at a given temperature is proportional to the concentration of the element in the solution.

A small proportion of atoms existing in their excited state emit the radiation of a wavelength which is characteristic of the elements. In emission spectroscopy, the intensity of radiation emitted by excited state atoms is measured.

The atomic absorption spectrophotometer employs a hollow cathode lamp for an emission source. A hollow cathode consisting of the element being determined and an anode are enclosed in a sealed off cylindrical glass tube filled with an inert gas such as neon or argon. When an electrical potential is applied, the gas atoms are ionized and the metal atoms are discharged from the hollow cathode. The metal atoms are excited by collision with ionized gas atoms and emit the characteristic radiation. The radiation is focused on to the flame and received by a detector via a wavelength selector. The wavelength selector is employed to separate the desired radiation from other spectrum lines. The selector for SP-90 was a monochromator using a 30° rear aluminized silica prism. The signals from the detector are amplified and recorded on a chart recorder.

Interference with magnesium analysis

Various elements capable of forming stable mixed oxides with magnesium at high temperature interfere with the determination of magnesium. Elwell and Gidley (28) report interference in determination of 6 ppm Mg in the presence of 1,000 ppm of Al, Si, Ti, Hf, Th and Sr. The interference by these elements could be overcome by adding releasing agents strontium and lanthanum to combine with the interfering elements or by using a hotter flame of acetylene-nitrous oxide (73). No slags employed in this research contain an excessive amount of interfering elements as reported in section 3.1. except silicon in the $Na_2Si_2O_5$ melt. The silica was expelled as the volatile silicon tetrafluoride by treatment with hydrofluoric acid and hydrochloric acid as will be described later. During the earlier stage of analysis, it was noticed that magnesium was severely suppressed when sample solutions were prepared with sulphuric acid. It may be (28) that magnesium and impurity element sulphates formed stable oxides, before being dissociated. This problem was easily overcome by using hydrochloric acid instead of sulphuric acid.

Calibration

The detection limit of magnesium quoted in text books lies between 0.0005 and 0.01 ppm. Normally samples were diluted so as to be in the region of 0.1 to 4 ppm of magnesium, well above the detection limit. Standard solutions for calibration were prepared for each melt. This was done by adding blank slags into standard solutions to introduce the same impurities, magnesium in particular, as sample solutions. A typical calibration curve for Mg in sodium silicate melt is shown in figure 4.4. For the calibration dried 'Specpure' grade magnesia was used supplied by Johnson Matthey and Company Limited.

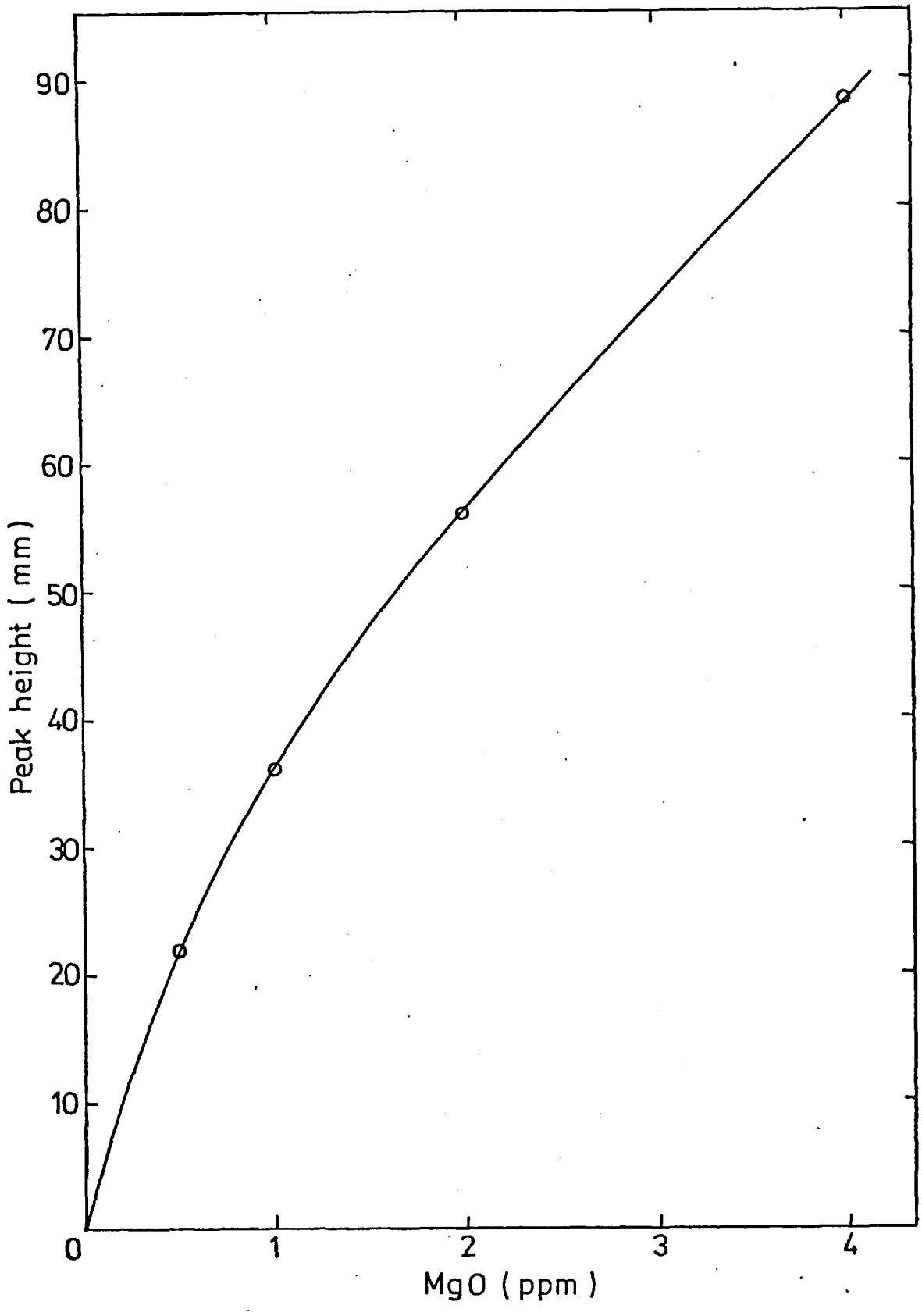

Figure 4.4. Typical calibration curve for MgO.

Analytical procedure

Melts procured by sampling loops were crushed and ground to a fine powder in a tungsten carbide percussion mortar. Either 0.02 or 0.04 gms of sample depending upon the quantity available was weighed into beakers and dissolved in warm distilled water. With sodium borate samples either 0.5 or 1 ml of analytical reagent quality hydrochloric acid was added to accelerate solution. When the samples dissolved completely these were transferred and diluted to either 50 ml or 100 ml graduated flasks.

As mentioned in the section on interference, silica had to be removed from sodium silicate samples. Normally 0.04 gms of sample were dissolved in 1 ml of hydrofluoric acid and 0.5 ml of hydrochloric acid in platinum crucibles. Adequate heat was carefully applied to avoid sputtering of the solutions from beneath and above the crucibles with an electric oven and a radiation heater. When the solution became pasty, the same quantities of hydrofluoric and hydrochloric acids and 1 ml of perchloric acid were added and the solutions evaporated to fumes of $HClO_4$. The solutions were diluted with distilled water and again evaporated to fumes to reduce the content of acids. When the solutions were reduced to less than 1 ml, these were diluted to 100 ml.

The operation of the instrument began by fitting a magnesium hollow cathode lamp and switching on. The following settings were made and left at least 15 minutes to stabilize the instrument and emission from the hollow cathode lamp.

Air flow rate	5,000 ml/min
Acetylene flow rate	1,500 ml/min
Wavelength	285.2 mμ
Cathode lamp current	3 mA

Distilled water was first admitted to the flame and emission from the lamp was set at maximum scale on a chart recorder with the help of gain settings. On introduction of solutions containing MgO, a reading

equivalent to an absorbed radiation by magnesium in the solution was obtained on the recorder. Standard solutions for calibration were always introduced before and after the sample solutions. Distilled water was admitted in between each sample solution to check the base line and to clean the capillary tubing, atomizer and cloud chamber.

4.4.3. Gas chromatograph

A gas chromatograph was constructed to follow reaction products in a gaseous form, these being CO and CO_2 evolved as a result of oxidation of carbon in the pores of MgO refractories under melts. The employment of a gas sampling valve enabled the operator to follow gases continuously during five minutes. A schematic block diagram of the gas chromatograph is shown in figure 4.5.

Columns

Two columns with a stationary phase of solid absorbent silica gel and molecular sieve were made to separate the gases - O_2, N_2, CO_2 and CO. Silica gel (40-60 mesh), capable of separating O_2/N_2 and CO_2, was packed into 1 foot in length, $\frac{1}{8}$" in diameter of steel tubing and molecular sieve 5A (30-60 mesh) for O_2, N_2 and CO, was packed into 6 feet in length, $\frac{1}{8}$" in diameter of steel tubing. Glass fibre was plugged into both ends of the steel tubing to retain the packed solid absorbent in position. The columns made were bent into a coil of about 3 inches in diameter and deactivated at 200°C for 48 hours. This was carried out with a flowing atmosphere of N_2 through the columns. Initial and subsequent occasional deactivation of the stationary phase was required to remove moisture and trapped gas in solid absorbents, i.e. CO_2 in the molecular sieve. The columns were connected to a katharometer and accommodated in an oven kept at 72°C, as shown in the figure 4.5.

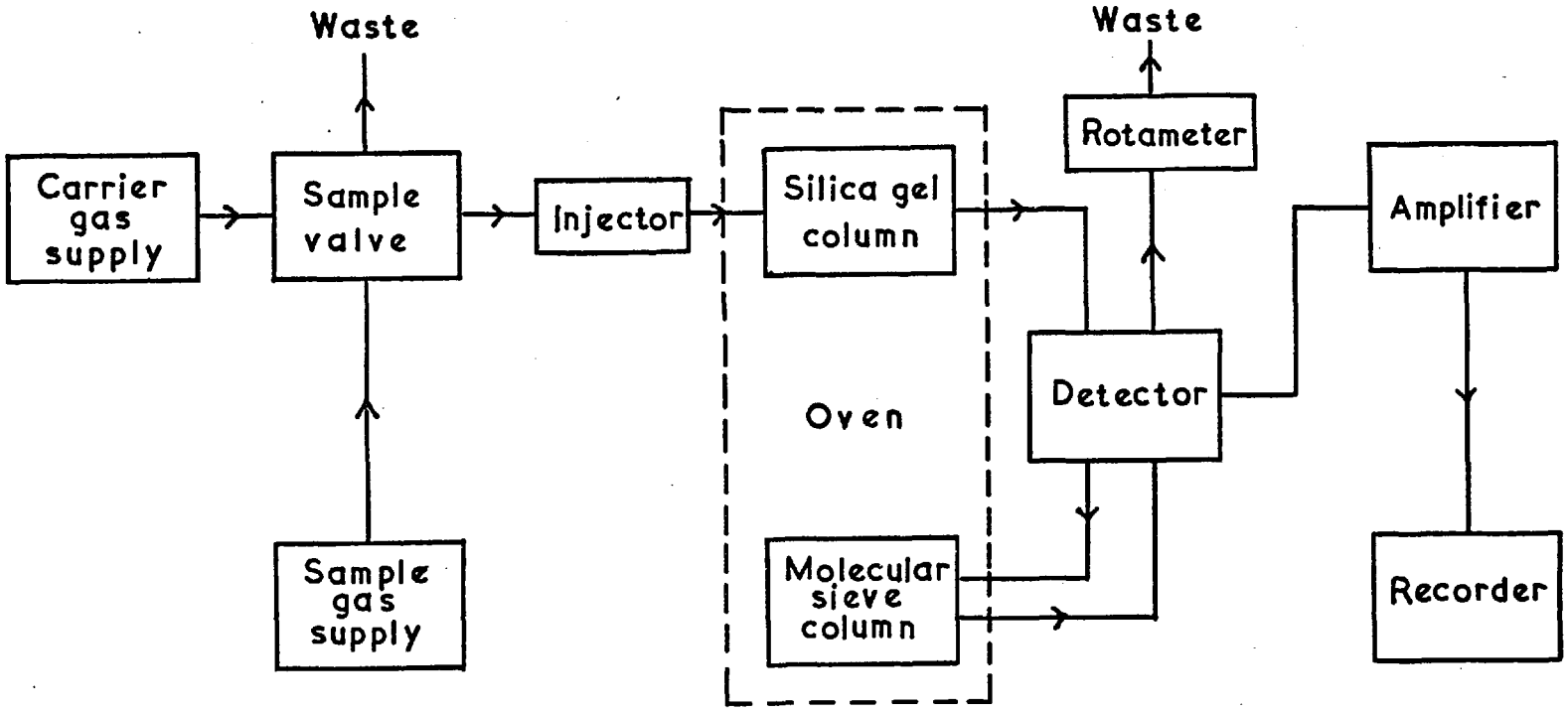

Figure 4.5. Block diagram of gas chromatograph.

Carrier gas and flow rate measurement

In order to obtain a rapid response on a thermal conductivity type detector, hydrogen was used as a carrier gas which has the highest thermal conductivity, for the response depends on the difference in conductivity between the sample gas and the carrier gas.

The hydrogen flow rate was kept constant at 20.5 ml/min with an inlet pressure of 5 lb/in^2 and regulated by a cylinder head regulator. The flow rate of the gases was measured by a soap bubble flow meter. During the course of the run when a constant reading of flow rate was necessary, a rotameter was used.

Sample injection and calibration

A manual gas sampling valve with 1 ml sampling loop, supplied by Pye Unicam Limited, was used for sample injections. Gases from the furnace chamber were arranged to pass through the 1 ml loop of sampling valve continuously to waste. By turning the knob on the sample valve, the gases contained in the sampling loop at that moment were injected into the chromatographic column with the carrier gas. The knob was left in the injection position for more than five seconds to ensure all the sample gases were washed out considering carrier gas takes about 3 seconds to remove the gases in the loop.

For calibration, gases were introduced through the injection port sealed by a septum of self sealing silicon rubber. A gas tight 'Hamilton' injection syringe was used for an injector.

A series of known quantities of individual gases was injected to obtain a calibration curve. Although pure gases were drawn from pressurized rubber tubing by the syringe flushed out several times, a small amount of air was always present. This amount of air was measured and subtracted from the pure gas. A typical calibration curve for CO and CO_2 is shown in figure 4.6. The recorder used contained an electronic integrator with which the area of the peak could be measured. However, calibration by

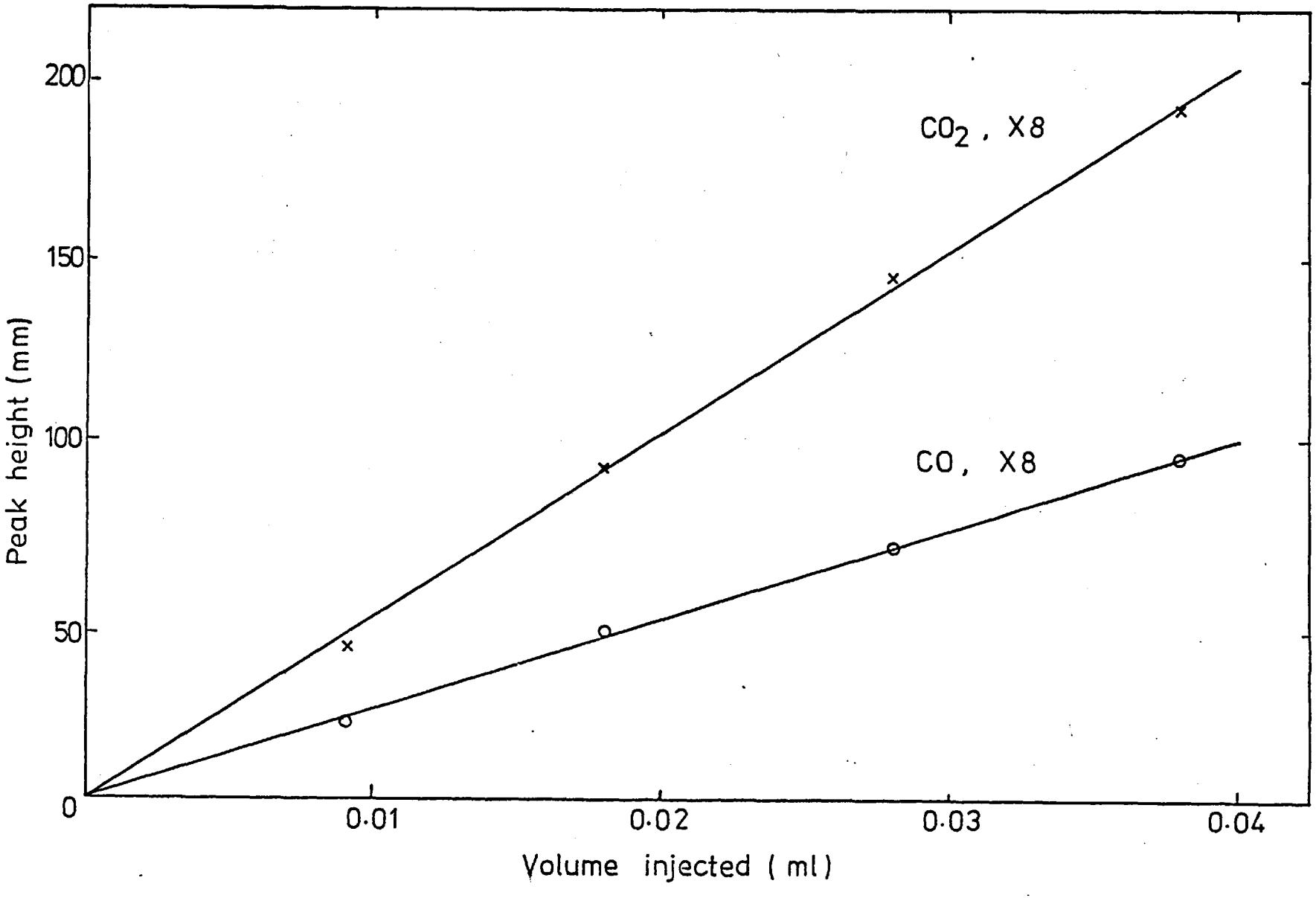

Figure 4.6. Typical calibration curve for CO and CO_2.

a peak height measurement was found to be more accurate than by the integrator. Hence the height of the peak was always measured for the calibration.

Detector

Microkatharometer type MK 158 manufactured by the Taylor Servomex was used for a detector. This differential thermal conductivity type detector using platinum resistance wires embedded in two gas tight compartments, was connected to a Wheatstone Bridge circuit. Five volts was applied to the platinum wire to be heated. A constant flow of the carrier gas balances the bridge circuit. As soon as the sample gas enters one side of the katharometer, a change in temperature of the wire is caused as a result of differences in thermal conductivity between the sample gas separated by the column and the carrier gas. The temperature difference causes an imbalance in the bridge circuit. The degree of imbalance was amplified and recorded on a chart paper recorder.

Analytical procedure

The column temperature and the carrier gas flow rate was first checked and adjusted to the desired value before the instrument was switched on. Then 5 volts was applied to the platinum resistance wire in the katharometer and the instrument was left on for more than half an hour to warm up.

When an experimental run is commenced as described in the section 4.3, gas analysis was performed every five minutes along with the sampling of the melt. After the stirring experiment was terminated, gas analysis was continued until all the CO/CO_2 gas was released from the furnace chamber.

During the course of the run, the release of sodium vapour was noticeable especially with sodium silicate melt above 1,300^{o}C. This was collected by a glass fibre plug made between the furnace chamber outlet and gas sampling valve inlet.

At the beginning of the research, it was intended to carry out experimental runs in flowing N_2 atmosphere at just above atmospheric pressure (i.e. 2 or 3 cm of mercury). However, due to convection currents set up within the furnace chamber, it was impossible to measure the flow rate. This was overcome by using a glass fibre plug as described above and raising the pressure to 10.5 cm of mercury. In this condition reasonably reproducible readings of flow rate could be determined.

CHAPTER 5

OXIDATION OF CARBON UNDER MELTS

5.1. Introduction

5.2. Previous work

5.2.1. Oxidation of carbon in air

5.2.2. Oxidation of carbon under melts

5.3. Experimental

5.4. Discussion of results

CHAPTER 5

OXIDATION OF CARBON UNDER MELTS

5.1. Introduction

Graphite exists in abundunce in nature as micro-cystalline flakes mixed with clay and other impurities. This impure natural graphite has been extensively used in the manufacture of crucibles and as a component of electrode graphite. Graphite is anisotropic, consisting of layers of covalently bonded, hexagonally arranged carbon atoms held together by weak Van der Waals forces. Use is made of its enhanced thermal conductivity parallel to the layer planes to increase the heat transfer in crucible walls.

Dodd and Green (26) report a trial of plumbago brick as a refractory lining in a steel ladle. Similar material has more recently been used in the boshes of iron blast furnaces but the largest amount of graphite used in industry is synthetic, manufactured from petroleum coke with a coal-tar pitch as a binder. The pitch is then carbonized at about 900^{o}C and the baked carbon is converted to crystalline graphite by heating at a temperature of about 2,800^{o}C, normally leaving porosity of about 30%. In addition pyrographite is assuming some importance where enhanced anisotropic properties are required such as resistance to oxidation in the basal planes. It has been suggested that this form might occur in pitch-impregnated refractories under working conditions.

Among the usage of carbon as a material, the exothermic reaction of carbon with oxygen has been one of the major sources of energy. The endothermic reaction with carbon dioxide and steam provides gaseous fuels that are again utilized as an energy source. On the other hand, carbon is used as a material where good oxidation resistance is desirable. For example, as an electrode material and nozzles in rockets. Efforts have therefore been made to improve oxidation resistance with some

success where coatings are used.

Numerous researches have been carried out on the combustion of carbon by chemical reaction. It is beyond the scope of this review to cover the whole field of carbon gasification. It has been reviewed by Walker, Rusinko and Austin (97), Field, Gill, Morgan and Hawksley (34), and more recently by Lewis (61). The following section on carbon oxidation will therefore be confined to the relevant topics for later discussion.

5.2. Previous work

5.2.1. Oxidation of carbon in air

Since the classical work on carbon combustion by Tu, Davies and Hottel (94), the overall reaction mechanism has been divided into two regions. In the low temperature range (C - E, Figure 5.1.), the rate process is controlled by the chemical reaction of the reactant and the carbon, where the rate is strongly dependent on temperature but practically independent of gas velocity. At the higher temperatures (A - C, Figure 5.1.), diffusion through the laminar gas layer formed at the carbon surface prevails, where the rate is almost independent of temperature but is dependent on the gas velocity. The plot of the combustion rate of carbon in air reported by Tu et al. (94) is shown in Figure 5.1. together with the rate observed by the author (69) in earlier work.

The energy of activation for the former process quoted in the literature varies widely depending mainly upon the type of carbon used. Walker et al. (97) report that the activation energies are found to vary from 17 to 100 ± 30 Kcal/mol. Wicke (102), working with crushed electrode carbon finds a value of 58 ± 4 Kcal/mol. More recently Lewis (61) states in his review that there is now general agreement that for graphites containing less than 5 ppm impurities the activation energy for oxidation in a dry gas is between 60 and 62 Kcal/mol. Accordingly, he emphasises

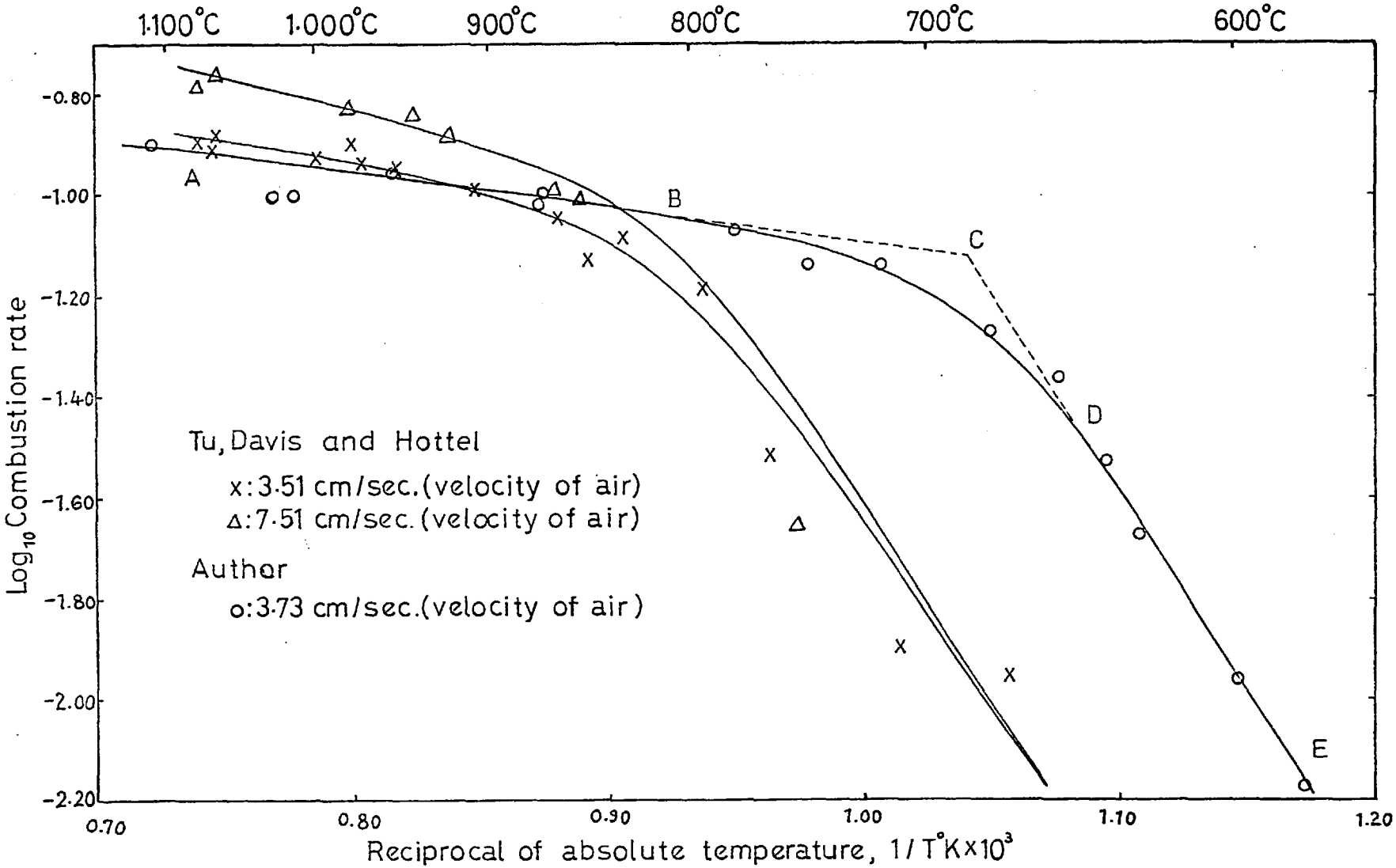

Figure 5.1. Arrhenius plot of the rate of oxidation of carbon in a steady flow of air.

that the observed values of E of less than 60 Kcal/mol apply to a reaction which is predominently catalytic in nature. This remark is in support of work reported by Heuchamps and Duval (45) who found 60 Kcal/mol with a clean graphite, but a value between 35 and 38 Kcal/mol with a contaminated graphite. These authors also report that the more contaminated the graphite the lower the ratio of CO to CO_2 in the product.

In addition to the two reaction mechanisms mentioned above, Wicke (102) states that there is an intermediate region (B - D, Figure 5.1.) in the case of porous specimens. Here, the overall rate is controlled by the competition between diffusion and reaction inside the pores which are partly filled with reaction products. The observed activation energy in this zone is half the E value for chemical reaction.

When the pores are completely filled with the reaction product and the laminar gas layer with its concentration gradient external to the specimen is established, the rate-controlling step is transport of gas molecules from the bulk of the gas to the surface of the specimen. Many workers (94)(25) found an empirical relationship in which the oxidation depends on the square root of gas velocity in this zone. The energies of activation reported were 2.4 Kcal/mol by Tu et al. (94), below 8 Kcal/mol by Day (25) and 4 Kcal/mol by Park (69).

The composition of reaction products, the CO/CO_2 ratio, particularly the primary products of the oxidation of carbon, has also been the subject of various workers. Arthur (1) measured the CO/CO_2 ratio in the temperature range 460 to 900°C, using $POCl_3$ as an inhibitor of the secondary reaction in the gas phase oxidation of carbon monoxide. He finds that the ratio can be expressed as

$$CO/CO_2 = 10^{3.4} e^{-12,400/RT}$$

over the temperature range investigated. The CO/CO_2 ratio as a function of temperature is reproduced in Figure 5.7.

Using a high flow rate of oxygen over the carbon specimen to minimize secondary oxidation of CO, Day (25) finds that carbon dioxide is a primary product of carbon oxidation. On the other hand, Blyholder and Eyring (8) report that CO is the predominent primary product.

The CO/CO_2 ratio in a dry air stream of 4 cc/sec was measured by Wicke (102) whose results are also reproduced in Figure 5.7. Using the retarding agent for the CO oxidation - $POCl_3$ - with the same flow rate of air, he finds the primary CO/CO_2 ratio is in agreement with that of Arthur and the CO/CO_2 ratio increases with increasing temperature.

Walker et al. (97) summarize in their review on this topic that:-

1) Carbon dioxide, as well as carbon monoxide, is a primary product of carbon oxidation;
2) The ratio of the primary products CO/CO_2, generally is found to increase with increasing temperature;
3) It is not well established that the magnitude of the ratio of the primary products is solely a function of temperature and independent of the carbon reacted.

5.2.2. Oxidation of carbon under melts

Apart from its academic interest, the oxidation of carbon by liquid oxides is important in both the ceramic and the metallurgical industries. Oxide refractories are often used under reducing conditions in the presence of carbon as in the iron blast furnace. The carbon electrode in an arc melting furnace is eaten away by an oxidation process. Undoubtedly, the interaction between carbon and iron oxide-containing slags is important in iron and steel making industry not only to a metallurgist as the production of steel relies on the carborthermic reduction of iron, but also to a ceramist as the corrosion resistance of carbon-containing refractories used in an oxygen steel making vessel is dependent upon carbon removal. For the last reason, the author (69) looked into the problem earlier and the present work continues this study.

In spite of its importance, a relatively small amount of work has been reported in the literature on the mechanism of reaction between carbon and slags. This may be due to experimental difficulties in obtaining meaningful results. The oxidation of carbon is an exothermic reaction and there is no satisfactory way of determining the temperature of the interface accurately where the reaction takes place. The problem of a slag container arises particularly if iron oxide is present in the slag. The rate of oxidation differs with the type of carbon employed depending upon the degree of graphitization and impurities content. All these add to the fact that research in this area is difficult and conclusions drawn by different research workers are not in good agreement.

Dancy (23) studied the reduction of pure liquid FeO and Fe_3O_4 by carbon in molten iron. The value of apparent energy of activation of the reduction for FeO was 43 Kcal/mol and for Fe_3O_4 was 37 Kcal/mol. Although no conclusion was drawn regarding the rate controlling step for the reaction, the factors contributing towards the high energy of activation were considered important. For example, the viscosity and surface tension of the components which may influence gas evolution and the rate at which the reactants reached the interface.

Fulton and Chipman (36) studied the reduction of silica in a slag containing 45% SiO_2, 38% CaO, 17% Al_2O_3 by carbon saturated iron in a graphite crucible. The rate observed was very slow and nearly independent of stirring. From these results combined with the high energy of activation observed of 130 Kcal/mol, they conclude that the rate was controlled by chemical reaction. Also suggested is that the step is associated with the breaking of Si - O bonds.

Shurygin, Boronenkov, Kryuk and Revebtsov (88) studied the kinetics of reaction between graphite and FeO in melts containing CaO - SiO_2 - Al_2O_3 by Levich's rotating disc method at the temperature range of

1,400 to 1,520°C. From the fact that the weight loss of the specimen obtained was dependent only slightly on the angular velocity, gasification of carbon at the interface was assumed to be the rate controlling process. This conclusion was further supported by the value of corresponding energy of activation with that of carbon gasification in air, 38 - 52 Kcal/mol.

The study of kinetics of the oxidation of carbon in zinc containing slag, 56.0% FeO, 9.05% ZnO, 25.8% SiO_2 and 7.2% Al_2O_3, was reported by Chumarev and Okunev (17) using a similar technique to Shurygin et al. Similar observations on the non-dependence of the the oxidation rate of carbon with intensified mixing of melt and the corresponding value of energy of activation, 38 Kcal/mol, lead them to conclude that chemical reaction was the rate controlling process.

Chumarev and Vlasova (18) studied the reduction of zinc oxide in a $CaO - SiO_2$ melt by determining the value of the CO/CO_2 ratio in the reaction product. From the fact that the CO/CO_2 ratio increased with increasing temperature, they concluded that the reaction rate was controlled by the CO production stage. Again the same value of energy of activation for oxidation of carbon 38 Kcal/mol was obtained.

Fay Fun (33) conducted experiments with slags containing up to 40% FeO in $CaO - SiO_2$ at just above 1,600°C by immersing a graphite rod as a reductant. As the slags were contained in a magnesia crucible, an appreciable amount of MgO entered the slag due to dissolution. The increase in MgO was approximately compensated by the decrease of FeO. Fun concluded that neither the chemical reaction nor gas phase diffusion could be counted as the rate-limiting stage because the observed rates fall between the calculated ratio of the chemically controlled graphite gasification and predicted rates from gas phase diffusion. However, the work contains interesting observations on the increasing rate of oxidation with increasing FeO concentration which could be explained by the mode of bubble generation. For example, strings of bubbles were

formed at higher than 10% FeO whilst the bubbles were generated individually one after another below 10% FeO, thus agitating the slag the more the higher concentration of FeO. Therefore, bubble evolution was suggested as an important parameter for the reaction.

Davies, Hazeldean and Smith (24) studied the kinetics of oxidation of carbon in iron oxide - lime - silica slags over the temperature range 1,400 to 1,500°C. These authors concluded unequivocally that gas phase diffusion of reaction product, CO_2, across a boundary layer is not rate controlling as the calculated rate did not agree with the observed rate. This conclusion was further supported by an experimentally obtained high value of apparent energy of activation, 67 Kcal/mol, compared with the value of a few Kcal for gas phase diffusion. Chemical reaction control was considered unlikely as the predicted rate was 1.6 times higher than the experimentally observed rate. However, attention was again drawn to the importance of the gas evolution step in the rate process.

In his earlier work, the author (69) investigated the oxidation of electrode carbon under $NaVO_3$, $Na_2B_4O_7$, and $Na_2Si_2O_5$. As the Arrhenius plot of oxidation rate of carbon in the melts is reproduced in Figure 5.2., the equality of the apparent activation energy 21-25 Kcal/mol in each melt lead to the suggestion that there may be a common phenomenon prevailing. The rate controlling process suggested was a diffusion controlled process, possibly by carbonate anions, diffusing through a carbonate rich boundary layer at the interface. The suggestion was reinforced by a similar value of activation energy for viscous flow of molten sodium carbonate, 26 Kcal/mol as reported by Janz (52). However, the suggestion needed further experimental confirmation that will indicate whether or not a boundary layer existed. Levich's (59) rotating disc method as is extensively used for the confirmation of a diffusion controlled process, was considered suitable in addition to the stagnent

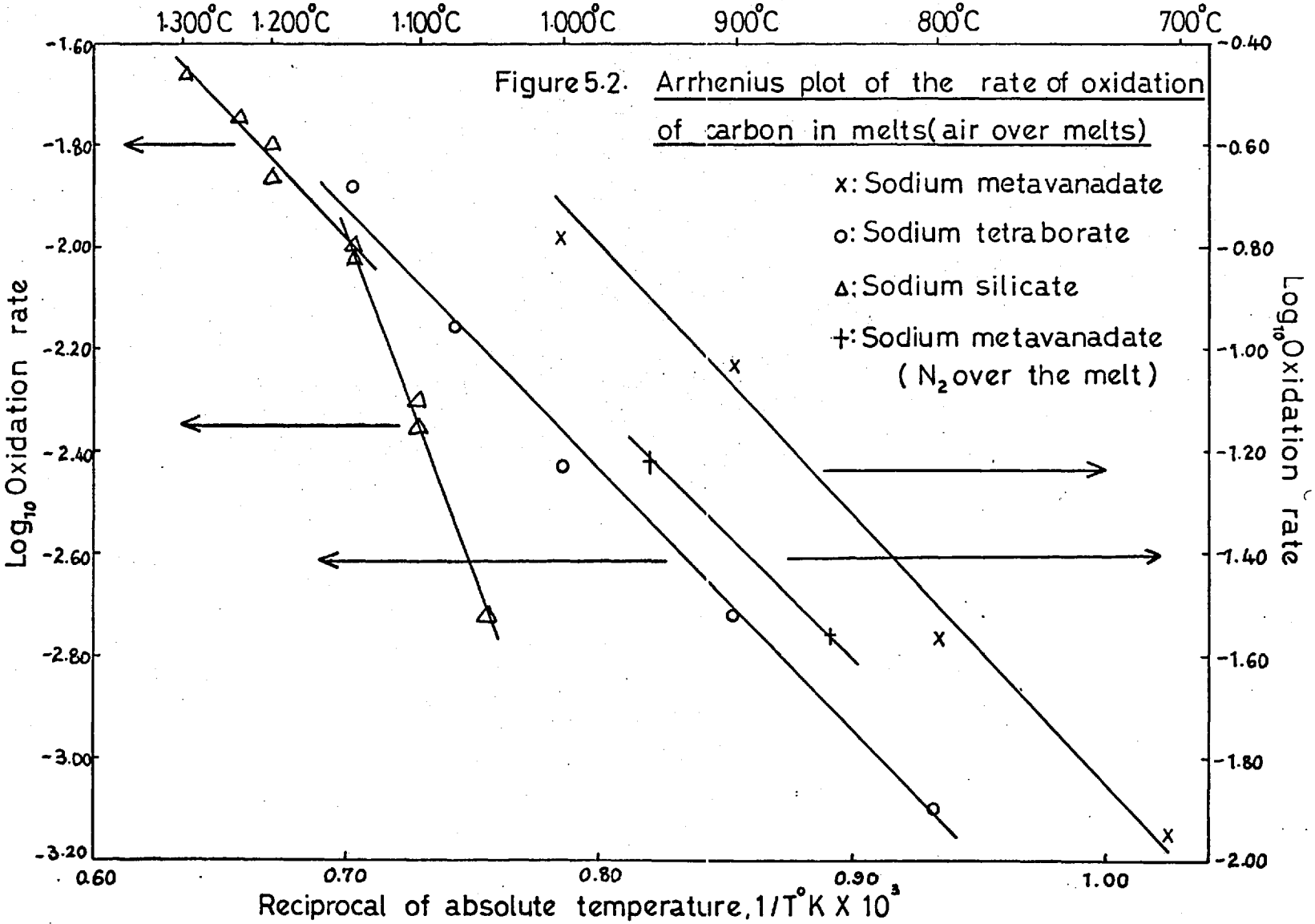

Figure 5.2. Arrhenius plot of the rate of oxidation of carbon in melts (air over melts)

oxidation experiment under natural convection. The reaction products, the ratio of CO/CO_2, were followed by gas chromatograph. The detailed experimental technique and discussion of results obtained follow.

5.3. Experimental

The carbon specimens, in the form of cylindrical discs, were cut about 1.5 cm long from the carbon rod (CY9) of about 1.6 cm diameter supplied by Morganite LTD. Both sides of the disc surfaces were ground on successive grades of emery paper. During the grinding the length was adjusted to vary not more than ± 0.1 cm. A hole of 0.5 cm in diameter was drilled at the centre of one end of the specimen to fit in one end of a mullite extension tube (10 A material tube supplied by Andermann Limited, London) by push-fit. Those specimens whose extension tube was not central were rejected.

The preweighed specimen held by its extension tube was mounted in a 3-jaw chuck which allowed adjustment of the extension tube so that the specimen ran true. The chuck was driven by a variable speed motor; the speed of this was measured by a cyclometer.

The melt of 200 gm was contained in a platinum crucible. The temperature of the furnace was controlled by a thermocouple placed near the windings by on-off controller. The melt temperature was measured by a separate platinum-rhodium thermocouple dipping into the melt and left at the same spot. As the oxidation of carbon is a strongly exothermic reaction, usually 5 - 8°C rise of temperature was observed. Reaction temperature was taken from measurements made during the run rather than the pre-set temperature.

The carbon specimen, preheated up to about 400°C, was brought down into the middle of the melt without allowing it to reach thermal equilibrium with the melt, to avoid weight losses by oxidation in air; similarly, the oxidized specimen was removed directly from the melt to

the cooler part of the furnace tube, below 400°C. Immediately after the specimen was immersed into the melt, a microswitch started the motor on its preset speed.

Melt adhering to the carbon specimen was leached off in warm water followed by diluted hydrochloric acid solution before being dried and weighed to a constant weight. The surface area of the specimen was determined by measuring with a micrometer screw gauge.

For the stagnent experiment, the specimen cut from a 'CY9' carbon rod of about 3 cm in diameter was used. The rod was cut into pieces of about 3 - 4 mm thick and these discs were cut in the middle to form two half-moon shapes to be fitted in two rings of the platinum holder previously used by Faruqi (32). The specimen held in the platinum holder supported by an extension refractory tube was vertically immersed into the melt for the predetermined time. The apparatus and other experimental technqiues were the same as those described above.

To follow the reaction products of carbon oxidation, a gas chromatograph in conjunction with the apparatus described in the Chapter 4 was used. The carbon specimens were prepared in the same way as for the stagnent experiment described above.

The atmosphere above the melt was exposed to air except for the measurement of the reaction products for which the atmosphere was nitrogen.

5.4. Discussion of results

The combustion rate of carbon in the melts together with the oxidation rate in air, is listed in Table 5.1. with the viscosities of the respective melts. As can be noted, it is shown that the lower the viscosity, the higher the rate of oxidation as far as those melts are concerned, the rates being $NaVO_3 > Na_2B_4O_7 > Na_2Si_2O_5$.

As the melts are ionic in nature, the oxygen should be carried to the carbon surface as anion complexes. If the transport of reactant to

the carbon surface in a melt phase was controlling the rate process, the apparent energy of activation for combustion should then be closely related to the energy of activation for viscous flow. However, the E values for combutstion (E_K) does not correlate the E_η values of melts as is shown in Table 5.1. It suggests that the explanation given above does not seem to be valid.

Table 5.1.

Oxidant	Combustion rate ($gm/cm^2/hr$) 1,000°C	Viscosity (poise) 1,000°C	900°C	Refs.
$NaVO_3$	'0.1060' (N_2 over melt)	0.066	0.089	(41)
	0.1653 (air over melt)			
$Na_2B_4O_7$	0.0037 (air over melt)	-	'2.0'	(87)
$Na_2Si_2O_5$	'0.0007' (air over melt)	'1.097'	-	(9)
Air	0.4110 (17.5 cc/s)			

	E_K (Kcal/mol)	E_η (Kcal/mol)	
$NaVO_3$	22 (973 - 1,273°K)	9	(41)
$Na_2B_4O_7$	23 (1,073 - 1,343°K)	56	(87)
$Na_2Si_2O_5$	24 (1,423 - 1,573°K)	38	(9)
Air	31 (below 1,000°K)		
	4 (above 1,000°K)		

' ' : by extrapolation

On examining the weight loss/unit area versus time curves for sodium borate melt illustrated in figure 5.3., it can be first seen that the carbon begins to oxidize about 900°C. This was observed earlier by Khundkar (54), who studied the reduction of the melt by carbon powder.

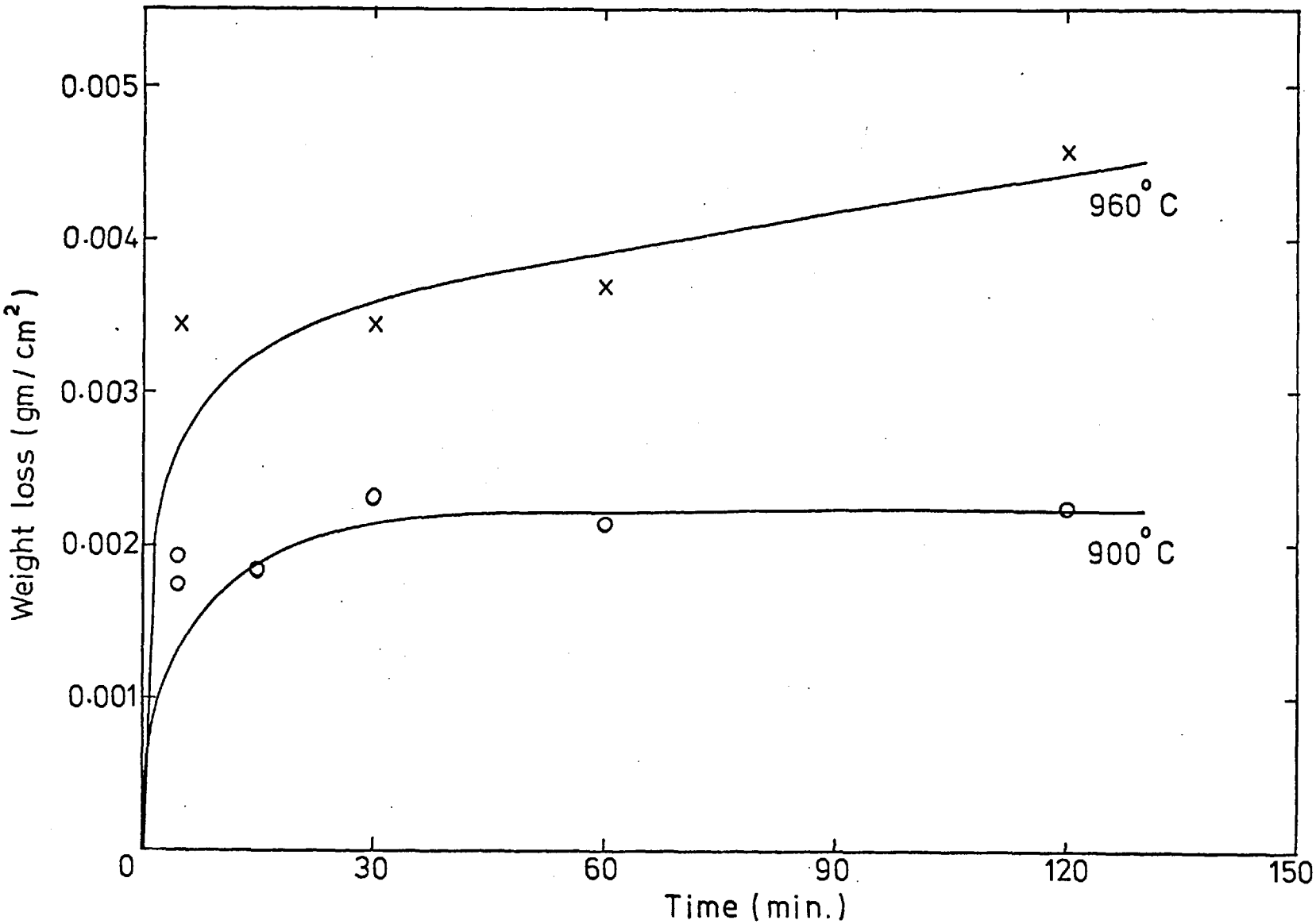

Figure 53. Weight loss v. time plot for carbon oxidizing in sodium tetraborate.

The curve at 960°C shows a parabolic section that could be taken as an indication of a transport controlled process. If, however, the transport control was operative, it could be considered in two aspects:-

1) gas phase transport control

2) liquid phase transport control.

In view of the fact that the reaction products are gases, one could raise the question of whether gas phase diffusion can be rate controlling. However, the value of apparent activation energy of 23 Kcal/mol compared with the value of 4 Kcal/mol for gas phase diffusion makes this highly unlikely. As already mentioned in the section 5.2.2., the formation of a carbonate anion rich boundary layer could be expected considering the reaction products are CO and CO_2. However, again, the results of the rotating disc experiment disproved the suggestion as shown in figure 5.4. The higher initial oxidation rate, shown in the figure 5.3., could be explained in terms of oxidation of carbon by air trapped in the pores of the specimen and dissolved oxygen in the melt, and oxidation while the specimen was released out of the melt.

The result of the rotating disc experiment show a decrease of oxidation rate with increasing rotation speed (see figure 5.4.). This is a direct confirmation of the similar observation made by Shurygin et al. (88) who studied the reduction of FeO - containing melt by solid carbon and Chumarev et al. (17) from their study of the reaction between carbon and ZnO containing slag. Both authors offer the same explanation i.e. that the increasing rotation speed decreases the bubble life at the interface. It seems to imply that secondary oxidation of carbon by CO_2 in the bubble may be predominent and rate-controlling.

Turning now to the weight loss/unit area versus time plot for the oxidation of carbon in sodium vanadate melt shown in figure 5.5., a straight line relationship indicates a typical example of a reaction - controlled process. It seems to agree with the near independence of the

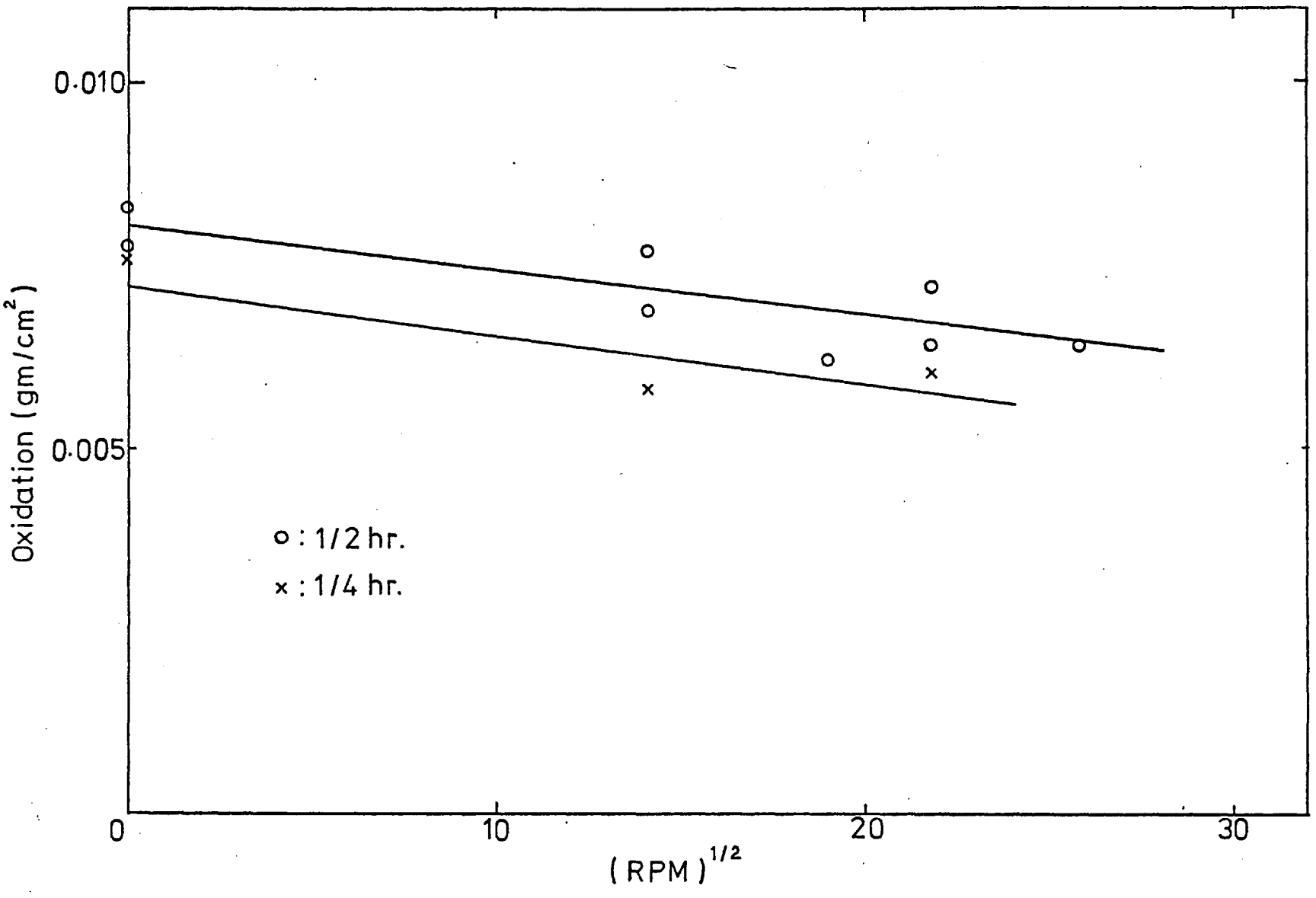

Figure 5.4. Square root of rotation speed v. weight loss of carbon in sodium tetraborate at 890°C.

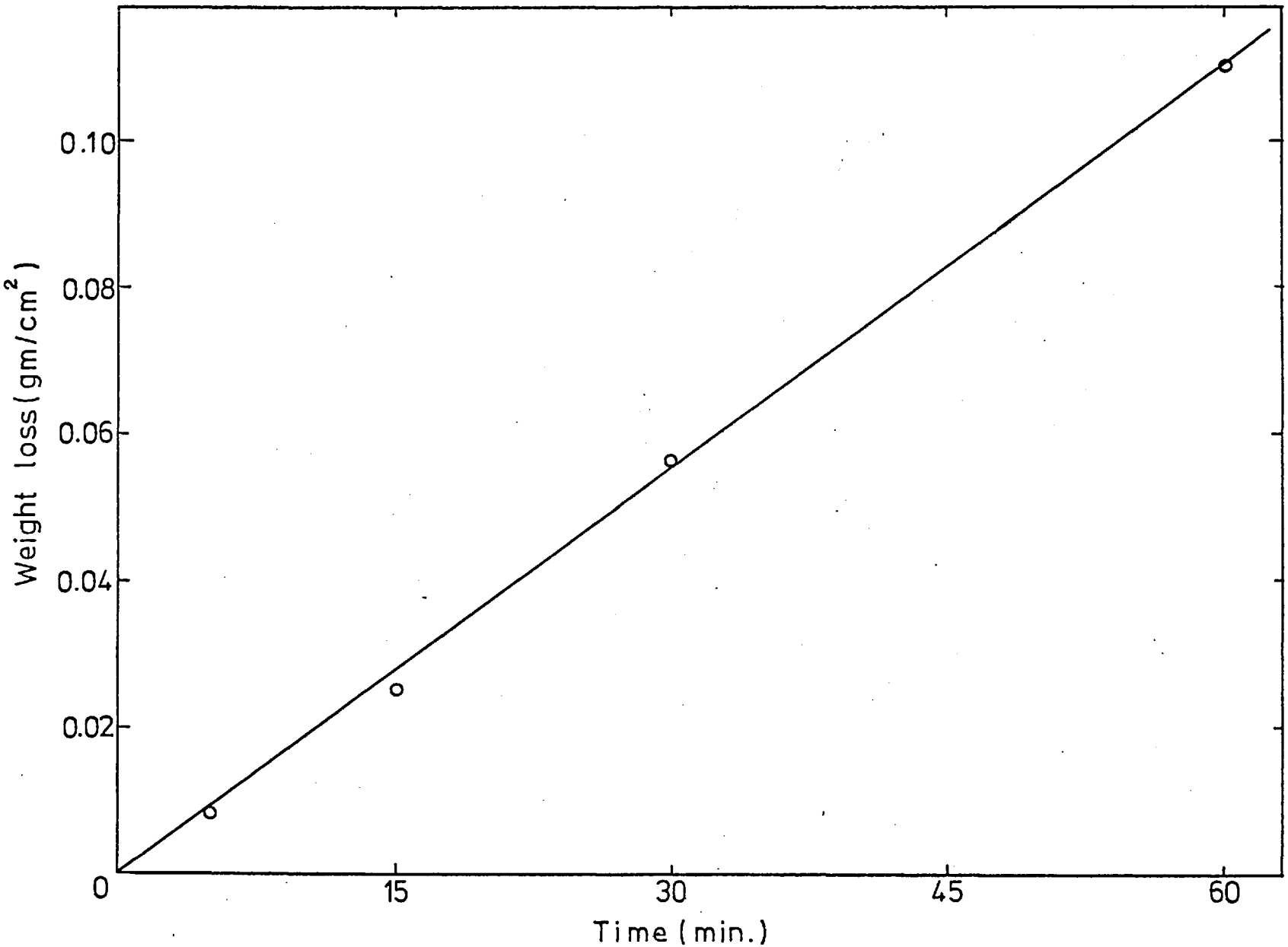

Figure 5.5. Weight loss v. time plot for carbon oxidizing in sodium metavanadate at 900°C.

of oxidation on the rotation speed as shown in figure 5.6. Therefore, again, the possible formation of a carbonate rich boundary layer does not seem to be the rate controlling process. And neither can gas phase transport control be considered the case for the same reasoning as in sodium borate melt.

While the discussion in the above paragraph seems to support a reaction controlled process, it should be pointed out that a different rate of oxidation with air or nitrogen atmosphere above the melt, shown in the figure 5.2. is indicative of a transport controlled process. This is the analogue of the oxidation mechanism in air by transport controlled process where the oxygen pressure and air velocity made the rate different. And unlike the observation made on dependence of rate of carbon oxidation on the rotation speed in sodium borate melt, a slight tendency in sodium vanadate for increase of oxidation rate with increasing rotation speed could be taken as an indication that the gasification of carbon by CO_2 may not be significant. The predominent reaction product, CO_2, as shown in figure 5.7., of the oxidation seem to support this remark.

Although no further work was carried out in sodium disilcate melt the ratio of CO/CO_2 (the reaction products) was followed in the temperature range 1,300 to 1,400°C. The results are also plotted in figure 5.7. in comparison with those obtained by Chumarev et al. (18). As can be seen, the results are in good agreement and follow the general finding in air that the CO/CO_2 ratio increases with increasing temperature.

An effort was made to throw light on the oxidation state of reduced melts by electron spectroscopy for chemical analysis (ESCA) without much success. As would be expected, this was because the surface of the melts oxidized in the ambient atmosphere and the instrument was only capable of detecting 50 Å in depth from the surface.

As the foregoing discussions have shown, it is not possible to draw unequivocal conclusions with respect to the rate controlling process

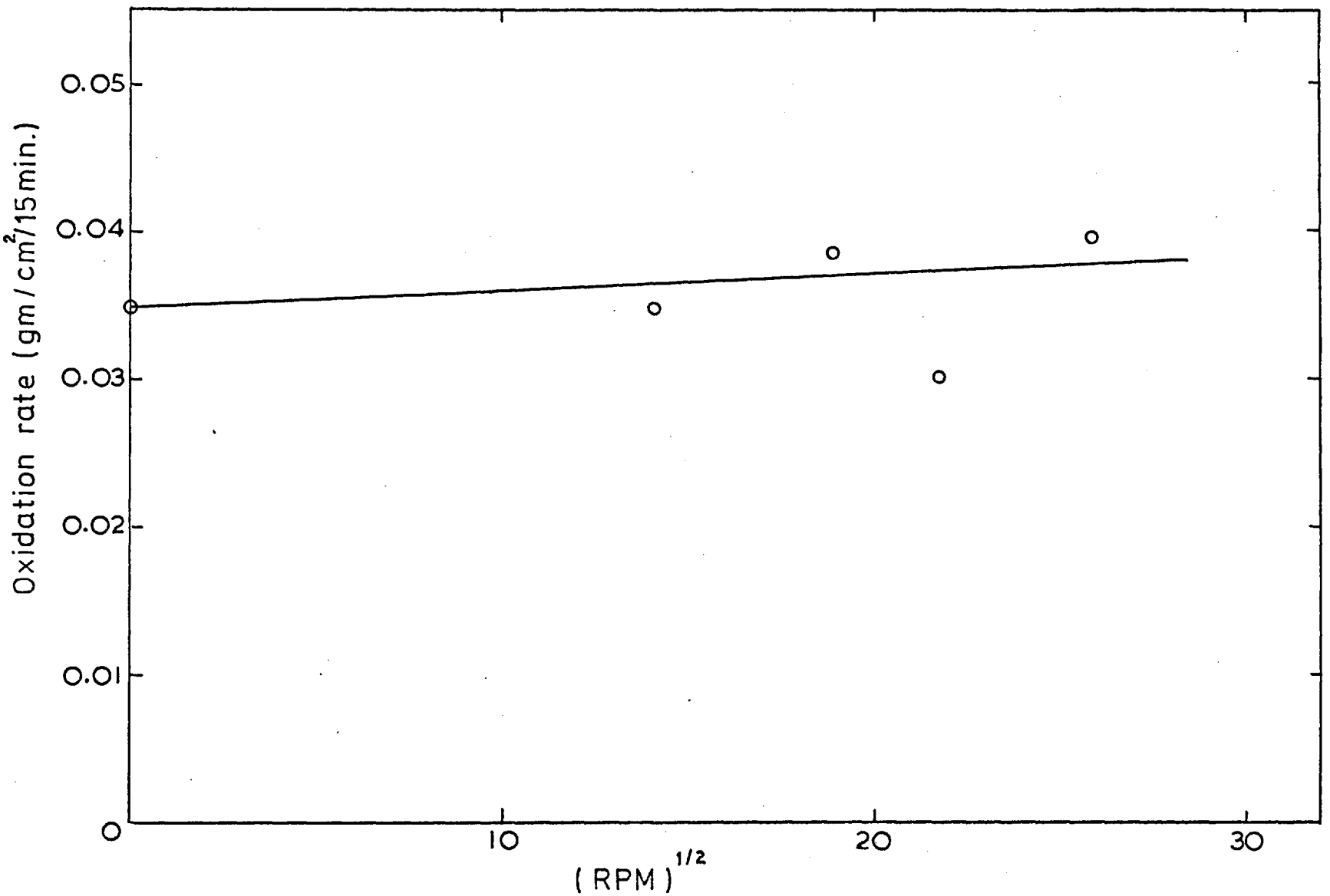

Figure 5.6. Square root of rotation speed v. weight loss of carbon in sodium metavanadate at 895°C.

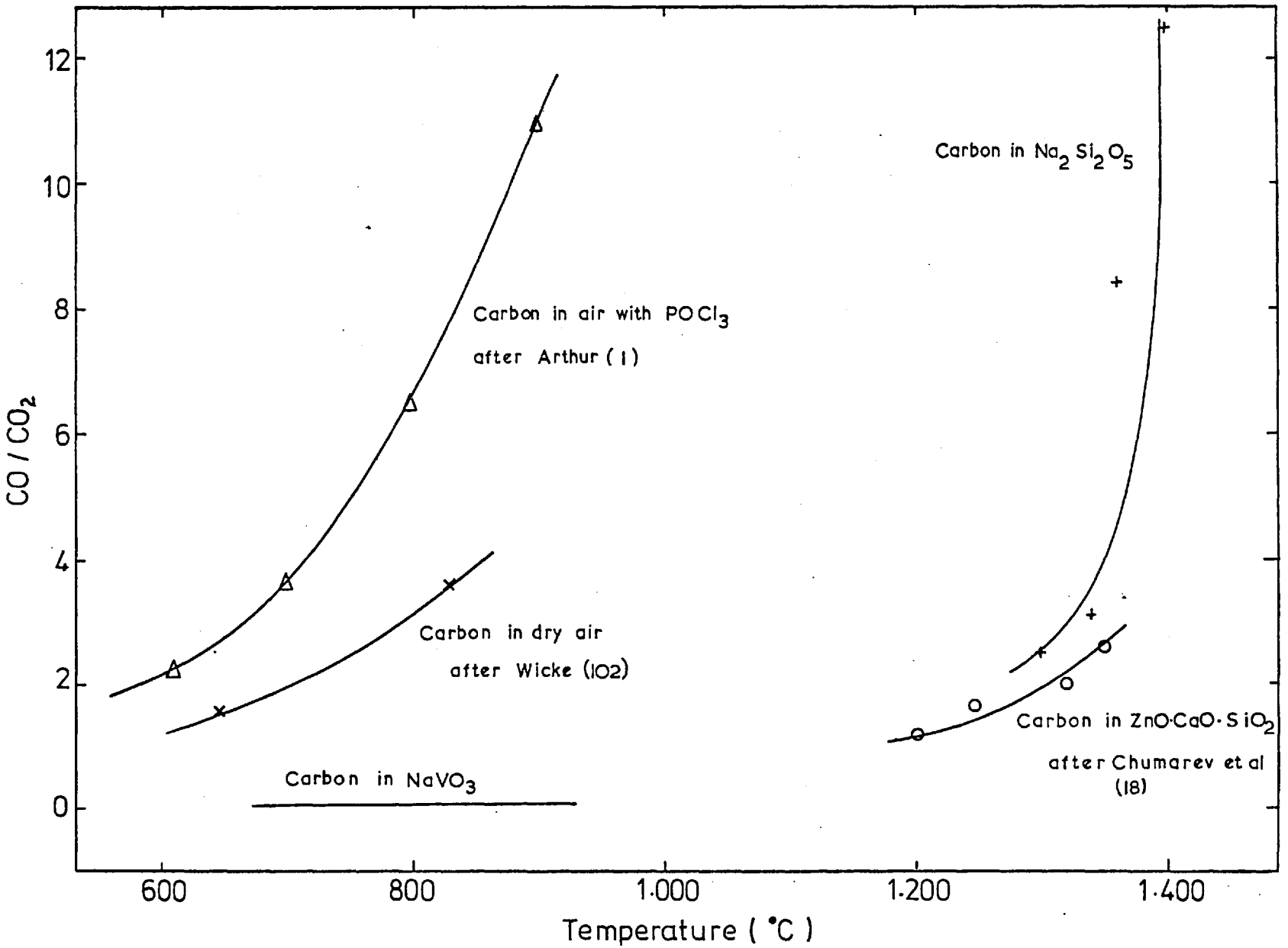

Figure 5.7. The CO/CO_2 ratio as a function of temperature.

in the oxidation of carbon in vanadate melt, as determined in this investigation. Further work should be directed to understand other important parameters affecting rate process such as gas bubble generation and detachment from the carbon surface which are essential features of the reaction.

CHAPTER 6

STUDIES OF REFRACTORY - MELT INTERFACES BY ELECTRON MICROPROBE ANALYSER

6.1. Introduction

6.2. Experimental

6.2.1. Sample preparation

6.2.2. Electron microprobe analyser

6.3. Examination of interfaces

6.3.1. Alumina - melt interfaces

6.3.2. Magnesia - melt interfaces

CHAPTER 6

STUDIES OF REFRACTORY-MELT INTERFACES BY ELECTRON MICROPROBE ANALYSER

6.1. Introduction

It is now well established that dissolution at refractory-melt interfaces is by the following processes:-

1) diffusion (or transport) control

2) chemical (or surface) control.

One of the significant differences in these two dissolution processes is the existence of a solute rich diffusion layer when a refractory corrodes in a melt by a diffusion controlled process. A typical example of an experimental result is best shown, when weight loss/unit area of refractory is plotted against time, as a parabolic curve that indicates the formation of a diffusion layer. Once the layer is set up in the steady state, the dissolution process is controlled by the diffusion of reactant to, or the product away from the interface through the diffusion layer. Under forced convection normally achieved by rotating either the rods(75) or the discs (21) of refractory, the rate of dissolution is increased with the speed of rotation.

When a refractory dissolves in a liquid by a chemically controlled process, there would be no build up of a diffusion layer. This situation arises when the diffusivity of reaction products is faster than the rate of the chemical reaction at the interface. The corrosion process is then controlled directly by the reaction at the interface of refractory-melt. In this instance, the plot of weight loss/unit area of refractory versus time shows a straight line relationship. Furthermore, the corrosion rate of the refractory would not increase under forced convection.

During the course of the present studies, the interfaces between refractory and melt were subjected to electron microprobe

analysis (EPMA) in order to investigate:-

1) the distribution of corrosion product in the melt

2) the penetration of the melt into the refractory.

6.2. Experimental

6.2.1. Sample preparation

All the specimens for the EPMA studies were specially prepared by a technique known as the crucible test which has long been used for a slag test. This test, mainly of a practical nature, provides information regarding the corrosion and penetration of the slag into the crucible.

The crucibles used were cylindrical shaped fully sintered alumina and magnesia supplied by Morgan Refractories Limited and Thermal Syndicate Limited respectively. The relatively low-melting melts sodium borate and sodium vanadate were kept in alumina crucibles at 900°C for two hours. The corrosion temperature for the sodium silicate melt was raised to 1,300°C for the same period of time. Knowing that magnesia was of relatively higher solubility than alumina from a prior investigation by Barham (2), the corrosion time for magnesia crucibles was reduced to one hour.

After the heat treatment, the melts were quenched at room temperature by taking the crucibles out of the furnace. The crucibles with solidified melts were cut horizontally by a diamond wheel before these were mounted in a plastic. The mounted samples were then ground and polished using SiC papers and diamond polish with 'White Spirit' as cutting fluid. The surface of the specimens was then vacuum sputtered with carbon to yield a conducting surface so as to avoid surface charging by the electrons.

6.2.2. Electron microprobe analyser

The electron microprobe analyser is a useful instrument for

investigating microvolumes of a solid to reveal the distribution of chemical elements present. The instrument is also useful for examining surface features of solids pictorially from the images formed on a cathode-ray tube by a scanning electron beam. It offers information for identifying the phases, studying the textures of ceramics in general and for following change of chemical composition due to the reactions occuring. An article by Ruddlesden (82) covers the capabilities and limitations of the instrument for studying ceramic materials.

The analysis is carried out by an electron beam of about 1 μm diameter which strikes the conducting surface of the specimen. This produces emission of characteristic X-rays of the elements present in the specimen. The intensities of emitted X-rays are analysed by X-ray spectrometers that employ suitable crystals for diffracting X-rays according to Bragg's equation.

Among the capabilities of EPMA most useful information on the refractory - melt interface is drawn when the concentration of the elements is followed graphically by traversing the probe across the interface. Quantitative analysis of the solute concentration - distance relationships in the diffusion layer can be made from the trace, based on the assumption that the intensities of X-rays are approximately proportional to the concentrations of the elements to be determined.

In addition to the study by graphical traces of X-rays, pictorial study of images formed on a cathode-ray tube as a result of the electron beam scanning a specimen was also carried out. These are:-

1) X-ray emission image

   The X-ray image is produced in the form of dots when the X-ray spectrometer output is applied to the cathode-ray tube. The density of dots is proportional to the concentration of the element concerned.

2) Back-scattered and absorbed electron images

   These images are formed when the electrons in the beam

back-scattered or absorbed by the specimens, are collected and displayed on the screen. The contrast of both images is dependent on atomic number variation in the specimen. As the intensity of back-scatterd electrons is strong with high atomic numbered elements, the area where heavy elements are present is shown bright. An absorbed electron image shows the area where heavy elements are present as darker. These images were useful in locating the area for X-ray trace analysis as it gives an overall picture of the interface.

The electron probe microanalyser used was a JEOL JXA-3A manufactured in Japan.

6.3. Examination of interfaces

6.3.1. Alumina - melt interfaces

Alumina - $NaVO_3$

Photographs of X-ray images of Al, V and Na at the alumina - $NaVO_3$ interface are shown in figure 6.1. together with the electron image of the same area. At first sight, it can be seen from the X-ray dot pictures that V ions along with Na ions penetrated the pores and grain boundaries of polycrystalline alumina. This supports earlier observations made by Safdar (83) and Park (69) on similarly treated alumina test pieces. Both authors have found in a separate research that the corroded polycrystalline alumina was discoloured and the penetrated melt could not be leached out completely with a suitable acid.

Evidence of vanadium ion penetration into a refractory have also been reported earlier in the literature. Lambertson (56) found vanadium pentoxide penetrated evenly throughout a slagged high alumina fireclay brick from a naval boiler burning fuel oil. Pask and Parmelee (70) reported that vanadium ions from a V_2O_5 melt diffused into a commercial flint glass. Two types of diffusion were considered to take place into glass from a melt by these workers:

Figure 6.1. Electron microprobe photographs of alumina - sodium metavandate interface (left to right)

(a) BEI (Comp) of the interface (160μm across) - the melt is shown as light area

BEI (Topo) of the interface

(b) X-ray dot picture of vanadium at the interface

X-ray dot picture of sodium at the interface

(c) X-ray dot picture of aluminium at the interface

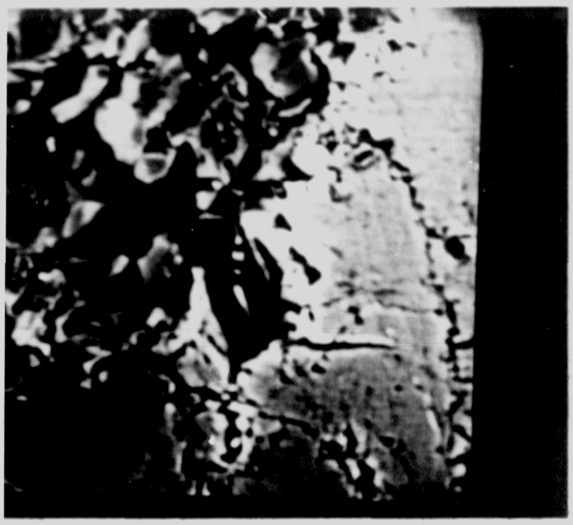

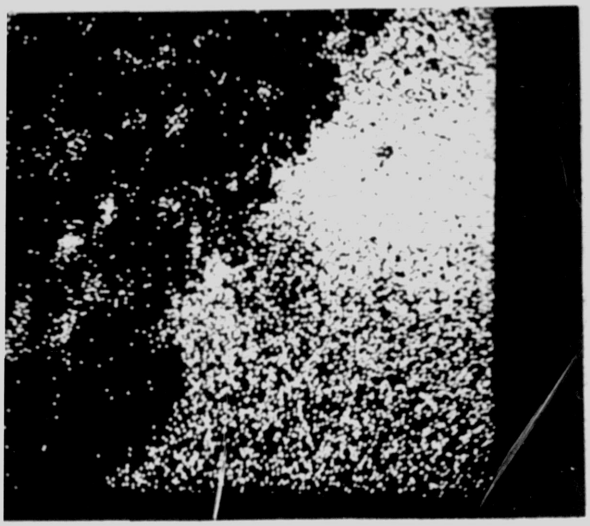

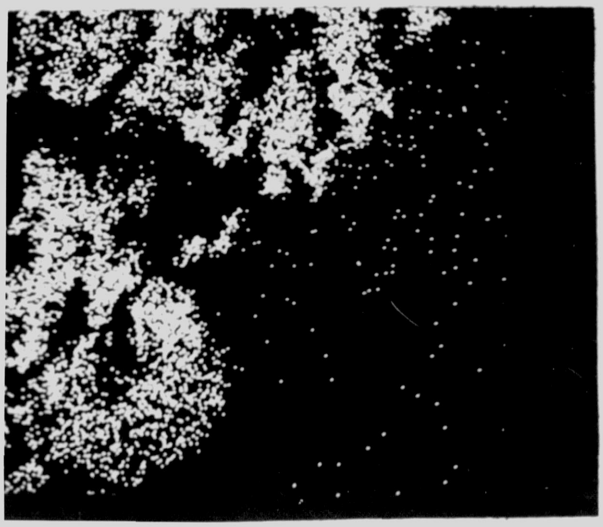

1) replacement of alkali ions within the glass with cations from a melt if both ions are present in a glass and a melt

2) penetration of diffusing particles into the 'holes of the glass' if the glass is thermally treated to provide the passage for the particles.

In his study Goldman (38) concluded that no ionic penetration was present when transparent refractories - sapphire and silica glass - were subjected to V_2O_5 melt. Evidence for the assumption was that the refractories were not discoloured even though vanadium ion is a strong colouring agent. Later, Haxell (41) confirmed that no penetration was observed on both refractories corroded in V_2O_5 melt at around 1,000°C by the EPMA scan. It is most likely that the finding by Pask and Parmelee (70) occurs with a glass containing alkali ions by the combination of both types of diffusion mentioned above, but not with silica glass where ion exchange is not possible and diffusion is only possible via 'holes'.

Safdar (83) even suspected ionic penetration may occur into single crystal alumina from the evidence of density increase of corroded sapphire specimens measured by a mercury balance. However, as found by Haxell, present evidence does not support this hypothesis. Neither vanadium nor sodium ions were detected by an electron-probe in the corroded sapphire specimen. To check the density increase of corroded sapphire specimen observed by Safdar, the measurements were repeated by the author and the results are tabulated in table 6.1. together with those obtained by Safdar. During the corrosion experiment, an enhanced corrosion due to metal contact (76) was avoided by hanging the sapphire specimen from a sintered alumina tube placed horizontally through the pre-drilled hole on the specimens, because an enhanced corrosion evidenced by 'pitting' on the surface was suspected to be a source of air bubbles during the measurement. Air bubbles included in the volume of the specimens under mercury will obviously introduce errors. The assembly was hung by a platinum wire passing through the supporting alumina tube

and lowered into melts as such.

Table 6.1.

Density of sapphire before and after corrosion

Melt	Temperature °C	Density of Sapphire (gm/cm^3)			
		Safdar		Author*	
		before corrosion	after corrosion	before corrosion	after corrosion
$NaVO_3$	900	-	-	3,984	3,982
	900	-	-	3,978	3,983
80%$NaVO_3$ /	800	3,922	3,939	-	-
20%Na_2SiO_3	900	3,922	3,953	-	-
	1,000	3,922	3,968	-	-
$Na_2B_4O_7$	800	3,922	3,957	-	-
	900	3,922	3,962	3,977	3,990
	900	-	-	3,974	3,980
	1,000	3,922	3,966		

* Density of mercury was taken as 13.541 at 22°C from the data collected by Bigg (6).

The density increases obtained by Safdar amount to an average of 0.91% whereas the present measurements indicate an average value of 0.14%. It may be noticed that the density increase of specimens corroded in sodium borate was more significant from the present results. This is most likely due to the surface effect of specimens during the measurement rather than ionic penetration. The difference in transparency of the specimens, shown in figure 6.2., seems to bear this out. As reported by Faktor, Fiddyment and Newns (31) that corroded corundum surfaces were chemically polished in V_2O_5 melt, so the surfaces of sapphire were polished in sodium borate melt where diffusion control is also operative. However, when chemical control is present such as sapphire in sodium vanadate melt, it was shown (83) that surface feature such as ledge formation was revealed. This leaves the surface less transparent.

Figure 6.2. Top, sapphire specimen as cut by diamond wheel

Middle, sapphire specimen corroded in $NaVO_3$ melt for an hour at 900°C

Bottom, Sapphire specimen corroded in $Na_2B_4O_7$ melt for an hour at 900°C

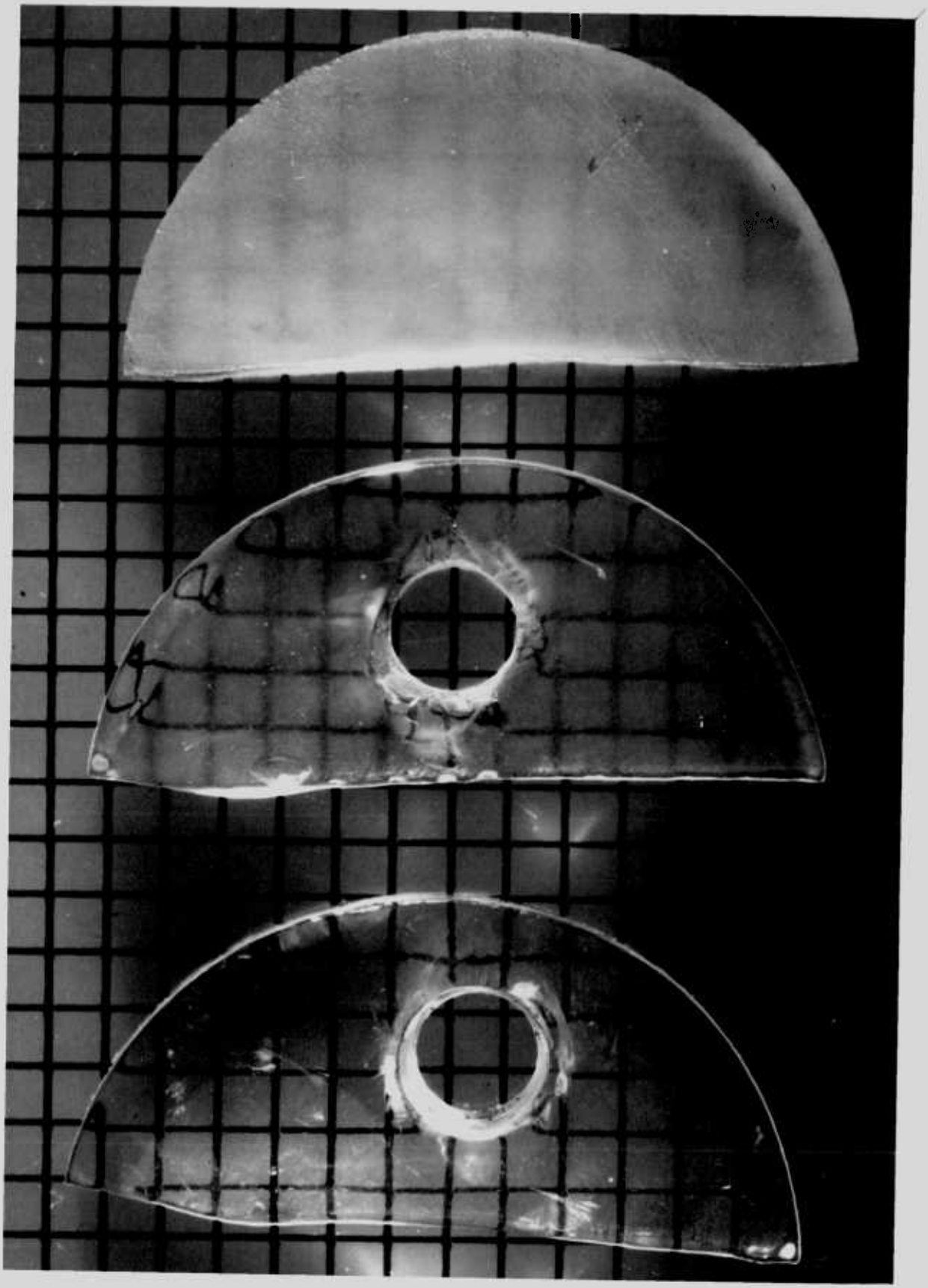

From the evidence obtained by electron probe studies, it could be concluded that penetration of ions takes place into polycrystalline alumina from a vanadium containing melt. This may be achieved through the grain boundaries where rapid diffusion paths are available for the diffusing ions. The diffusing units are expected to include vanadium and sodium cations and oxygen anions as these ions are small in size; mixing of melts with grain boundary impurities is a possibility to be borne in mind.

X-ray traces of two elements, one from a melt and the other one from a refractory, across the interfaces were followed on a chart recorder to obtain concentration of elements-distance relationship. An absorbed electron (AEC) trace was simultaneously recorded to identify a hole or crack in the specimen. These are indicated by a considerable increase in AEC together with fall of X-ray traces of elements. Reproduced recorder trace of aluminium and vanadium from an interface of polycrystalline alumina - $NaVO_3$, shown on figure 6.3., confirms the corrosion process was by chemical control as postulated by Faruqi (32). As can be seen, the concentration of aluminium falls off sharply with an increase of vanadium concentration. It does not show the existence of a solute rich boundary layer. Also to be noticed from the figure is penetration of vanadium into the pores and grain boundaries as discussed above.

Alumina - Sodium silicate

The dissolution of alumina in sodium silicate melt was studied by a number of workers (74)(32)(2) who concluded with an agreement that a diffusion controlled process was operative. The present electron-probe study of the interface confirms these earlier conclusions and shows clearly the existence of a solute rich boundary layer as shown in figure 6.4. It is to be noticed from the figure that concentration of aluminium is dropping off exponentially with distance away from the refractory

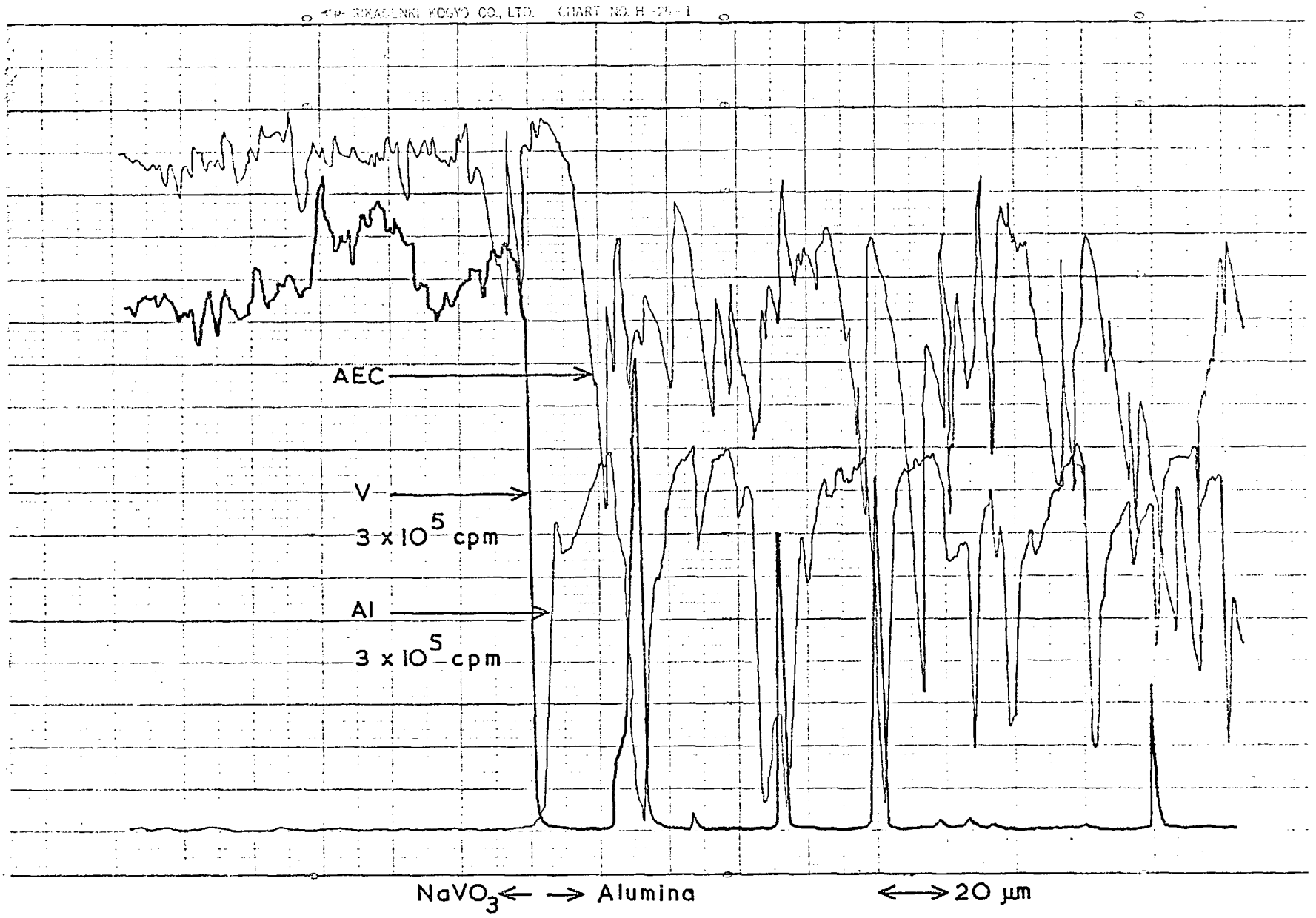

Figure 6.3. Electron microprobe trace of Al and V across the polycrystalline alumina–sodium metavanadate interface.

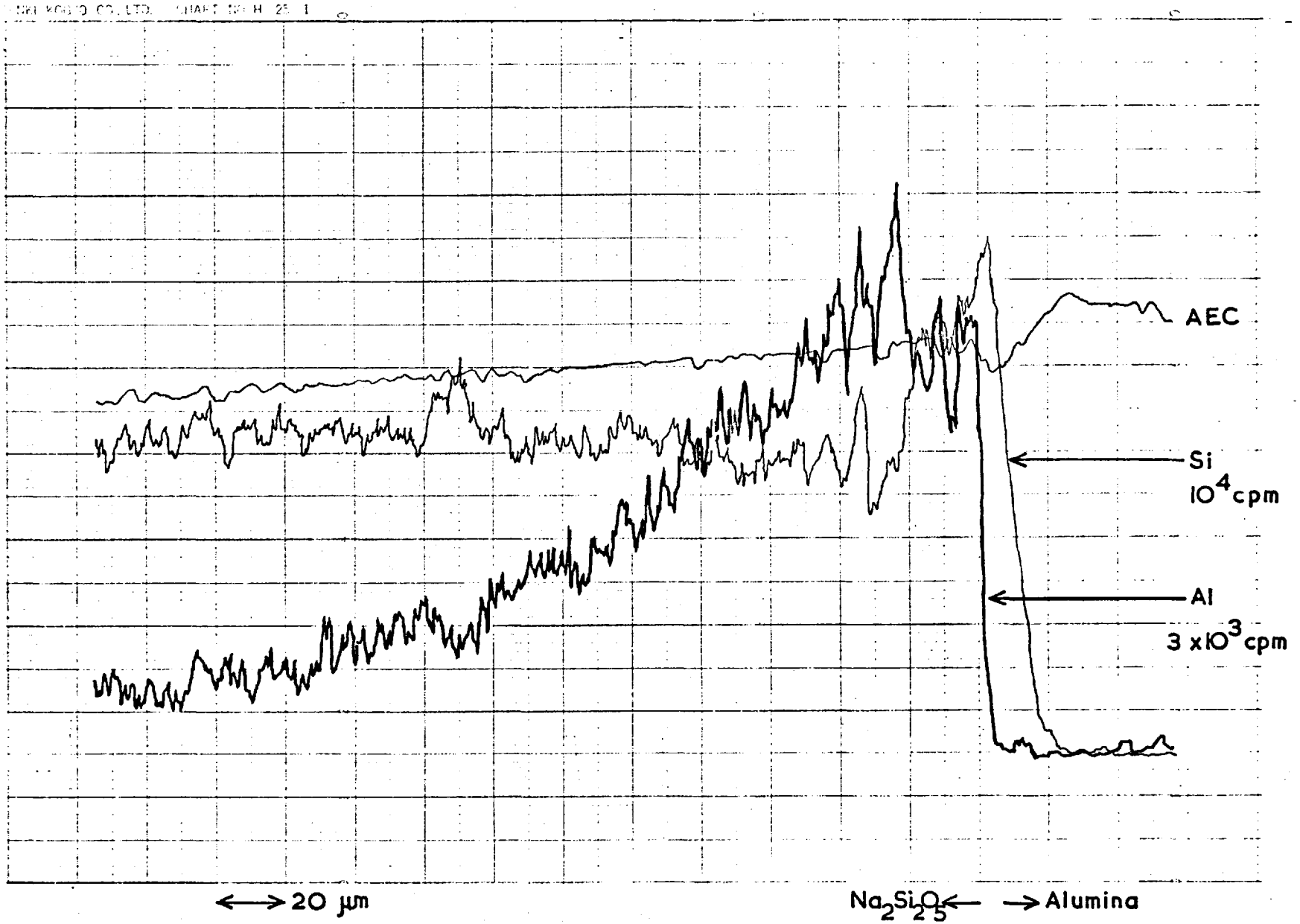

Figure 6.4. Electron microprobe trace of Al and Si across the polycrystalline alumina-sodium disilicate interface.

surface and then levelling off to a constant lower level. An approximate quantitative analysis of aluminium concentration was carried out, with the help of Mr. P.R. Monk of Analytical Services Laboratory of the College, by standardising aluminium against alumina (ruby). Taking aluminium as 53% of alumina, then the aluminium concentrations at various points were estimated and tabulated in table 6.2. together with those of $Na_2B_4O_7$ melt.

Table 6.2.

Concentration of aluminium variation in the diffusion layer

	$Na_2Si_2O_5$ 1,300°C	$Na_2B_4O_7$ 900°C
Distance µm	Al Wt. %	Al Wt. %
0	12.5	19.3
40	7.3	12.2
80	4.7	9.7
120	3.4	8.6
160	2.2	5.9
200	1.7	3.8
240	1.3	3.2
280	-	2.1

The thickness of the diffusion layer (δ) formed in sodium tetraborate and sodium silicate melt were shown, in figures 6.4 and 6.5., to be about 220 and 200 µm respectively. It is of interest to compare these values with calculated values of the Nernst diffusion layer (δ) as expressed by Reed and Barrett (76),

$$\delta = \frac{2Q_o}{(C_s - C_o)\rho}$$

where , Q_o : dissolution of refractory (gm/cm^2) during the time taken to build up the diffusion layer

C_s : saturated concentration (gm/gm)

C_o : bulk concentration (gm/gm)

ρ : density of melt (gm/ml)

The necessary experimental data were extracted from earlier works as referenced and the calculated values are listed in table 6.3. with those of the observed values. The values of effective diffusion layer thickness (δ^*) were determined by extending the tangent to the concentration profile (20) as shown in figure 6.9. These are also tabulated in table 6.3. Owing to the errors involved in the determination of oxide in both the bulk concentration and the boundary layer, need for a rule to determine the edge of the boundary layer does not arise.

Table 6.3.

Comparison of the boundary layer thicknesses

		$Na_2Si_2O_5$	Na_2SiO_3	$Na_2B_4O_7$
Temperature (^oC)		1,300	1,330	900
Q_o (gm/cm^2)		0.0039(32)	0.0038(2)	0.0074(69)
C_s (gm/gm)	obtained	0.263 (60)	0.0250(60)	-
	observed	0.236	-	0.364
ρ (gm/ml)		2.221 (42)	2.153 (2)	2.048 (69)
δ (cm)	calculated	0.013	0.014	-
δ (cm)	observed	0.020	-	0.022
δ^* (cm)	effective	0.0085	-	0.010

The values of C_s of alumina in sodium silicate were taken from $Na_2O \cdot SiO_2 - Al_2O_3$ diagram, shown in figure 6.10., constructed from the $Na_2O - Al_2O_3 - SiO_2$ ternary phase diagram (60) by reading off melting points of compositions from the alumina corner to an appropriate $Na_2O \cdot SiO_2$ composition. The saturated concentration of alumina in $Na_2B_4O_7$ could not be obtained as $Na_2O - Al_2O_3 - B_2O_3$ phase diagram is not yet available.

From the table, it can be seen the value of C_s observed by EPMA in sodium disilicate is in good agreement with the value of C_s obtained from the figure 6.10. This fact confirms an earlier assumption by Reed (74) that a melt at the interface is saturated with refractory where

diffusion control is operative. Also to be noticed is the calculated value of δ is of the same order of magnitude as the value obtained by EPMA.

Having obtained the thicknesses of the boundary layer by EPMA, mean convection diffusion coefficents of Al_2O_3 in sodium silicate melt were calculated using the Nernst-Brunner equation,

$$K = D(\text{or } D^*) \frac{(C_s - C_o)\rho}{\delta(\text{or } \delta^*)}$$

where. K : steady state corrosion rate ($gm/cm^2/sec$)

D : mean convective diffusion coefficient (cm/sec)

D* : D calculated based on δ^* (cm/sec)

C_s : saturated concentration (gm/gm)

C_o : bulk concentration (gm/gm)

ρ : density of the melt (gm/ml)

δ : diffusion layer (cm)

δ^* : effective diffusion layer (cm)

Data used for the calculation were tabulated in table 6.4. together with the calculated diffusion coefficients. During the calculation assumptions were made as follows.

1) δ may not alter over the temperature range of 100°C. This assumption is based on Barham's calculated value of δ which was shown to be constant above 1,300°C

2) the same δ for sodium disilicate could be taken for sodium sodium metasilicate. In fact the calculated values of δ were quite close to each other as shown in the table 6.3.

Table 6.4.

Calculated values of the mean convective diffusion coefficient for alumina

		K gm/cm^2/sec x10^{-6}	ρ gm/ml	C_s gm/gm	D cm^2/sec x10^{-8}	D* cm^2/sec x10^{-8}
$Na_2O \cdot 2SiO_2$	1,250°C	0.44	2.232	0.250	1.59	0.68
	1,300°C	0.62	2.221	0.259	2.16	0.92
	1,350°C	0.83	2.214	0.270	2.79	1.19
		(32)	(42)			
$Na_2O \cdot SiO_2$	1,300°C	2.00	2.163	0.243	7.61	3.23
	1,350°C	2.94	2.145	0.254	10.80	4.59
	1,400°C	4.25	2.130	0.264	15.10	6.42
		(2)	(2)			

The plot of calculated diffusion coefficients as a function of reciprocal of absolute temperature are shown in figure 6.11. together with reported diffusion coefficients for various species in sodium silicate melt. It is interesting to note that the apparent energy of activation (E_D) calculated from the slope of lines amounts to 30-39 Kcal/mol. indicating the fundamental process for alumina diffusion, in the melts of varying Na_2O : SiO_2 ratio, was similar.

Although calculated diffusion coefficients are not claimed to be very accurate because of assumptions made for the calculation and uncertainty in the data extracted from the literature, it does show a higher diffusivity of Al_2O_3 in sodium metasilicate than sodium disilicate at a given temperature. In view of the fact that the former melt is less viscous than the latter at the same temperature (see figure 6.12.), one would expect higher diffusivities in the former melt considering the Stokes-Einstein equation relating diffusivity and viscosity (η),

$$D = \frac{kT}{6\pi r\eta}$$

where, D : diffusion coefficient (cm^2/sec)

k : Boltzmann's constant

r : radius of diffusing species (cm)

η : viscosity (gm/cm.sec)

The apparent energy of activation for alumina corrosion (E_K) in sodium disilicate and metasilicate are 40 Kcal/mol (32) and 39 Kcal/mol (2) respectively. These values are similar to the activation energy for viscous flow of sodium silicate and sodium silicate with varying alumina concentration up to saturated melt composition. A plot of log η of the melts, obtained from the literature as referenced, against the reciprocal of the absolute temperature is shown on figure 6.12. The fact that log η is linear with 1/T indicate all melts obeyed the empirical relationship,

$$\eta = A\, e^{-E_\eta/RT}$$

E_η of the melts calculated using the slope of the lines all fall into 34 $\sim$ 40 Kcal/mol which are similar to the values of E_K quoted above. The fact that the values of E_η of sodium silicate and the sodium silicate saturated with alumina were similar, assuming the data were valid, may be taken as an indication that the fundamental flow process involved in these melts proceeded by a similar mechanism. Since viscous flow is known to be dependent upon movement of anions, it may be said in other words that the size of the flow limiting species were similar in these melts irrespective of alumina concentration following the 'discrete ion' theory postulated by Bockris, Mackenzie and Kitchener (9). These authors found in their study of viscous flow in binary liquid silicates that the addition of 10 mole percent of Na_2O to SiO_2 resulted in a drop in E_η from 140 Kcal/mol for pure SiO_2 to 50 Kcal/mol. Further addition of Na_2O up to 50 mole percent only lowered E_η to 32 Kcal/mol. The explanation given

by the authors for the high E_η for pure silica was that the flow process involved a sufficiently high energy to break Si-O bonds with a strength of 106 Kcal/mol (63). On the addition of metal oxide to silica, Si-O bonds break down to maintain homogenity in the melt with metal cations giving rise to the introduction of 'weak points'. As more metal oxide is added to silicate melt, more Si-O bonds are broken at random throughout the silicate three-dimensional lattice. These authors postulated a gradual decrease in the size of anions down to approximately 6 Å when the O/Si ratio reaches 3. The variation of E_η in sodium silicate as a function of composition is illustrated in figure 6.13. together with E_η for equivalent melts containing Al_2O_3 and E_D of alumina in sodium silicate melt.

In the absence of direct means of establishing diffusing species through the diffusion layer, it would not be without interest to speculate further based on remarks stated above. If similarity of E_η and E_D could be related to the dimensions of the diffusing species, it may be said that the dimensions of the diffusion controlling species was similar to that of anions of silicate melt containing 33 to 50 mol % Na_2O

Al_2O_3 - Sodium tetraborate

The corrosion of alumina in sodium tetraborate melt was studied previously (32)(83)(69) and it was agreed that a diffusion controlled process was operative. Evidence reported was:-

1) under natural convection, the corrosion increased parabolically as a function of time
2) under forced convection, the corrosion rate increased with rotation speed.

As a reproduced recorder trace of the interface shows in figure 6.5. the existence of a solute rich boundary layer further confirms the earlier conclusion.

The apparent energy of activation for the corrosion obtained from earlier work by the author (69) was 20 Kcal/mol which agreed well within

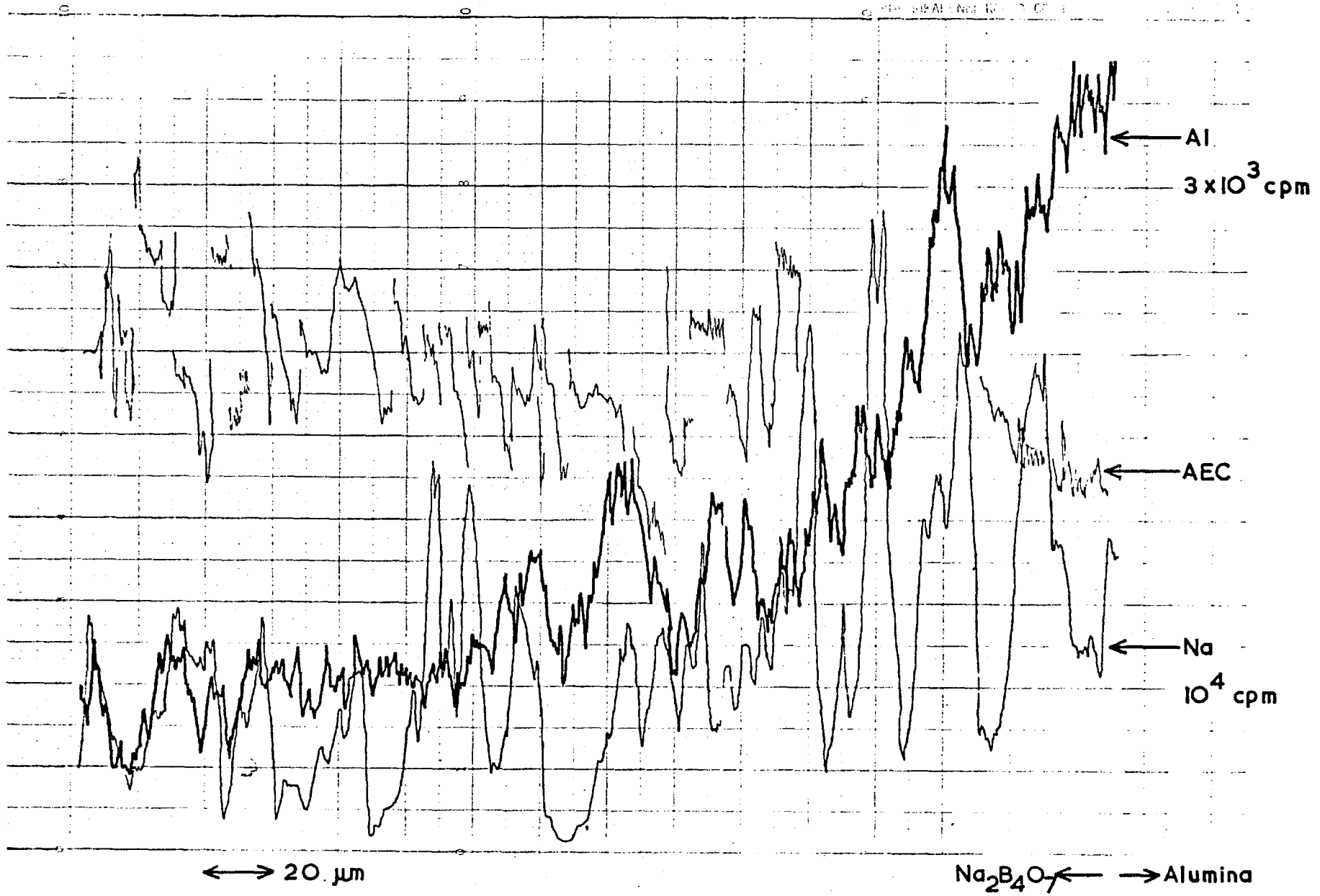

Figure 6.5. Electron microprobe trace of Al and Na across the polycrystalline alumina-sodium tetraborate interface.

experimental error with E_K value obtained by Safdar (83), 23 Kcal/mol.

Normally, it may be expected that anion complexes of reaction product, if the reaction product exists in ionic form, would control the dissolution process in silicate melts. In these instances E_K was either similar, as found by Barham (2) when alumina was corroded by sodium silicate or slightly bigger, as found by Reed (74) when alumina was corroded in calcium alumino-silicate melts, than E_η of the bulk melts.

However, the value of E_K, 20-23 Kcal/mol, in sodium borate melt does not relate to the value of E_η, 56 Kcal/mol (87) of the bulk melt, but is close to the value of E conduction (E_C), 20-22 Kcal/mol (62) of the bulk melt. From this similarity of the values of E_K and E_C, Safdar (83) concluded that the dissolution process may be controlled by the same mechanism as cationic movement. If the values of E_C and E_η were available for sodium tetraborate melt containing concentrations of alumina up to saturation and either one is similar to E_K, then one would expect the corrosion mechanism to be similar. However caution must be applied in dealing with borate melts as the melt is known to be more complex than silicate melts and a satisfactory model that will explain the structure is not yet available (63). Although both liquid borate and silicate containing metal oxide are ionic in nature, Mackenzie (63) states that the structure of binary liquid borate is grossly different from that of the silicate. In the binary liquid borate, E_η increases as metal oxide is added which is different from that of silicate melt as illustrated in figure 6.13. It has been thought that the temperature increases and the addition of metal oxide to B_2O_3 contribute to change BO_3 triangles to BO_4 tetrahedra. Richardson, F.D. (77) considered that this phenomenon may in part be the reason why E_η increases as metal oxide is added, because of the tendency mentioned above for boron to adopt a fourfold coordination with oxygen and for covalent B-O-B to be formed as cations become available to maintain the charge balance.

It is of interest to note that the rate of dissolution of alumina and mean convective diffusion coefficient of alumina diffusing in $Na_2B_4O_7$ melt at 900°C and in Na_2SiO_3 melt at 1,400°C were similar. The values are tabulated in table 6.5. together with the density and viscosity of the melts.

Table 6.5.

Comparison of the value of K and D in borate and silicate

Melt	Temp. °C	K gm/cm^2/hr	D cm^2/sec x 10^{-8}	η gm/cm.sec	ρ gm/ml
$Na_2B_4O_7$	900	0.0186	1.79	2.0 (87)	2.048
Na_2SiO_3	1,400	0.0153	1.51	1.8 (2)	2.130

Application of the Stokes-Einstein equation enables the average dimension of the diffusing species in these two melts to be compared. Although it is known (27) that the equation is not accurate enough to apply the diffusion data to calculate the radii of diffusing species in a glass, such comparisons are of interest as they allow one to speculate on the nature of the mean diffusing species. The value of viscosity needed is a mean value of the bulk melt and melt saturated with alumina for which data are not available at present. Therefore, the values of η of the bulk melt were used to compare the dimensions of diffusing species. For these reasons, absolute validity of the dimensions of diffusing species cannot be expected. Calculations were done as follows:

1. The size of diffusing species in borate melt at 900°C

The Stoke-Einstein equation was rearranged as

$$r = \frac{kT}{6\pi D\eta}$$

$$= \frac{1.38 \times 10^{-16} \times 1173}{6 \times \pi \times 1.79 \times 10^{-7} \times 2}$$

$$= 2.40 \times 10^{-8} \text{ cm}$$

2. The size of diffusing species in silicate melt at 1,400°C

$$r = \frac{kT}{6\pi D\eta}$$

$$= \frac{1.38 \times 10^{-16} \times 1673}{6 \times \pi \times 1.51 \times 10^{-7} \times 1.8}$$

$$= 4.51 \times 10^{-8} \text{ cm}$$

The ratio of radii calculated above is approximately 1 : 2 in borate and silicate melts. Going back to the previous section, it was postulated that the mechanism of dissolution of alumina in silicate melt was similar to the anionic movement in the silicate melt. The approximate linear dimension of silicate anions postulated by Mackenzie (63) was about 6-7 Å for $Na_2O \cdot SiO_2$. The dimension of diffusing species in borate melt would be about 3-4 Å using the above ratio. For comparison the radius of the sodium cation is 0.76 Å and the radius of an oxygen ion is 1.4 Å. Hence it is likely that the corrosion process is also associated with anionic movement.

6.3.2. Magnesia - melt interfaces

X-ray traces of magnesia - $Na_2B_4O_7$, $NaVO_3$ and $Na_2Si_2O_5$ interfaces are reproduced in figures 6.6. to 6.8. In contrast to the observation of vanadium ions penetration into the grain boundaries of polycrystalline alumina, no diffusion of vanadium ions into the matrix of polycrystalline magnesia was observed as the figure 6.7 shows.

Having been accustomed to the formation of rather thick boundary

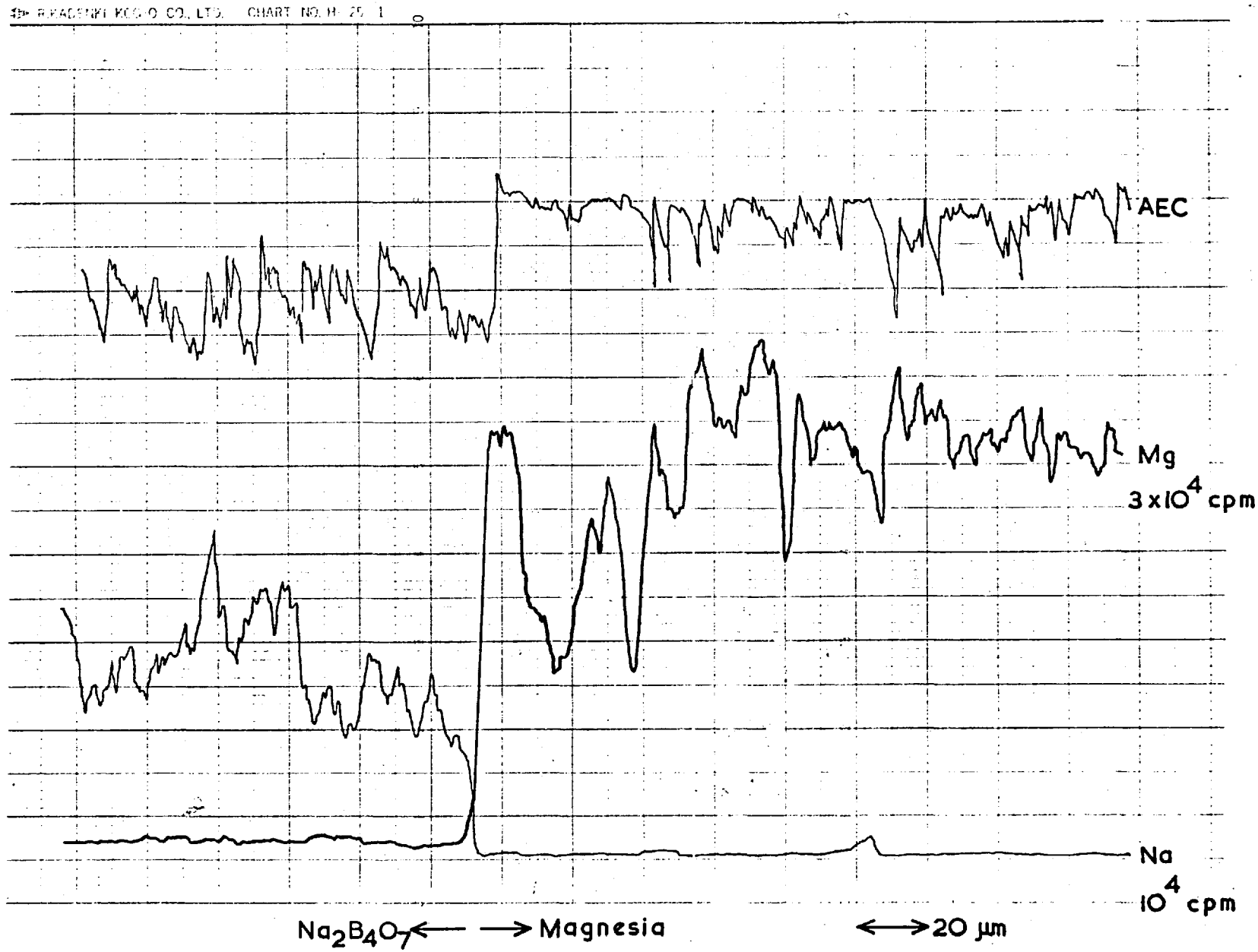

Figure 6.6. Electron microprobe trace of Mg and Na across the polycrystalline magnesia–sodium tetraborate interface.

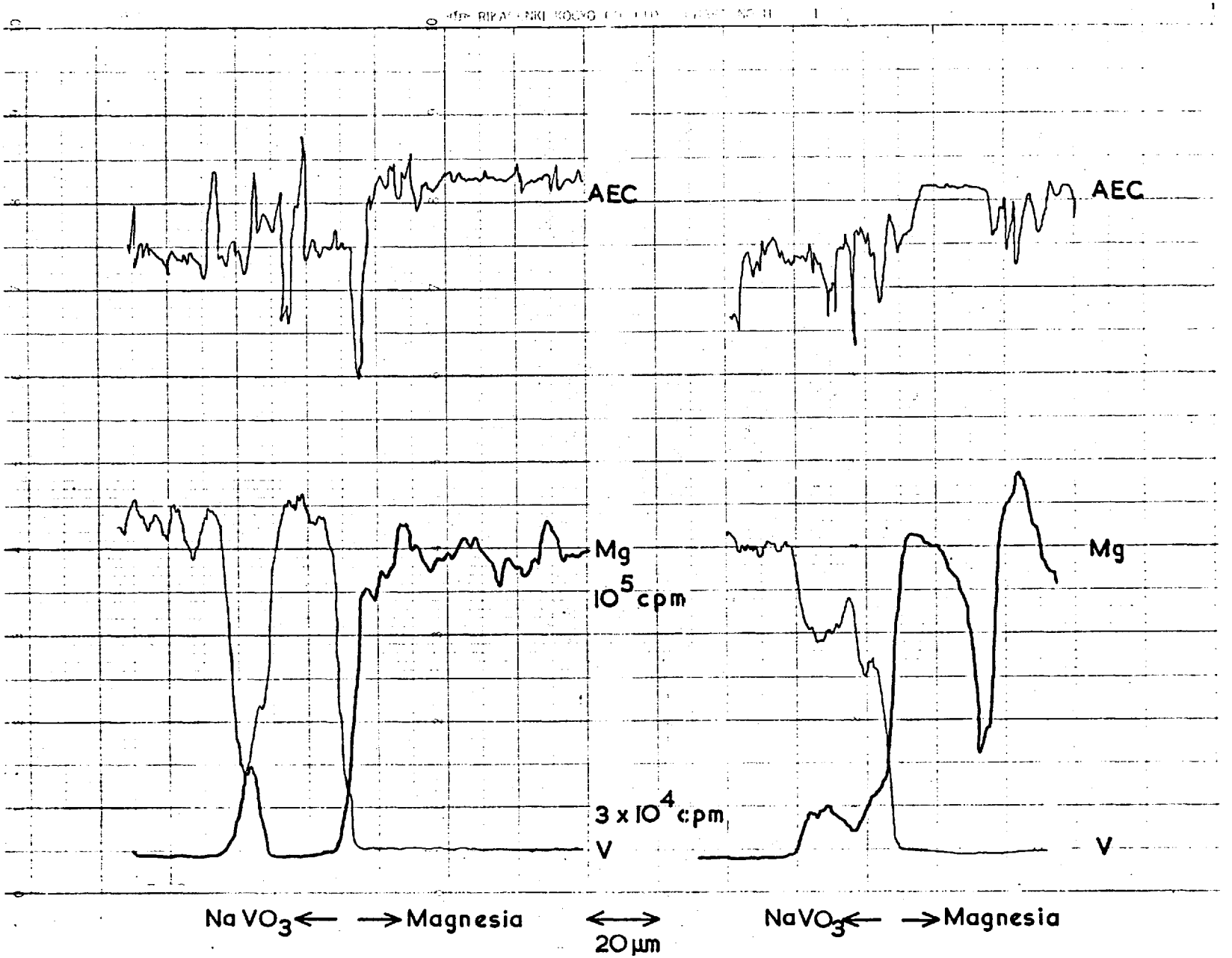

Figure 6.7. Electron microprobe trace of Mg and V across the polycrystalline magnesia–sodium metavanadate interface.

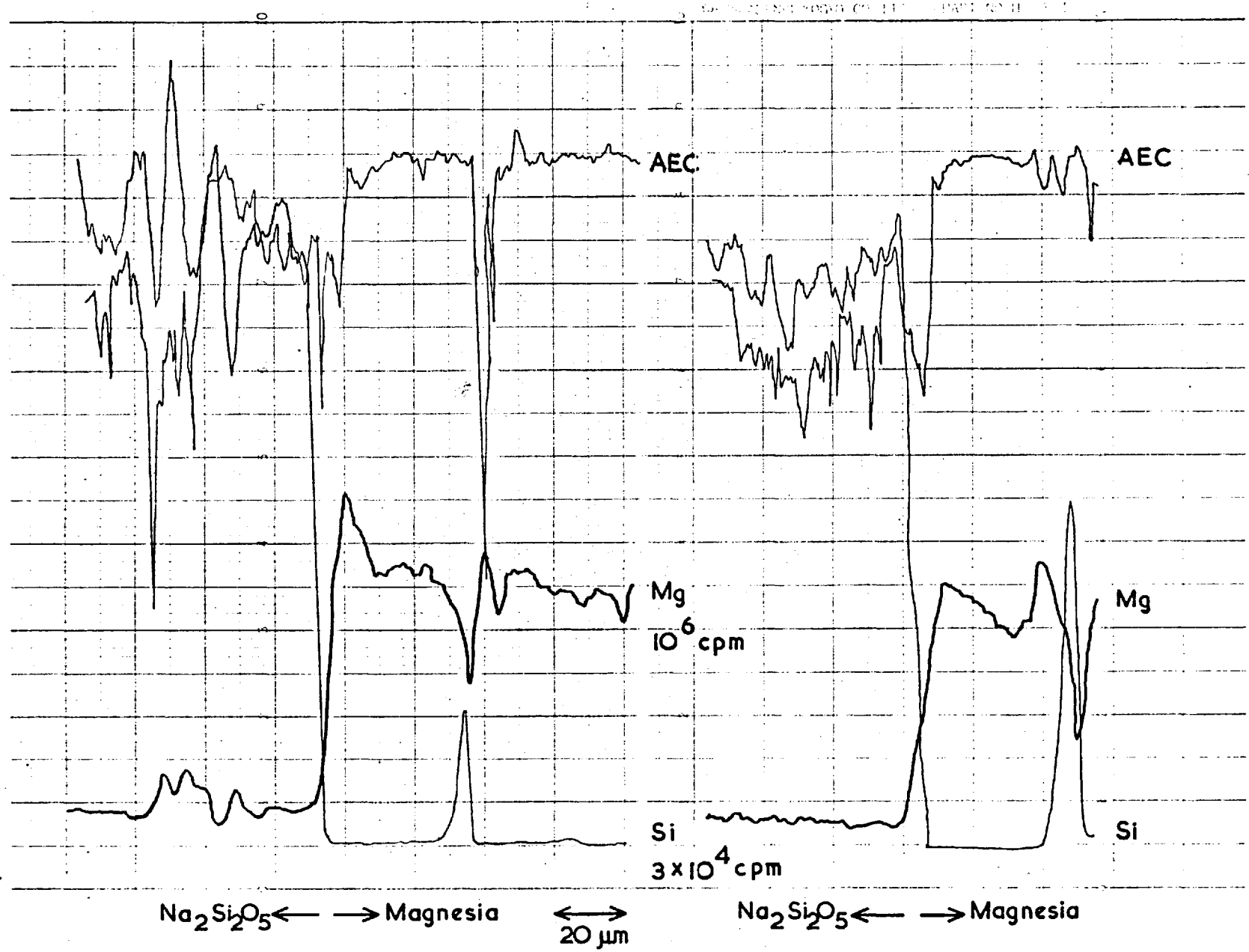

Figure 6.8. Electron microprobe trace of Mg and Si across the polycrystalline magnesia–sodium disilicate interface.

layers in the corrosion of alumina in borate and silicate melts, a sharp fall of magnesium concentration in the melts could be regarded as reaction control. However, surprisingly, a number of pieces of evidences from corrosion experiments under both natural and forced convection proved otherwise. The evidence will be discussed in detail in section 7.2. Incapability of detecting the boundary layer by EPMA scan should be regarded as an indication of the formation of very thin layer, i.e. as in the solution of sodium chloride in water studied by Wagner (96), knowing the limitation of resolution of the instrument is approximately 5 μm.

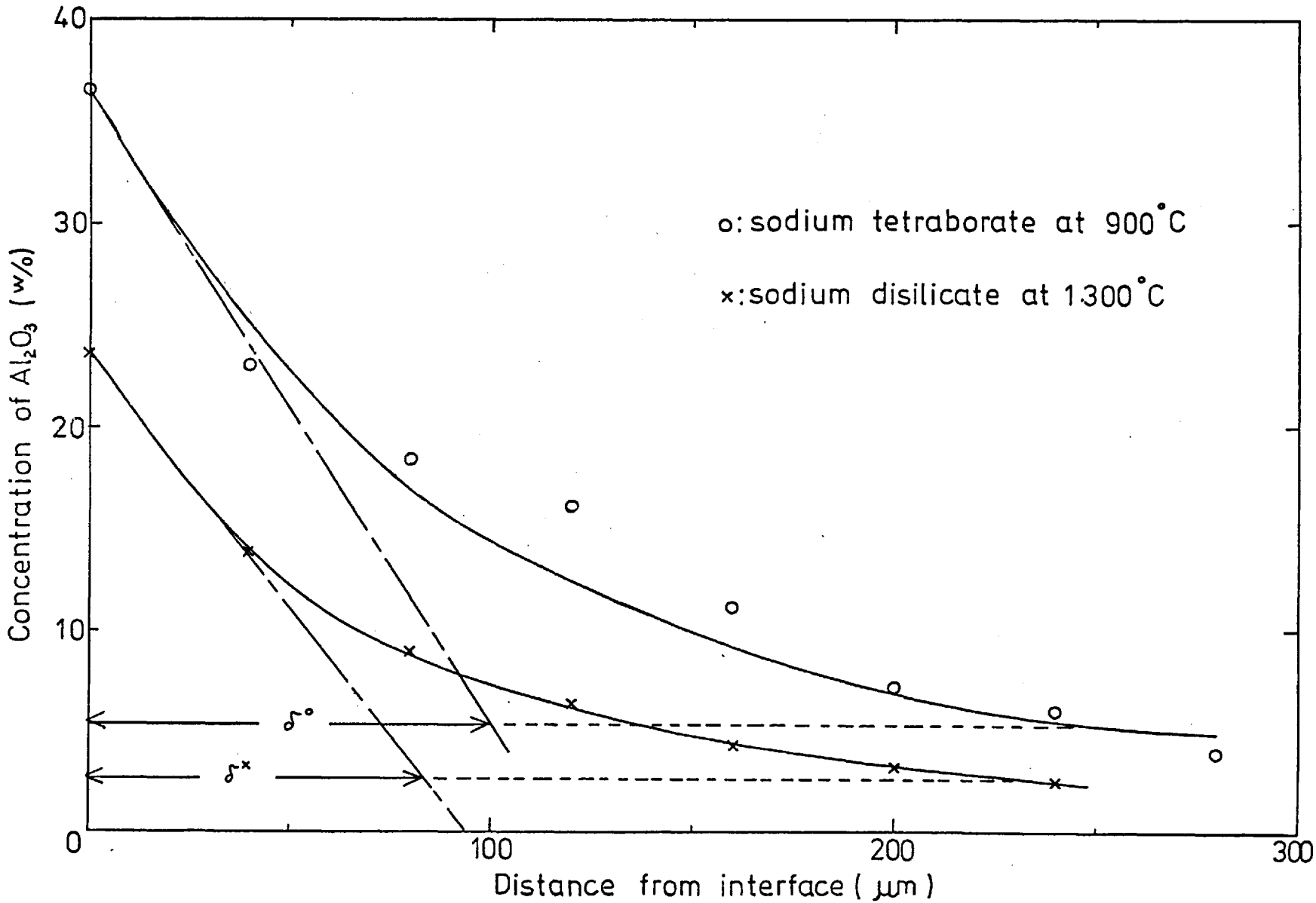

Figure 6.9. Determination of the effective boundary layer thicknesses.

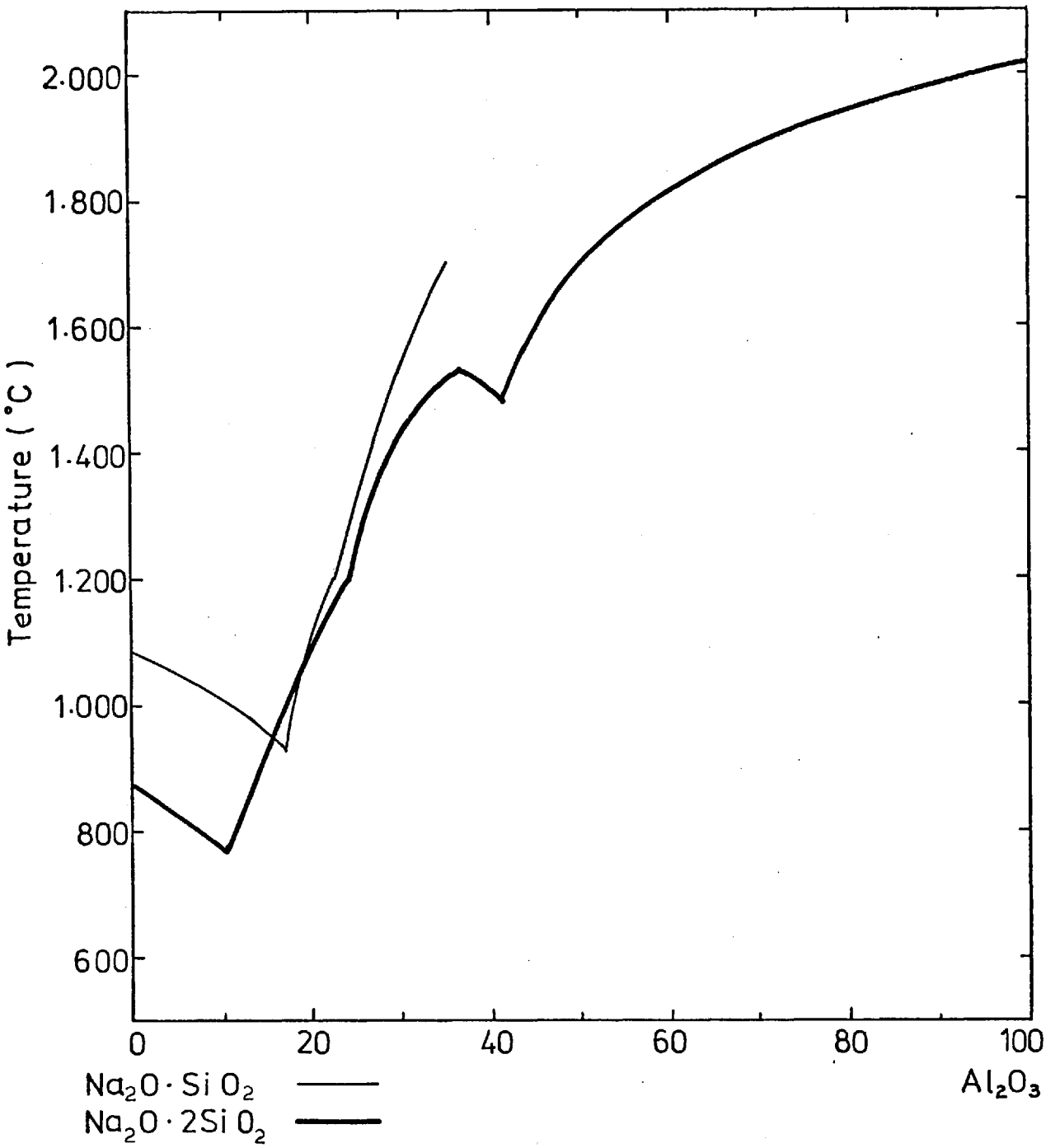

Figure 6·10. Alumina - sodium silicate phase diagram constructed from $Na_2O-SiO_2-Al_2O_3$ ternary phase diagram (60).

Figure 6.11. Diffusion coefficients for various diffusing species in sodium silicate melts

	Melt	Diffusing species	E_D	Reference
1 & 1*	$Na_2O \cdot SiO_2$	Sapphire	36 Kcal/mol	Author
2 & 2*	$Na_2O \cdot 2SiO_2$	Sapphire	30 Kcal/mol	Author
3	$Na_2O \cdot 2SiO_2$	Ruby	31 Kcal/mol	(92)
4	$Na_2O \cdot 2SiO_2$	Polycrystalline alumina	39 Kcal/mol	(92)
5	$Na_2O \cdot 2SiO_2$	Silica glass	29 Kcal/mol	(93)
6	$Na_2O \cdot 2SiO_2$	Silica glass	$\sim$ 95 Kcal/mol	(89)
7	$Na_2O \cdot 2SiO_2$	Na (self diffusion)	$\sim$ 10 Kcal/mol	(71)

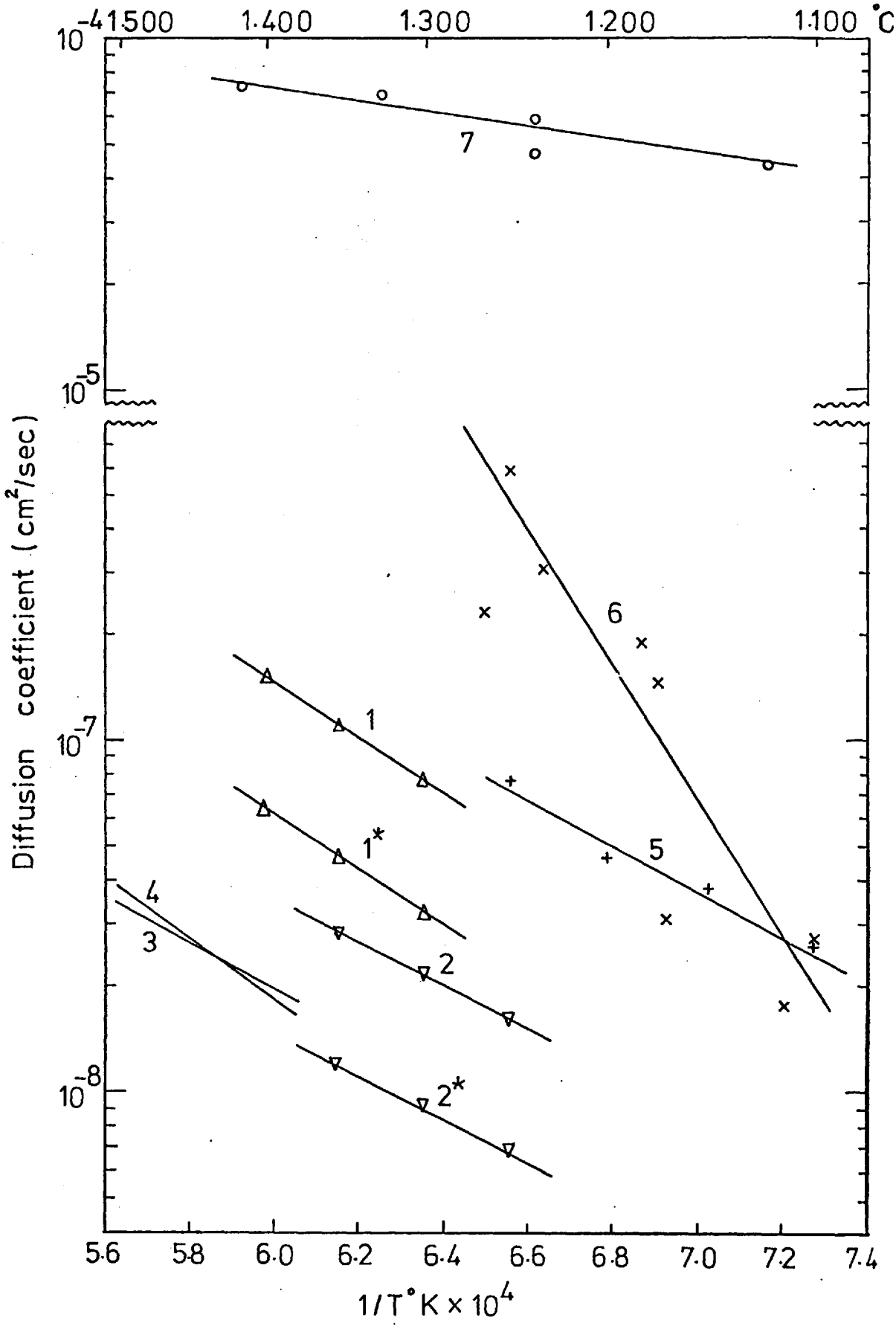
1500
1400
1300
1200
1100 °C
10⁻⁴
10⁻⁵
10⁻⁷
10⁻⁸
Diffusion coefficient (cm²/sec)
7
6
1
1*
5
4
3
2
2*
5.6
5.8
6.0
6.2
6.4
6.6
6.8
7.0
7.2
7.4
1/T°K x 10⁴

Figure 6.12. The plot of Log η as a function of the reciprocal of absolute temperature for:-

	Reference
1. $Na_2O \cdot SiO_2$	(2)
2. $Na_2O \cdot 2SiO_2$	(9)
3. $Na_2O \cdot 3SiO_2$	(9)
4. $Na_2O \cdot 3SiO_2$ + 6.9% Al_2O_3	(29)
5. $Na_2O \cdot 3SiO_2$ + 12.7% Al_2O_3	(29)
6. $Na_2O \cdot 2SiO_2$ + 28.8% Al_2O_3	(92)

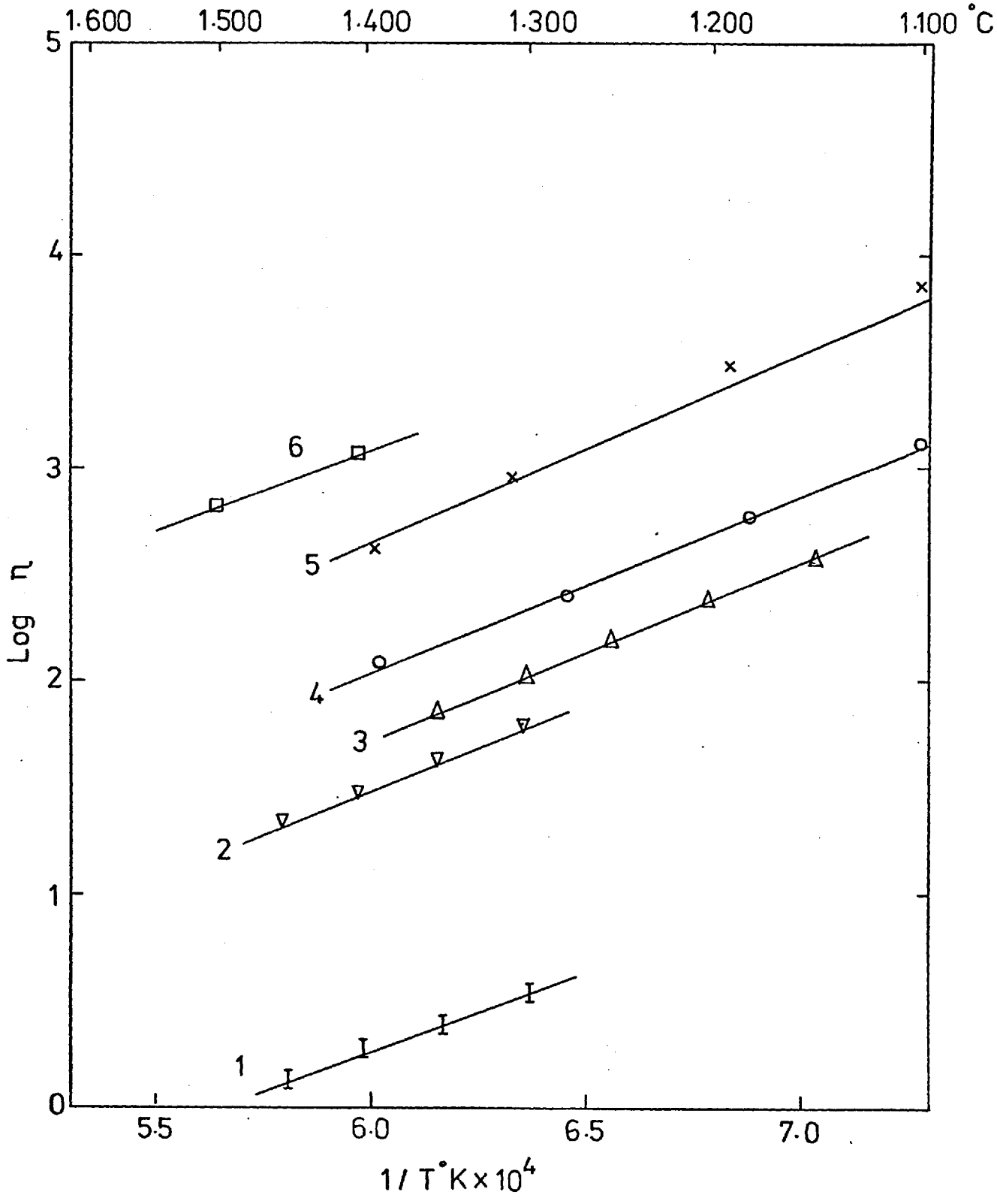
1.600
1.500
1.400
1.300
1.200
1.100 °C
5
4
3
2
1
0
Log η
6
5
4
3
2
1
5.5
6.0
6.5
7.0
1/ T°K x 10⁴

Figure 6.13. Energies of activation for viscous flow (E_η) in mixtures of Na_2O with SiO_2 and B_2O_3. (After Mackenzie) together with E_η for equivalent melts containing Al_2O_3 and E_D for alumina corrosion in sodium silicate

Δ : E_η for silicate containing 6.9 wt. % Al_2O_3 (29)

O : E_η for silicate containing 12.7 wt. % Al_2O_3 (29)

x : E_η for silicate containing 28.8 wt. % Al_2O_3 (92)

I : E_D for alumina corrosion

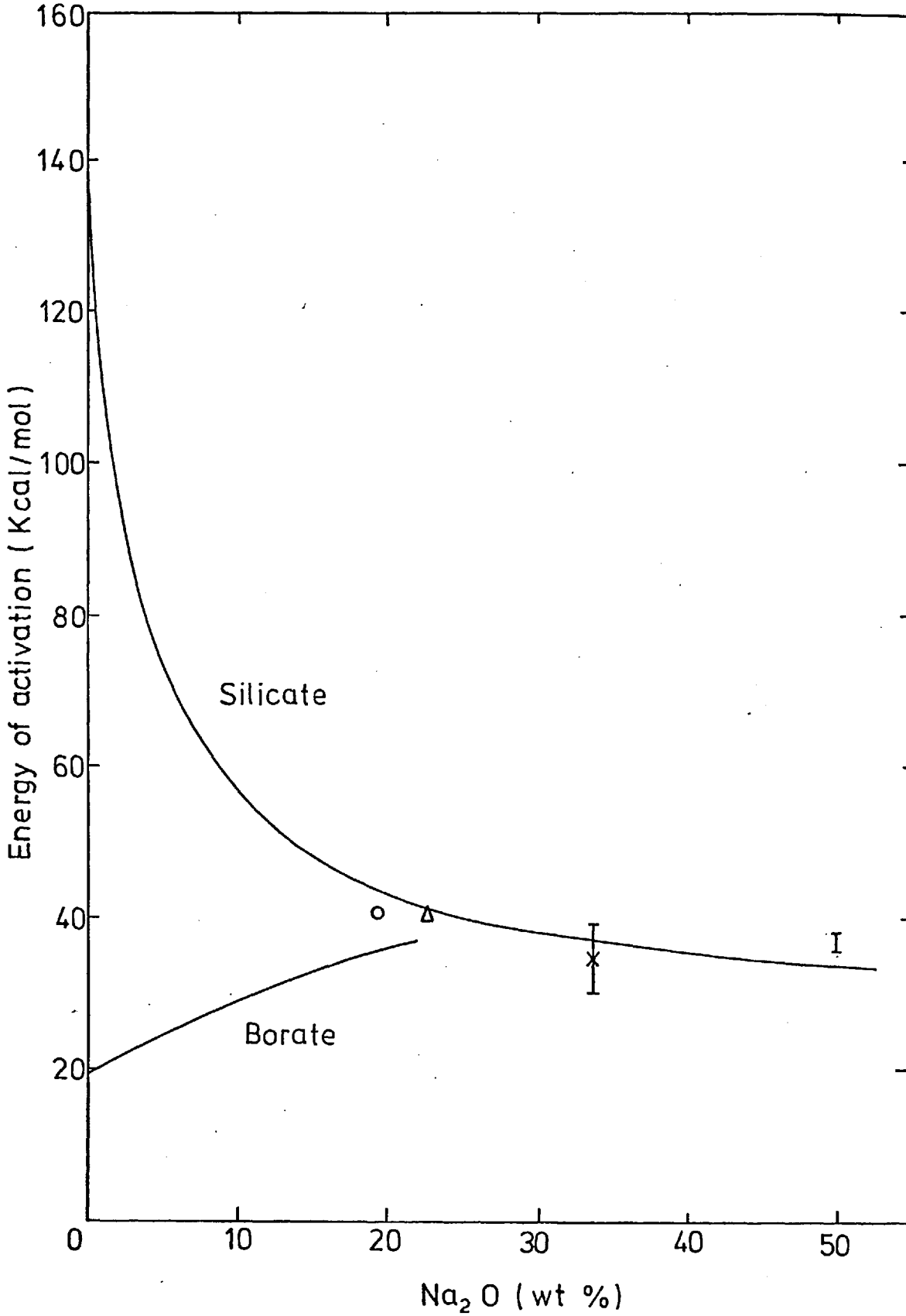
160
140
120
100
80
60
40
20
0
10
20
30
40
50
Energy of activation (Kcal/mol)
Na2 O (wt %)
Silicate
Borate

CHAPTER 7

DISCUSSION OF RESULTS

7.1. Accuracy of the technique employed

7.2. Dissolution of magnesia in melts under natural and forced convection

7.3. Corrosion of carbon-containing magnesia in melts

7.3.1. Corrosion of carbon-containing magnesia in sodium tetraborate melt

7.3.2. Corrosion of carbon-containing magnesia in sodium metavandate melt

7.3.3. Corrosion of carbon-containing magnesia in sodium disilicate melt

CHAPTER 7

DISCUSSION OF RESULTS

7.1 Accuracy of the technique employed

In order to follow the rate of corrosion of magnesia in melts by analysing representative samples taken out from time to time with the atomic absorption spectrophotometer, it was essential that the sampled melt should be representative of the whole. Therefore, stirring of melt was necessary for an effective mixing. The reasons as to why the present technique was chosen have already been explained in the section 4.1.

The mixing experiments with the stirrer at varying speeds of stirring were undertaken so as to ensure

1) homogenity of the melt toward magnesia concentration at various positions in the crucible

2) an optimum speed of stirring for an effective mixing.

The detailed experimental procedure and a discussion of results obtained will follow.

The melt chosen for this particular experiment was sodium tetraborate, because the viscosity of the melt at 900°C was similar to that of sodium disilicate at 1,400°C and the mechanism of corrosion of magnesia in both melts was previously known (2)(69) to be a chemically controlled process. However, the present work revealed that the reaction at the surface did not seem to be the rate determining process. This will be discussed in the section 7.2. Another advantage of using sodium borate melt was that the sampled melt could easily be brought into solution for analysis by A.A.S. whereas sodium silicate required another procedure of repeated fuming of acids for the removal of silica that might introduce an extra error. Most of all, the values of weight loss of MgO by weighing before and after the corrosion in the melt permitted a comparison with those obtained by an analysis. This was possible as an adhered melt could

be removed in warm water within a few hours without dissolving the single crystal of magnesia. Weight loss of MgO determined with three specimens in warm water for 24 hours gave an average value of only 0.041%.

The melt of 200 gms, contained in a fully-sintered alumina crucible of about 6 cm in diameter and 10 cm in length supplied by Morgan Refractories Limited was used for each run. When the melt attained the desired temperature the platinum stirrer with a single crystal of magnesia attached to it was lowered into the melt. The stirring for mixing whilst magnesia corrodes was followed at a fixed speed of rotation for each run. The experimental procedure was the same as those described in the section 4.3. except for a change of atmosphere above the melt from nitrogen to air. When the prefixed time had elapsed, prompt sampling with platinum loops was carried out during which the stirrer was taken out of the melt.

The crucible was then sectioned in two halves along a diameter after the melt was quenched at room temperature from an upright position. About 0.5 gm of glass was sampled from various positions of the glass, as numbered in the figure 7.1., for an analysis of magnesia to show its distribution.

The determination of the concentration of magnesia from the loops at various positions in the crucible at varying speeds of stirring are tabulated in table 7.1. together with the weight losses of specimens obtained by weighing before and after the run.

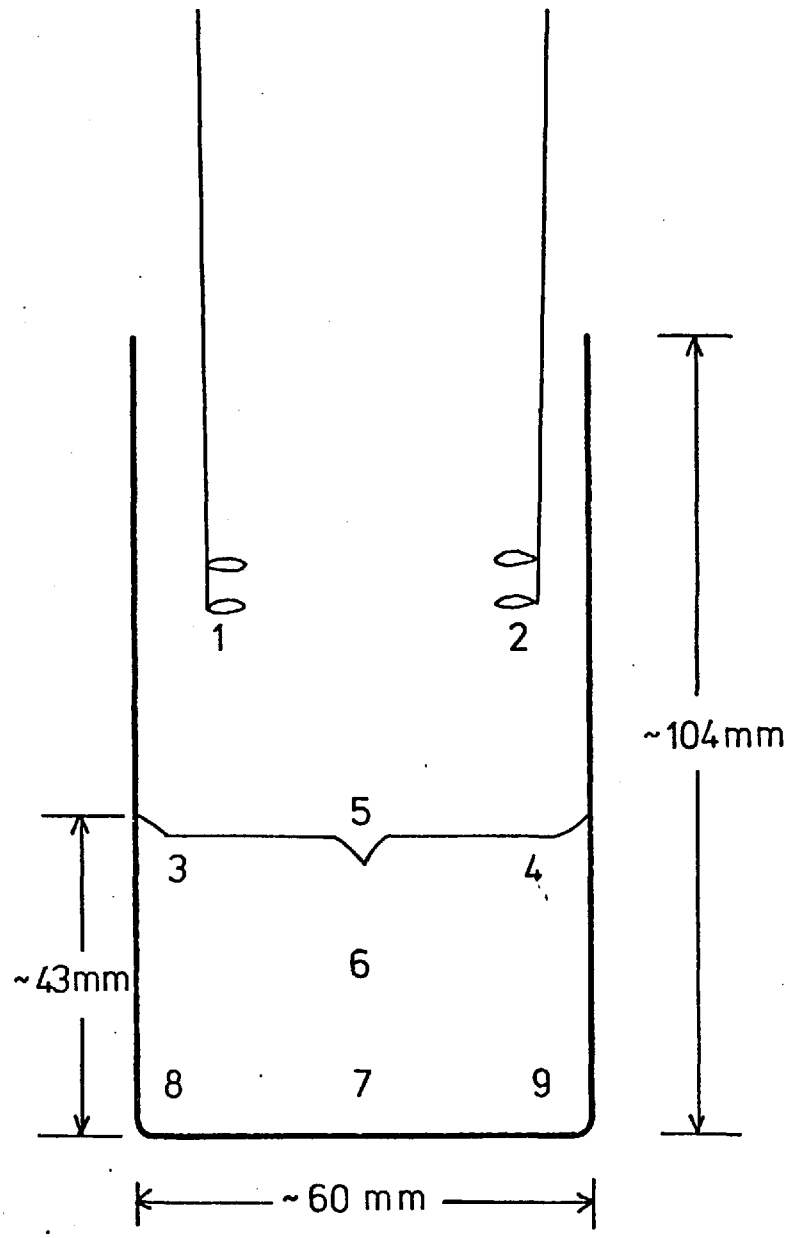

Figure 7.1. Sampling positions in the melt to reveal the degree of homogenity in respect to magnesia concentration produced by stirring ; numbers correspond to the numbers in the table 7.1.

Table 7.1.

MgO distribution in $Na_2B_4O_7$ melt

Temp ^{o}C = 900
Time (min) = 30

RPM / Position	0	79	164	318
1	0.055	0.325	0.521	0.520
2	0.015	0.320	0.508	0.530
3	0.030	0.340	0.508	0.515
4	0.100	0.315	0.508	0.515
5	0.075	0.315	0.508	0.520
6	0.115	0.350	0.457	0.515
7	0.030	0.350	0.508	0.500
8	0.000	0.350	0.470	0.505
9	0.275	0.340	0.445	0.500
xm_{1-2}	0.035	0.323	0.515	0.525
xm_{3-9}	0.089	0.337	0.486	0.510
xm	0.077	0.334	0.493	0.513
Wt. loss (x*)	0.087	0.331	0.489	0.550
$100 \times \frac{x^* - xm_{1-2}}{x^*}$	+59.8%	+2.4%	-5.3%	+4.5%

Key xm = mean value (gm)

x* = weight loss obtained by weighing before and after corrosion (gm)

To compare the relative variability of magnesia concentration, Karl Pearson's (65) coefficient of variation was calculated using the formula $v = 100\ s/xm$ where s is the standard deviation for which the formula is

$$s = \{\frac{1}{n} \sum_{i=1}^{n} (x_i - x_m)^2 \}^{1/2}$$

The values are tabulated in table 7.2. together with values of the rate of corrosion ($gm/cm^2/\frac{1}{2}hr$).

Table 7.2.

RPM	s, gm	v, %	$gm/cm^2/\frac{1}{2}hr$
0	0.073	94.81	0.0165
79	0.015	4.49	0.0598
164	0.026	5.27	0.0874
318	0.009	1.75	0.1120

As a plot of v against RPM is shown in figure 7.2., mixing achieved by stirring improves homogenity of the melt considerably compared to the unstirred melt while the increased speed of stirring decreases the variability only marginally. A similar indication can be noticed from a comparison of values obtained by the analysis of melt (1-2 in the figure 7.1.) with the value obtained by weighing of refractory before and after corrosion as listed in table 7.1. From this observation, the optimum speed of stirring was chosen to be 84 RPM bearing in mind that vigorous mixing would corrode the refractory faster and accordingly limits the time for the corrosion experiment, as the control of the corrosion process was by diffusion as will be discussed in section 7.2.

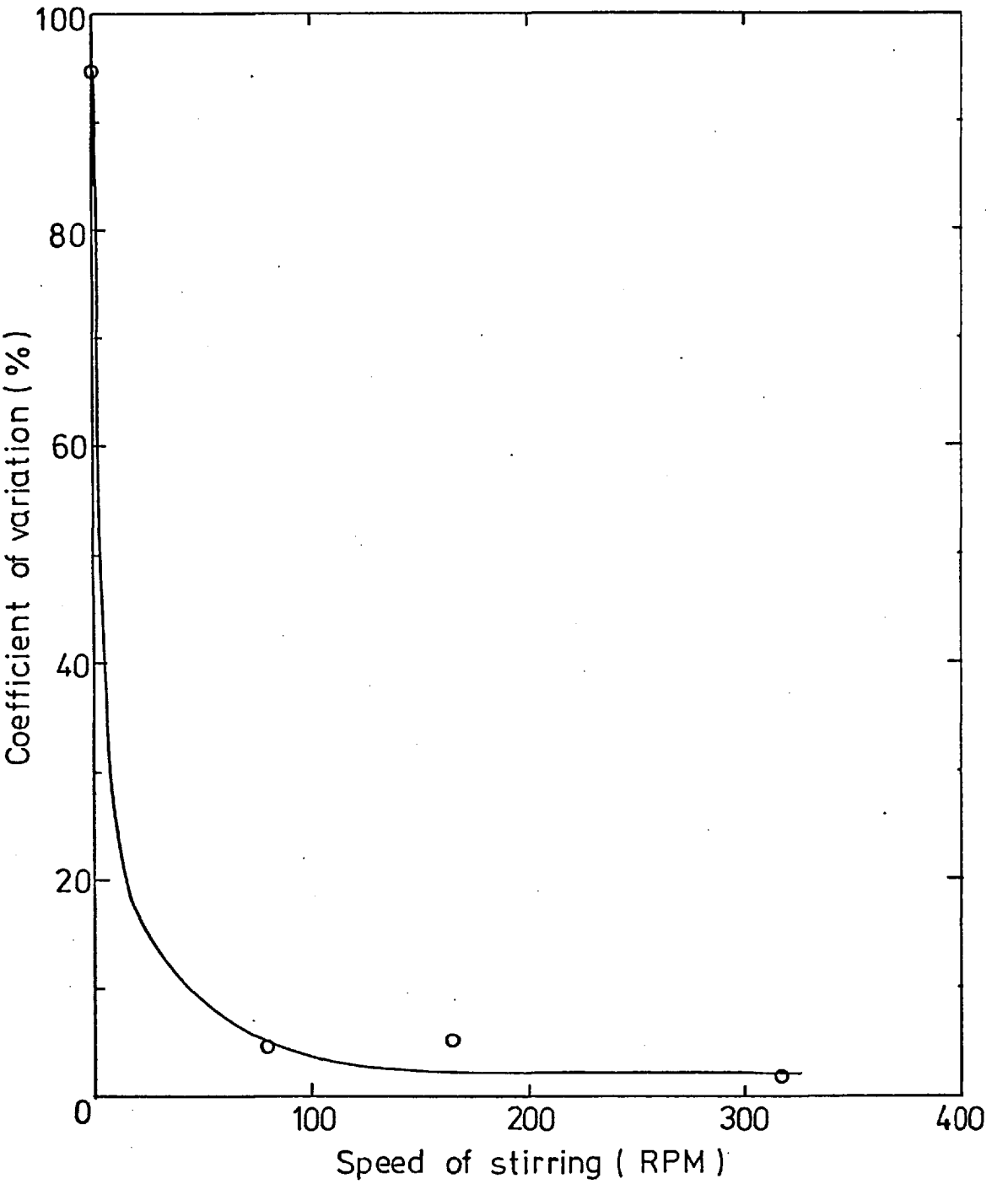

Figure 7.2. A plot of coefficient of variation of magnesia dissolution in sodium tetraborate as a function of speed of stirring.

In addition to the error introduced by an ineffective mixing as discussed above the main inaccuracy of the experiments was in the determination of weight loss by an analysis which has to go through many stages. Sources of error during these stages are from the following:-

1) weighing of powdered melt
2) preparation of an assay
3) the instrument, e.g. interference by other elements present in solution or noise due to sodium deposits on to the burner
4) calibration.

Some idea of the uncertainty introduced by the numerous stages in the analysis may be gained by comparing values so obtained with those obtained by the simple weighing of the specimen before and after each run.

	Expt. 1	Expt. 2	Expt. 3
Wt. loss by leaching	0.433	0.983	1.590
Wt. loss by analysis	0.405	0.980	1.605
Discrepancies	0.033	0.003	0.015
Uncertainty	7.62%	0.31%	0.94%

7.2. Dissolution of magnesia in melts under natural and forced convection

The dissolution of magnesia in sodium borate and sodium silicate melts under natural convection was studied previously by the author (69) and Barham (2). It was concluded that reaction at the interface was the rate controlling process. This conclusion was drawn on the basis that,

1) the plot of weight loss of magnesia (gm/cm^2) as a function of time gave a straight line passing through the origin (2)(69)

2) porous magnesia polycrystal corroded faster than single crystal in sodium silicate melt (2).

However, a number of pieces of evidence obtained in the present study under both natural and forced convection seem to support transport controlled dissolution.

A review by Bircumshaw and Riddiford (7) states that the dependence of dissolution rate (K) on the rate of stirring (RPM) has been observed during transport control in heterogeneous reactions. The relationship determined experimentally is

$$K \Rightarrow (RPM)^n$$

where n is 0.5 - 1 depending on the degree of tubulance. Reed and Barrett (76) tested the above relationship by rotating sapphire rods in $CaO.SiO_2$. Al_2O_3 melt and found n fell between 0.5 and 0.7. The present results on magnesia corrosion in sodium borate under forced convection seem to fulfil the above relationship, n being 0.5 as a plot of the corrosion rate against the square root of stirring rate (RPM) shown in figure 7.3. reveals.

Plots of the logarithm of the rate of corrosion as a function of the reciprocal of absolute temperature, shown in figure 7.4., indicate that the corrosion process was temperature dependent, obeying an equation of Arrhenius form

$$K = A \exp^{-E_K/RT}$$

where, K = corrosion rate ($gm/cm^2/hr$)

A = constant

E_K = energy of activation for the process (cal/mol)

R = gas constant ($cal/mol/^oK$)

T = absolute temperature (^oK).

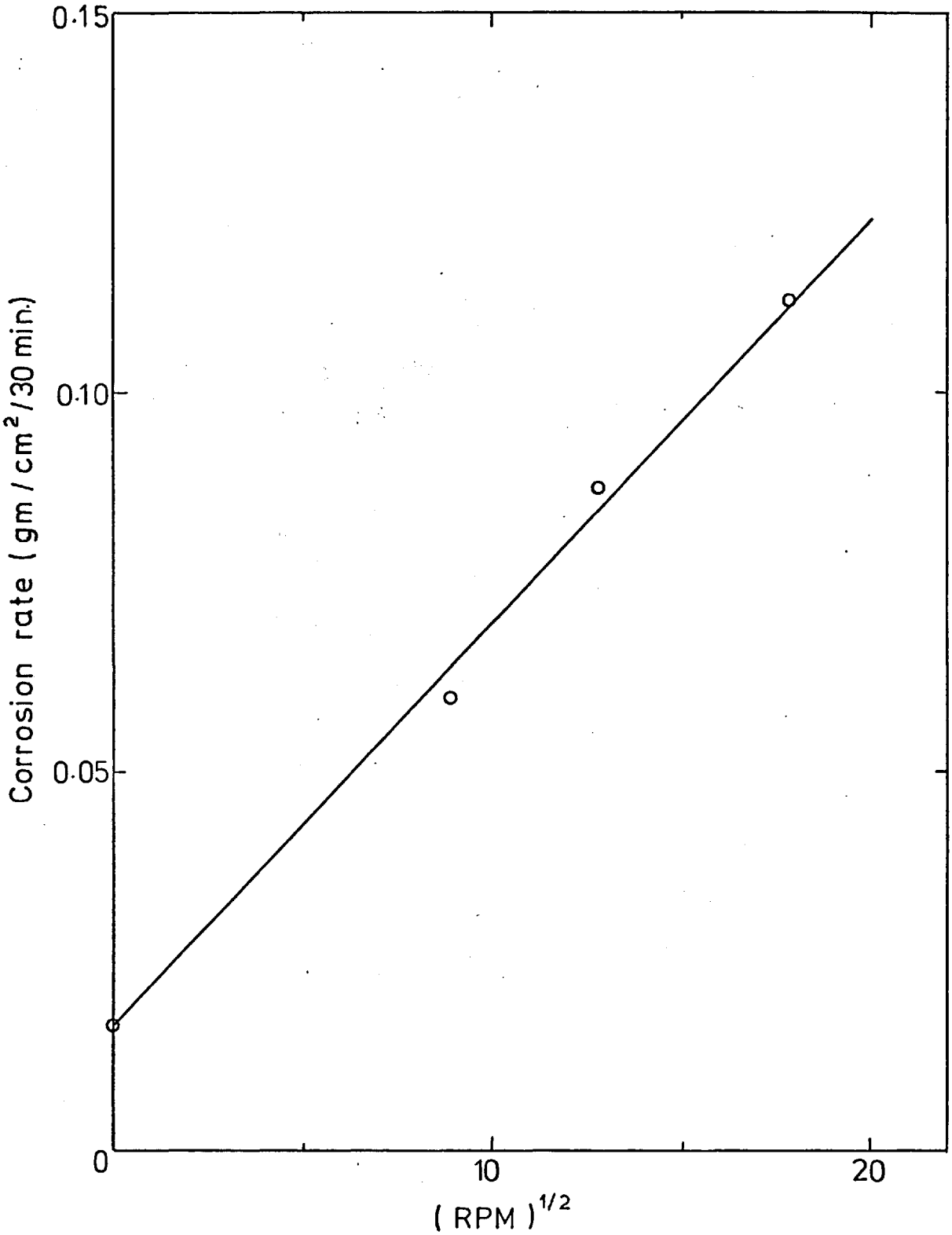

Figure 73. A plot of the rate of magnesia single crystal corrosion in sodium tetraborate at 900°C against the square root of stirring speed.

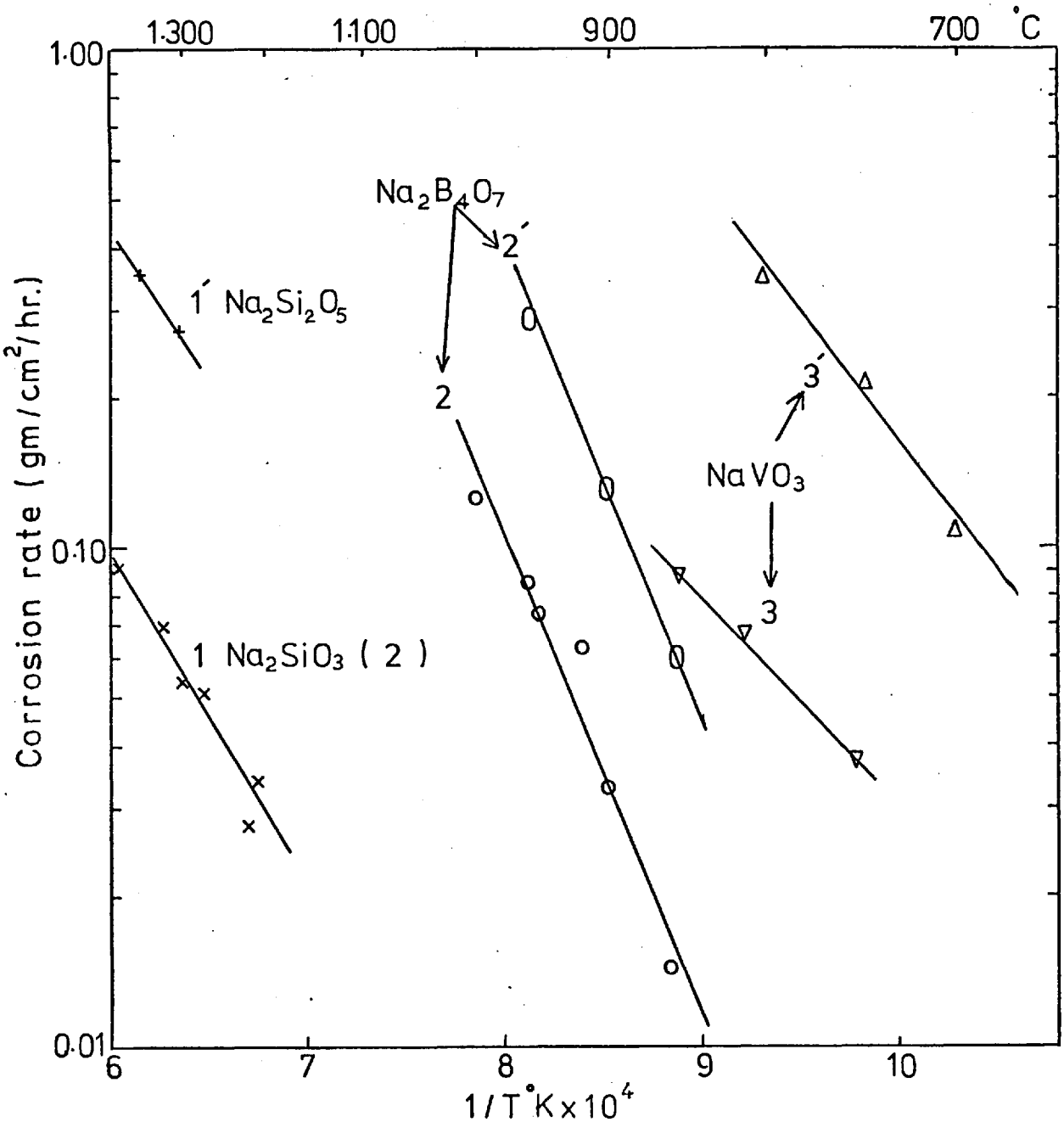

Figure 7.4. Temperature dependence of the corrosion rate of magnesia single crystal under natural (1,2,3) and forced (1´,2´,3´) convection.

Values of the calculated apparent energy of activation (E_K) using the slope of the lines are presented in table 7.3. As the values of E_K would represent activation energy for the diffusion process through the boundary layer if diffusion control is definitely operative, the magnitude of E_K may be compared with the values of activation energy for viscous flow (E_η) for the corresponding melt.

Table 7.3.

Energy of activation for magnesia corrosion and for viscous flow

	$Na_2Si_2O_5$	Na_2SiO_3	$Na_2B_4O_7$	$NaVO_3$
E_{K_1}	-	31 (2)	37 (69)	19
E_{K_2}	31	-	39	24
E_η	38 (9)	32 (9)	56 (87)	9 (41)
		36 (2)		

Key, E_{K_1} : E_K value in natural convection
E_{K_2} : E_K value in forced convection.

As can be seen, E_K values for magnesia corrosion in melts under both natural and forced convection ($\sim$84 RPM) are similar except for small difference of E_K values for $NaVO_3$ melt. Comparable observations on similar E_K values under free and forced convection were also reported in the literature by Cooper and Kingery (22) from their study of sodium chloride corrosion in glycerol. Under forced convection, if the flow velocity of a melt is increased indefinitely to a point where no boundary layer could be formed, then the reaction at the surface would be the rate controlling process. If this condition could be provided experimentally, the corrosion

rate would be constant irrespective of flow velocity and one would expect E_K values for the reaction and for diffusion through the boundary layer under natural convection to differ. In view of experimental difficulties, as may be expected, no reference is yet available for this comparison in relation to refractory corrosion.

However, it is worth noting that Reed (74) evaluated E_K values for chemical reaction by constructing a tangent to the curve at zero time from the parabolic section of the weight loss/unit area versus time curve for alumina corrosion in various silicate melts. Here the values of E_K for unsteady state (reaction control) were found to be somewhat lower than the E_K values for unsteady state (diffusion control). It is feasible that similarity of E_K values for magnesia corrosion in sodium borate in particular under both natural and forced convection would indicate that the fundamental processes involved in both case proceed by the same mechanism. Recapitulating, convective flow achieved by the stirring speed of $\sim$84 RPM diminished the thickness of boundary layer without altering the rate controlling process. The small difference in E_K value for $NaVO_3$ melt may be due to experimental error or to the change of mechanism. The data are not sufficient to ignore the former possibility whilst the E_K value for chemical reaction is not known to pursue the latter possibility.

Turning now to the values of E_K compared with the values of E_η of the melts, it can be seen that the E_K values do not relate to the values of E_η except those for sodium silicate. However, it must be emphasized that one may relate the value of E_K with E_η values for the melts containing high magnesia concentration up to the saturated concentration provided that the saturation concentration do not vary considerably over the temperature range investigated. But caution must be exercised in comparing these values because the E_K value results from several factors as stated by Samaddar, Kingery and Cooper (85),

i.e.

1. the liquidus composition and so the driving force for the dissolution process changes with temperature
2. the saturation concentration changes with temperature, so there would be corresponding changes in diffusion coefficient that have no relation to any activated process,

whereas the value of E_η represents a thermally activated single process (63).

Further useful evidence that indicates transport control of magnesia corrosion in $Na_2B_4O_7$ melt was drawn from the dependence of depth of corrosion on the distance from leading edge of the corroded specimen as shown in figure 7.5. This was first applied by Wagner (96) to the dissolving of a sodium chloride slab in water and further confirmed by Cooper and Kingery (22) and more recently by Cable and Martlew (11) who applied it to the corrosion of refractory in glass melt under natural convection. The rate of dissolution is

$$j = 0.5\ D\ (C_s - C_o)\ (\Delta\rho\ g/D\eta)^{1/4}\ x^{-1/4}$$

where, j = flux density from surface ($gm/cm^2/sec$)

D = diffusivity (cm^2/sec)

C_s = saturation concentration (gm/cm^3)

C_o = bulk concentration (gm/cm^3)

$\Delta\rho$ = density differences between saturated and bulk melt (gm/cm^3)

η = dynamic viscosity (poise)

g = gravitational constant ($gm/cm/sec^2$)

x = distance from leading edge of slab (cm).

The figure 7.5. shows the recession of the face of a totally immersed slab was proportional to the reciprocal of the fourth root of distance from the leading edge as the above equation predicted. The fact that the

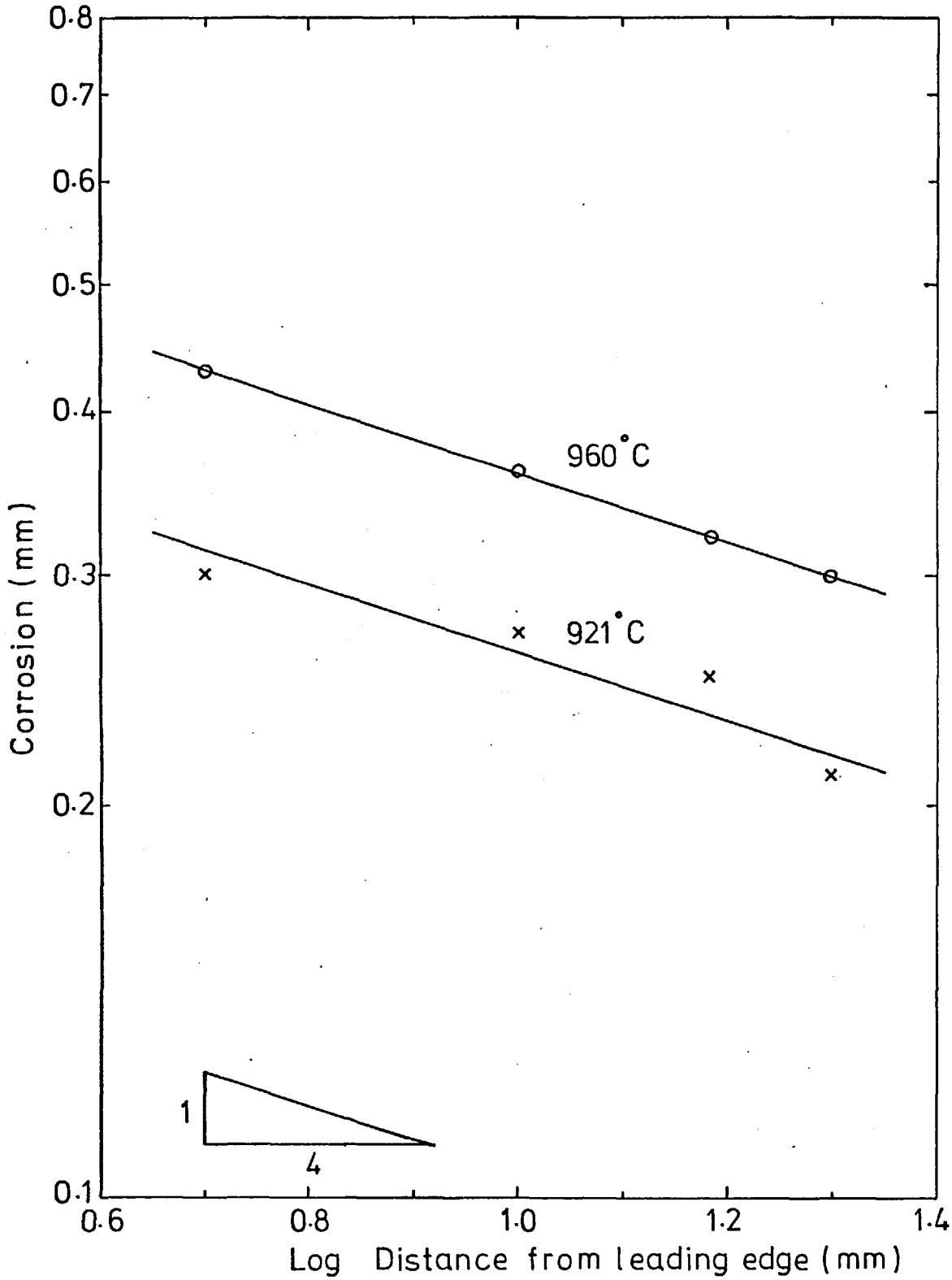

Figure 7.5. Logarithm of distance from leading edge against logarithm of magnesia corrosion in sodium tetraborate under natural convection.

upper edge of a slab was narrower than the bottom edge indicates that the dissolution of magnesia increased the density of bulk melt and consequently produced density promoted downward convective flow. This was confirmed by separate density measurements of $Na_2B_4O_7$ melts containing varying amount of MgO, as shown in figure 7.6. The density of the melt (ρ) was measured by the Archimedes' principle using a platinum bob and calculated by the following formula,

$$\rho = \frac{Wa - Wm}{V \times Et}$$

where, Wa = weight of platinum bob in air (gm)

Wm = weight of platinum bob in melt (gm)

V = volume of platinum bob (cm^3)

Et = volume expansion coefficient of platinum.

Figure 7.7. shows photographs of corrosion profiles of fully sintered magnesia cylinders rotated on their axes with varying speed in sodium borate melt at 900°C for half an hour. As the specimens used were in the form of crucibles supplied by the Thermal Syndicate Limited, due to the difficulty in procuring the rod of single crystal magnesia, it cannot be claimed that accurate quantitative measurements were made as the depth of removal from the bottom face could not be estimated. However, an average value of decrease in original diameter measured with a sharp knife-edge vernier caliper, down below the flux line and towards the bottom of the immersed sample indicates that the rate of corrosion increased with the rate of stirring as tabulated in table 7.4.

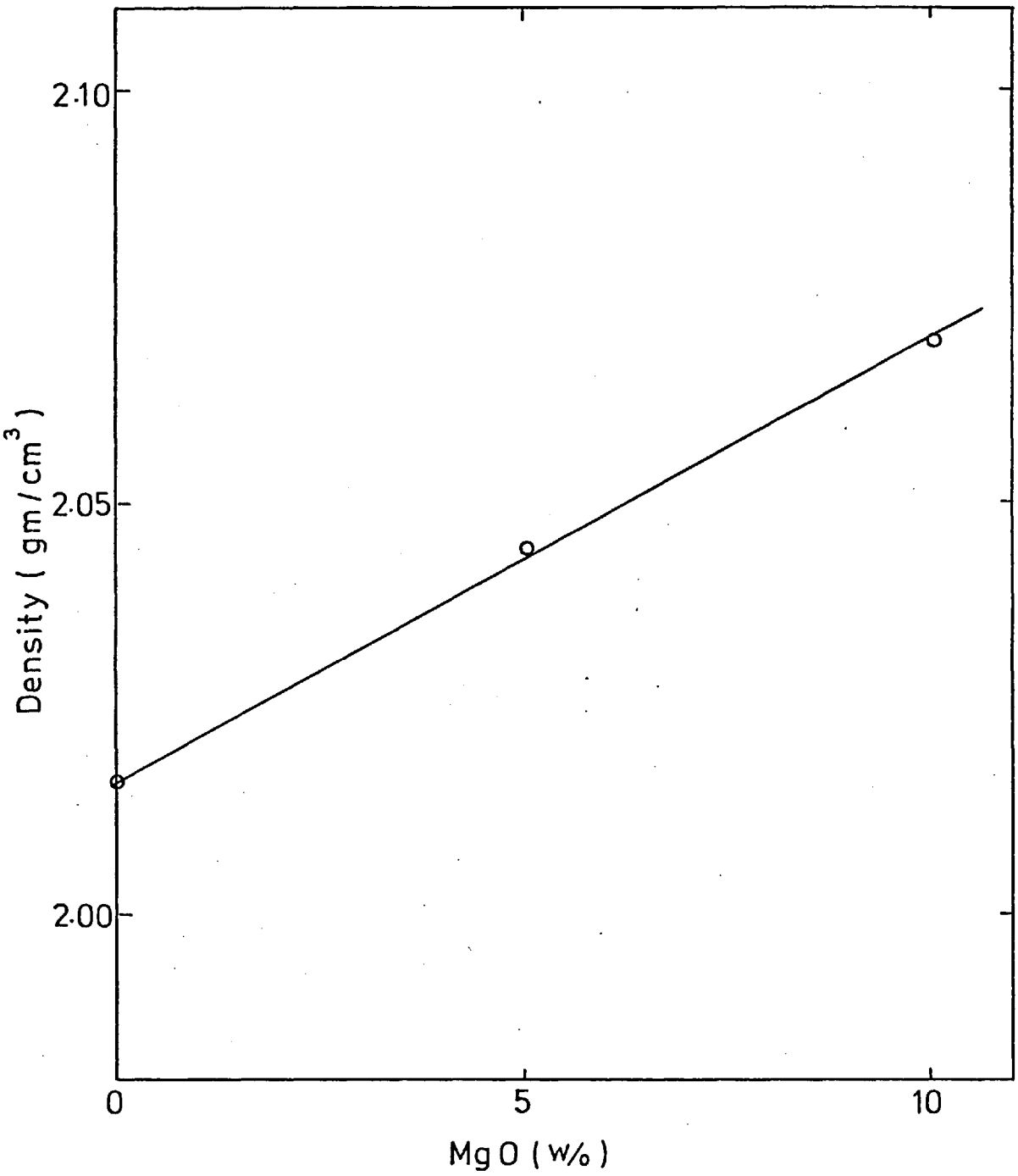

Figure 7·6. A graph to show density increase of sodium tetraborate with addition of Mg O at 900°C.

Figure 7.7. Corrosion profiles of fully sintered magnesia cylinders

1. uncorroded specimen

2. corroded under natural convection

3. corroded under forced convection (206 RPM)

4. corroded under forced convection (298 RPM)

5. corroded under forced convection (379 RPM)

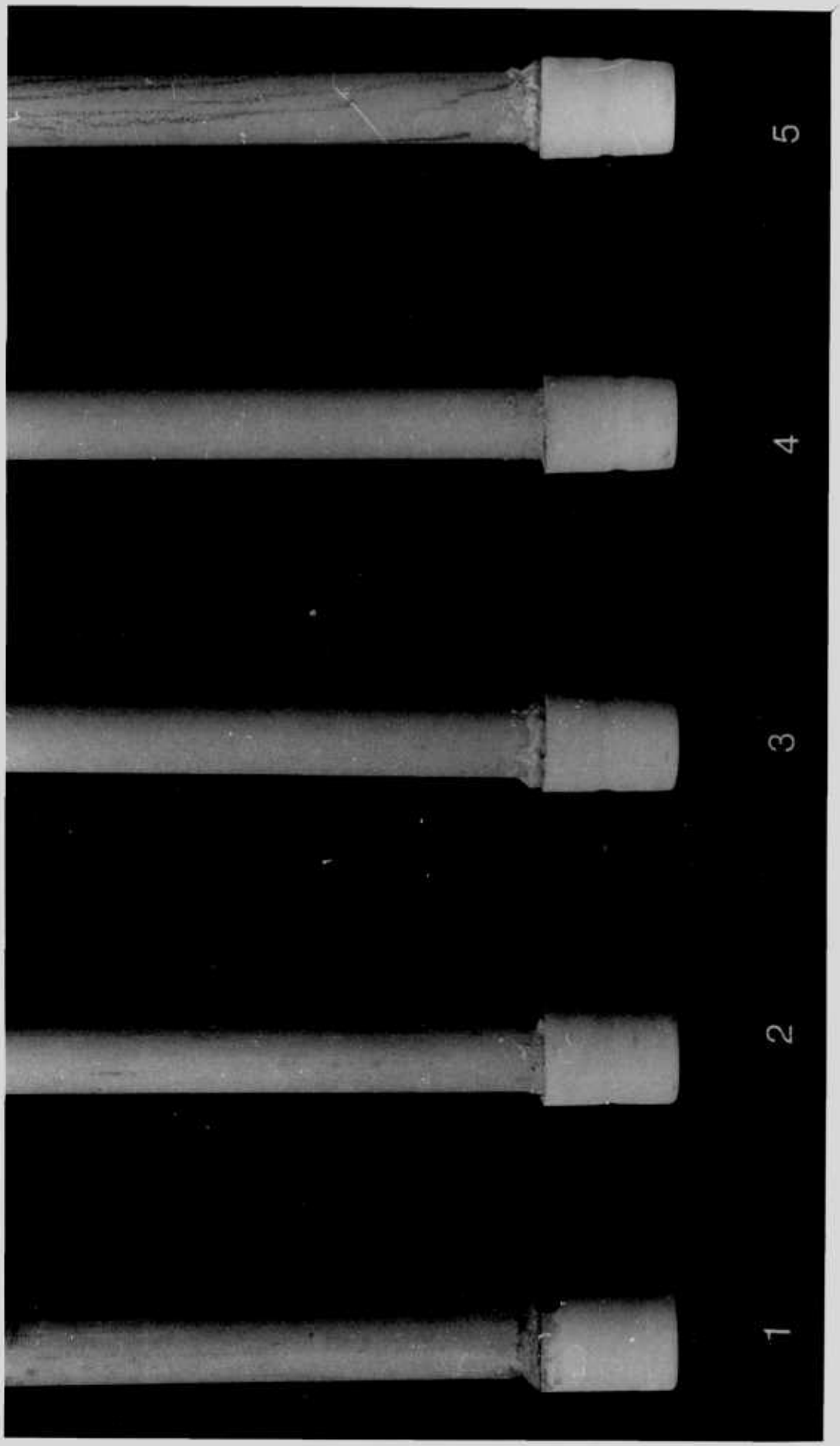
1
2
3
4
5

Table 7.4.

Magnesia Corrosion

Rotation Speed (RPM)	Corrosion (cm)
0	0.045
206	0.049
298	0.051
379	0.060

Another aspect of corrosion noticed from the photograph is an enhanced attack on the flux line where the liquid - gas - solid coexisted. A probable explanation of increased attack has been given by White, J. (100) as due to a surface tension effect. A groove observed on a sapphire rod immersed in $CaSiO_3 - Al_2O_3$ was considered to be due to the increase of surface tension of the melt with alumina addition by Cooper and Kingery (21). Vago and Smith (95) classified various patterns of flux line attack in terms of the surface tension effect and the presence of vapourisable components in the melts that attack the refractory. Cable and Martlew (11) obtained a satisfactory agreement between the observed value and that of calculated value of flux line attack based on Hrma's mathematical model(48) that the corrosion rate is dependent upon $(C_s - C_o)\{D^2(\sigma_s - \sigma_o)/\eta\}^{1/3}$ where σ_s is the surface tension of the saturated composition. These observations all add up to the probability that the flux line process is similar to forced convection driven by the surface tension gradient along the gas-liquid interface (12) that may be regarded as another indication for a transport controlled process.

Examining the details of evidence which led to the conclusion of reaction control for magnesia corrosion mentioned at the beginning of the section, the first point to be made is that the weight loss of refractory was followed by a continuous weighing technique. According to the details of the technique as described by Safdar, Barham and Barrett (84) the

technique has many advantages compared to the intermittent weighing technique (64), i.e. it enables one to follow the weight loss of the refractory that cracks on cooling by differences in thermal expansion between the refractory and slag, or that is soluble in acid, e.g. MgO. On the other hand, it has disadvantages such as:

1. an error would be introduced by vapour deposits on to the suspending wire,
2. gas bubbles trapped onto the specimen or hanging onto the suspending wire would cause a false reading
3. approximately 20-30 seconds are required for the balance to be balanced at the commencement of the run.

The author was led to suspect that if the diffusion layer establishes itself quickly to build up a thin layer, it may well be missed by the continuous weighing technique due to the third reason listed above. In order to throw some light on this supposition, the rate of magnesia corrosion in the melt was measured by the intermittent weighing technique. Indeed, a plot of weight loss/unit area values versus time did not go through the origin if the straight line is extended through the points as shown in figure 7.8. Although it could be argued that the weight loss values include solution occuring as the specimen was held above the melt to avoid cracking, there is an indication that the boundary layer is established quickly to form a very thin layer. Failure to detect the thickness of the boundary layer by EPMA and the above indication suggest that the layer would be a few microns thick.

Although previous work (2)(69) indicated reaction control of dissolution of magnesia in sodium borate and silicate, the fresh evidence given above leaves little doubt that once again the commonly encountered transport control is operative.

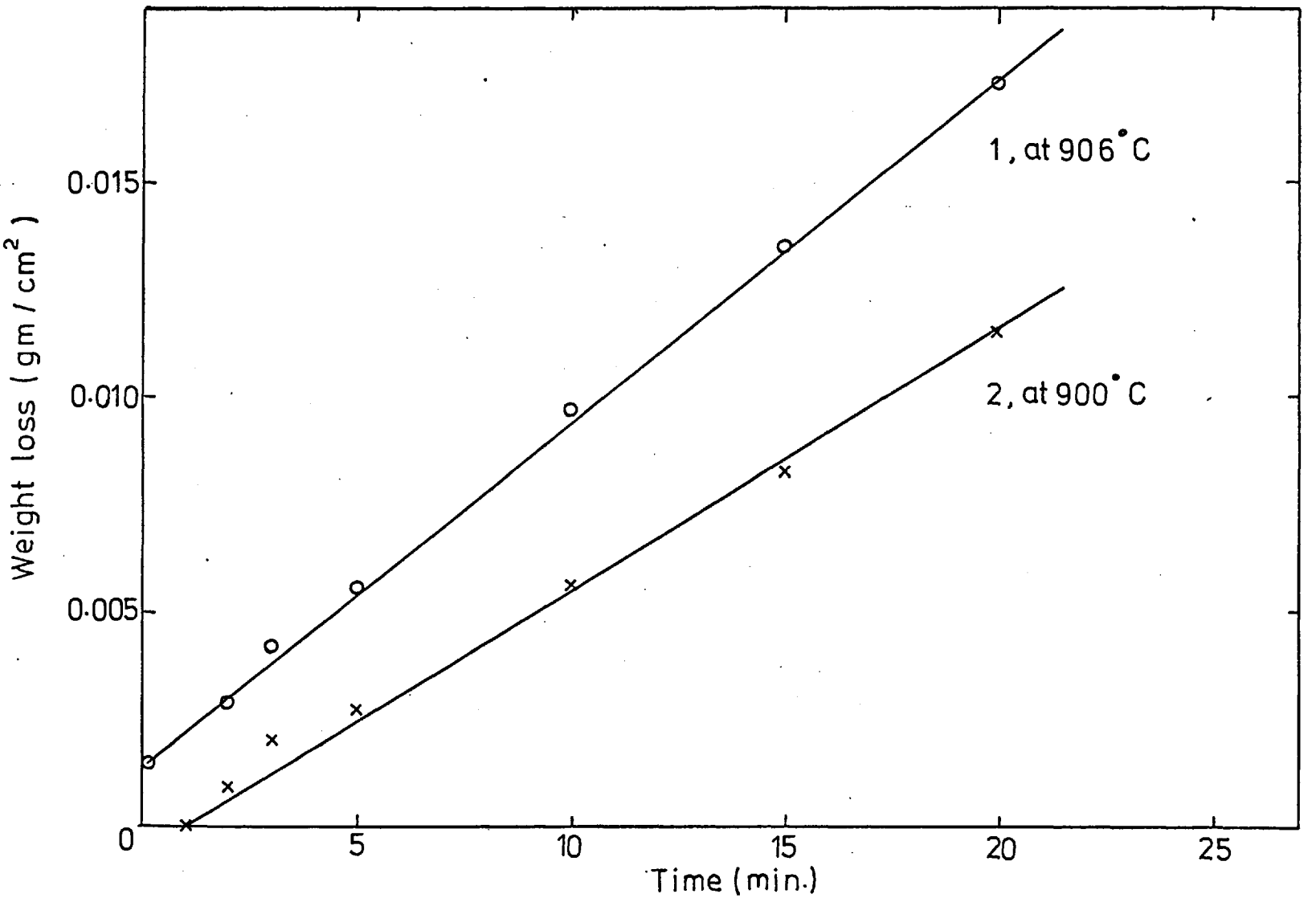

Figure 7·8. Dissolution of single crystal magnesia in sodium tetraborate by 1) static corrosion technique, 2) continuous weighing technique (69).

7.3. Corrosion of carbon - containing magnesia in melts

7.3.1. Corrosion of carbon - containing magnesia in sodium tetraborate melt

Figures 7.9. to 7.11. illustrate plots of weight loss/unit area (gm/cm^2) for single crystal and porous magnesia polycrystal without and with carbon respectively as a function of time at three different temperatures.

Examining first a plot for porous polycrystal corrosion compared with single crystal shown in figure 7.12., it reveals that the initial corrosion rate of porous magnesia was the same as single crystal even though the surface area of the porous magnesia specimen exposed to the melt is expected to be larger than the geometrical surface area measured. This is most likely because the melt, rich in solute if not saturated trapped inside the pores, had no effect on to the bulk melt being analysed. In this connection, the work of Faruqi (32) has shown that the pores of porous refractory were completely filled with saturated melt when diffusion control was operative provided that the boundary layer thickness is larger than half the pore diameter.

After the initial period of about ten minutes had elapsed, the slope of the curve showed that the corrosion rate of porous specimen is increased compared to that of single crystal. It would follow if it is borne in mind that the pores got enlarged due to attack of melt and subsequently the surface area exposed to the melt becomes larger than the geometrical surface area. Simple calculation at 40 minutes time interval show that about 17% of extra surface area was available in the porous specimen under attack by the melt.

Comparing the slope of curves for carbon-containing magnesia with corresponding porous polycrystal (as can be also seen in the figure 7.12.) reveals that the carbon in the pores (5.3 weight %) reduced the rate of corrosion of magnesia appreciably. This is likely to be achieved by the

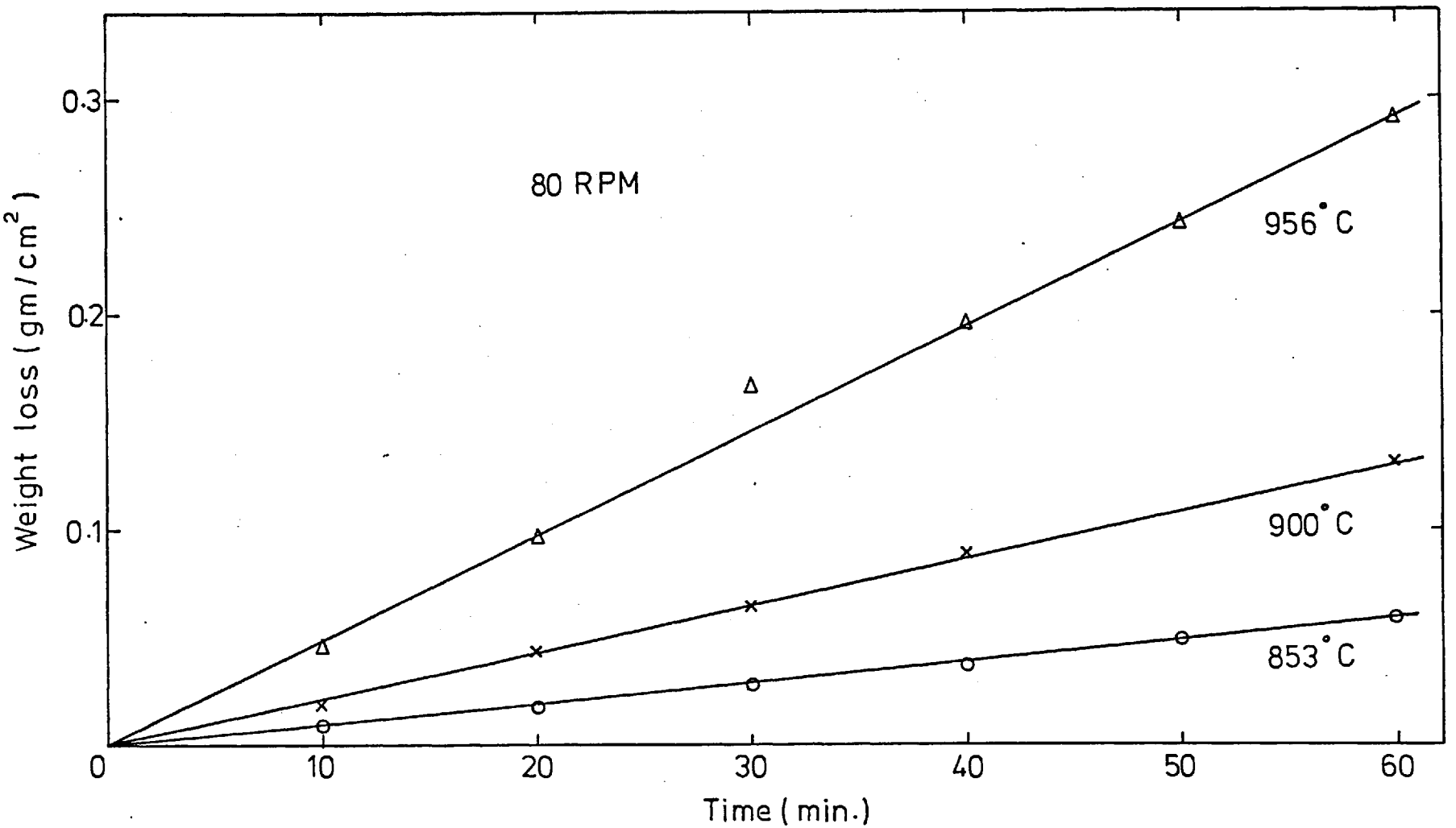

Figure 7.9. Corrosion of magnesia single crystal with stirring in sodium tetraborate.

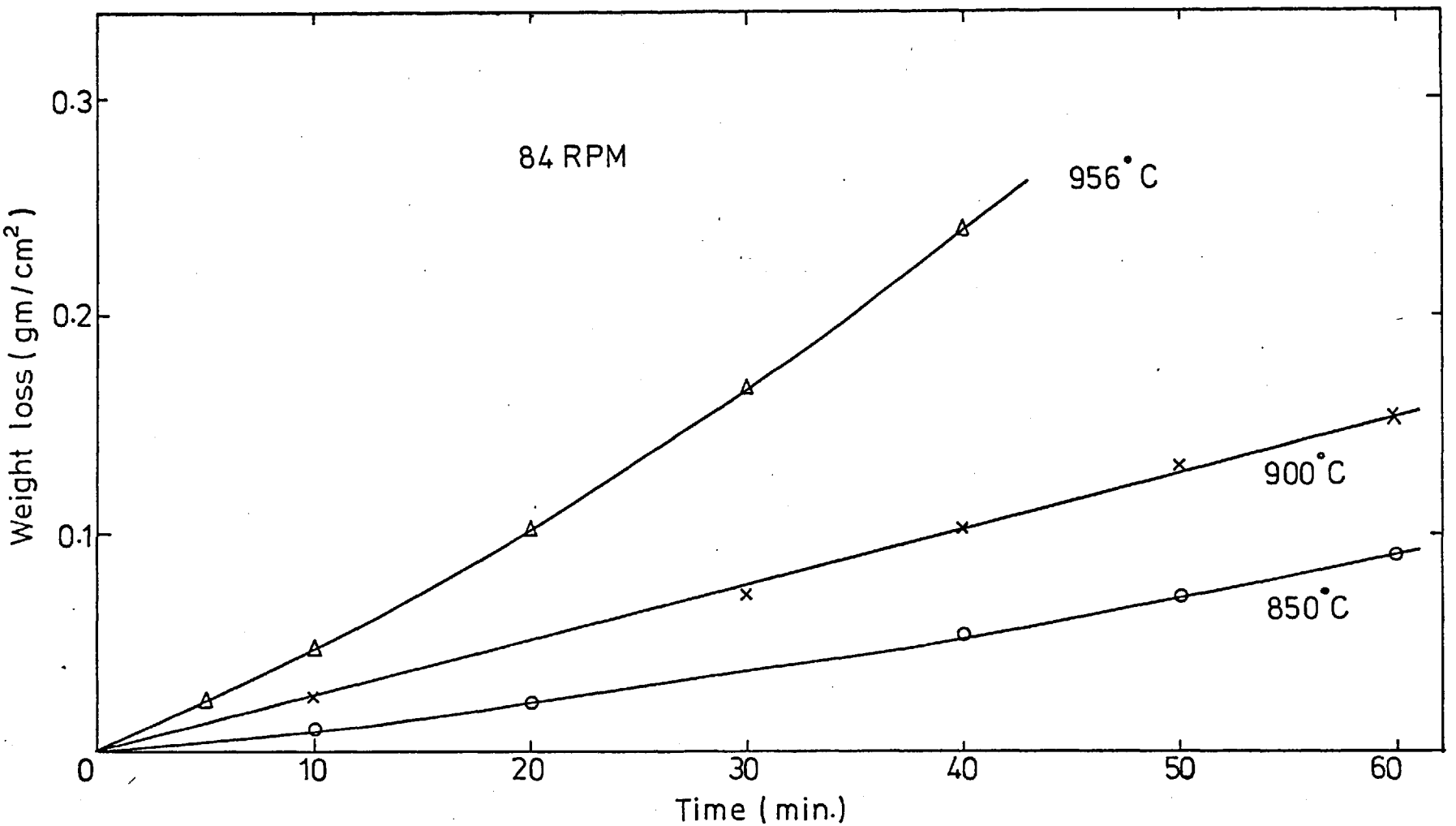

Figure 7.10. Corrosion of 32% porous magnesia with stirring in sodium tetraborate.

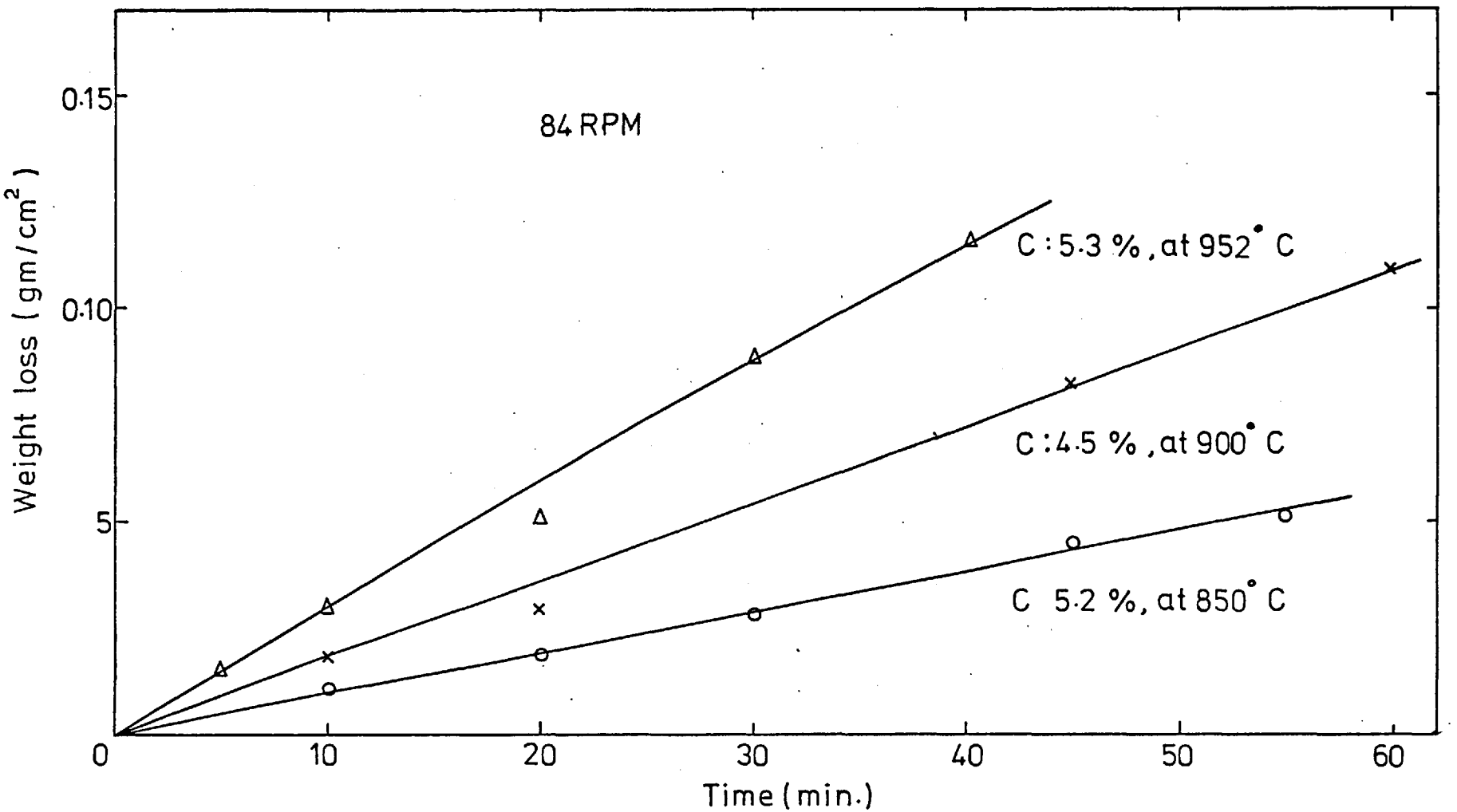

Figure 7.11. Corrosion of carbon-containing magnesia with stirring in sodium tetraborate.

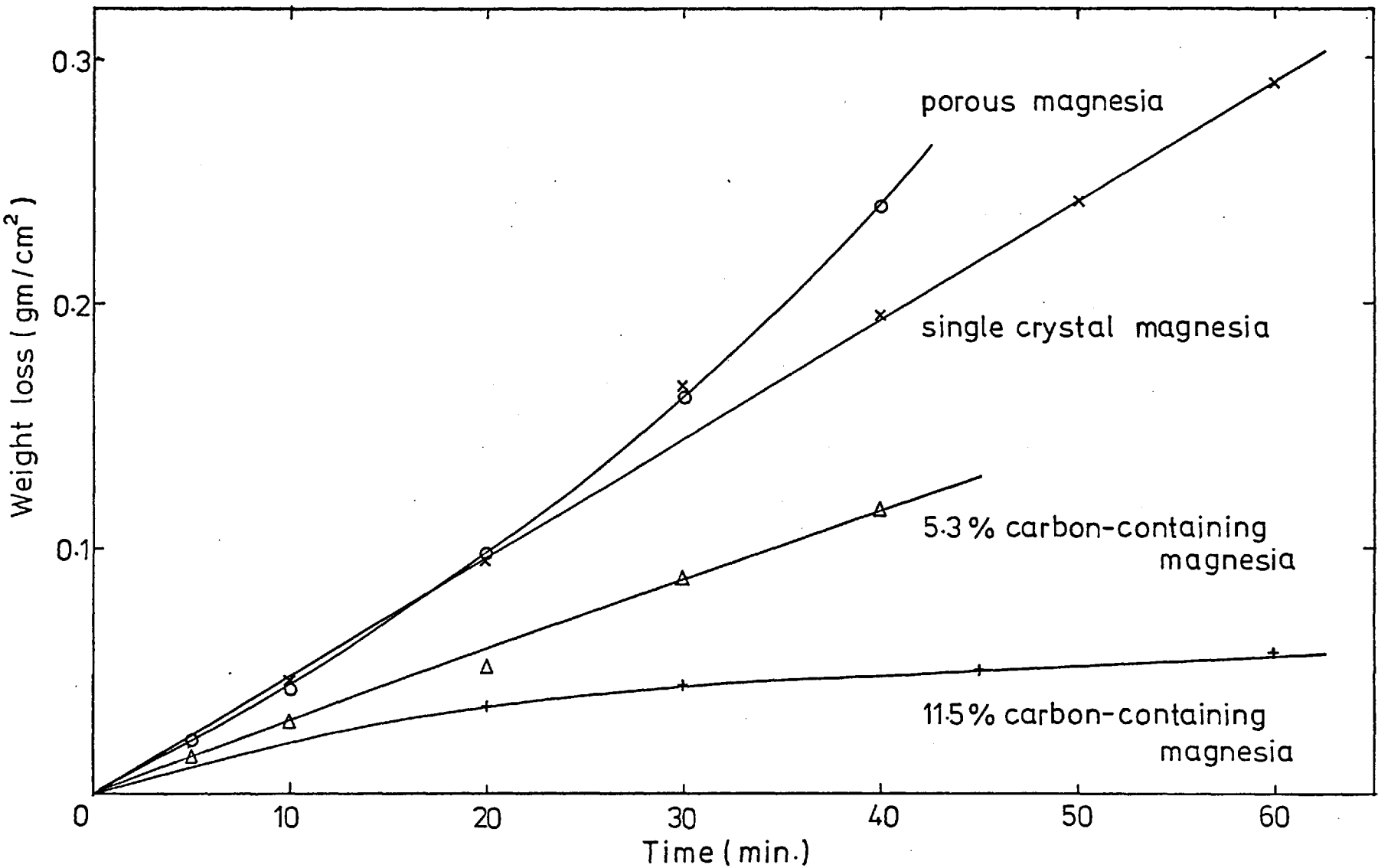

Figure 7·12. Corrosion of single crystal, carbon-containing magnesia and corresponding porous magnesia in sodium tetraborate at 952 - 956° C.

carbon that inhibited melt penetration through the pores. As a consequence, inside the pores would remain in an uncorroded state. Also the carbon would serve for pore blockage as the rate of oxidation of carbon in sodium borate was very slow at the temperature range investigated (up to 952°C). The reaction products evolved during the course of the run - 11.5 weight % of carbon - containing magnesia - is shown in figure 7.13.

During the course of the experiment, the corroded composite specimen - 5.3% carbon - containing magnesia - at 956°C was found to be covered with a carbon layer which was held there even after the corrosion experiment, a photograph of which can be seen in figure 7.14. This fact could account for the curvature shown in figure 7.12. when 5.3 % and 11.5% of carbon was originally present. It is postulated that the emergence of a carbon layer on the surface of the specimen, presumably of a skeletal structure (corresponding to its high porosity) provides the build up of a thicker boundary layer. This will slow up attack.

What is unlikely is that 5.3 weight % of carbon - containing magnesia indicates the greater resistance to corrosion of magnesia compared to that of zero porosity, single crystal magnesia. However, this is resolved when it is borne in mind that the recorded weight losses are of magnesia and that the carbon containing magnesia only exposed 68% of the area to the melt as compared with the single crystal (assuming Rosival's rule).

Table 7.5. shows the weight losses at the four different times calculated from the geometrical area and the microscopical area of magnesia together with those values of single crystal.

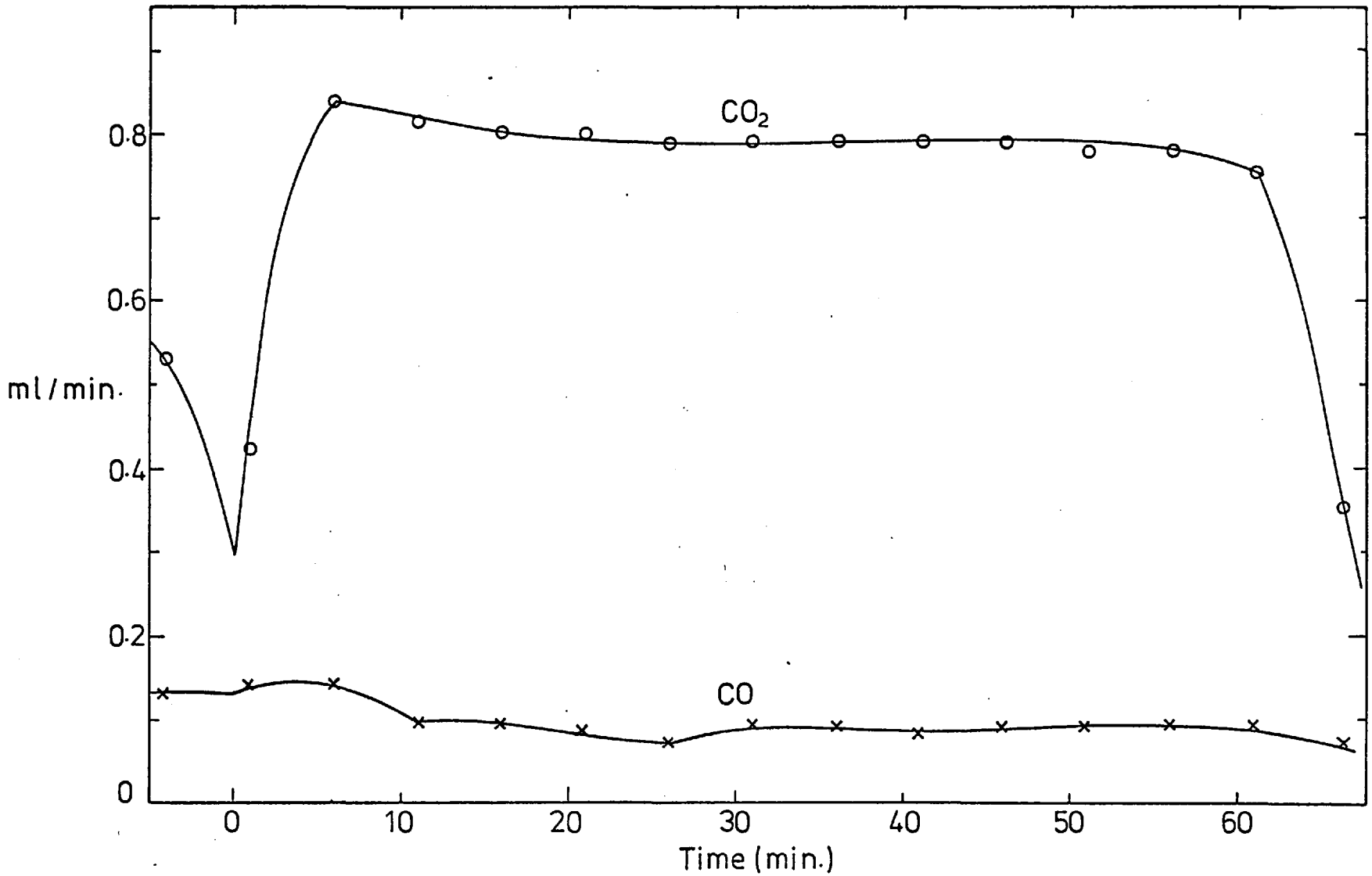

Figure 7.13. Evolution of gases during the corrosion of 11.5 % of carbon-containing magnesia in sodium tetraborate at 952° C.

Figure 7.14. Showing carbon surface on specimen after corrosion testing.

Table 7.5.

Time (Min.)	Carbon - containing magnesia: Wt.loss/ Geometrical area (gm/cm^2)	Carbon - containing magnesia: Wt.loss/ Corrected area (gm/cm^2)	Single crystal: Wt.loss/ Unit area (gm/cm^2)
10	0.030	0.044	0.048
20	0.051	0.075	0.096
30	0.088	0.130	0.146
40	0.116	0.171	0.194

As can be seen from the table, the values of weight loss/corrected area are close to the values of weight loss/unit area of single crystal. Discrepancies and further reduction of corrosion of magnesia by 11.5 weight % of carbon is considered to be due to the effect of the carbon layer explained above.

In conclusion, it may be said that if the carbon sufficiently fills the pores, the rate of magnesia corrosion can be reduced to that of single crystal. An approximate estimation show that about 3.2 weight% of carbon is required to achieve it.

7.3.2. Corrosion of carbon - containing magnesia in sodium metavandate melt

The plots of weight loss/unit area against time for single crystal, and porous polycrystal without and with carbon are shown in figures 7.15., 7.16. and 7.17. respectively. Also plotted in the figure 7.17. is an example of reaction product, CO_2, evolved during the course of run. It is to be noticed that maxima of reaction product evolved was recorded 7 to 8 minutes after the specimen was immersed into the melt as the reaction chamber above the melt had an empty volume of approximately 1 litre.

In contrast to the effect of carbon on the corrosion rate of magnesia in sodium borate melt, carbon in the pores enhanced the rate of corrosion of magnesia in sodium vanadate melt, as the rate of corrosion

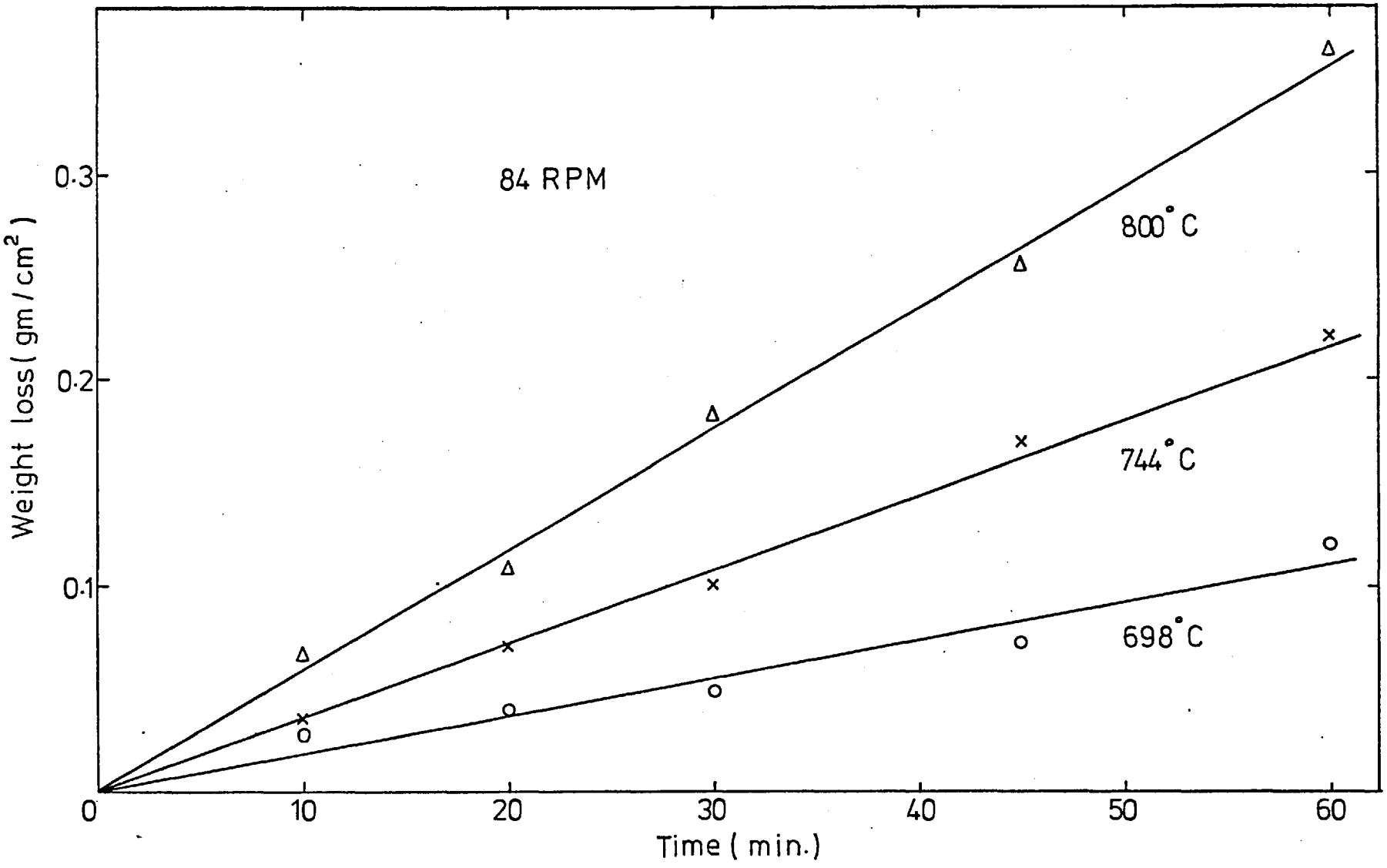

Figure 7.15. Corrosion of magnesia single crystal with stirring in sodium metavanadate.

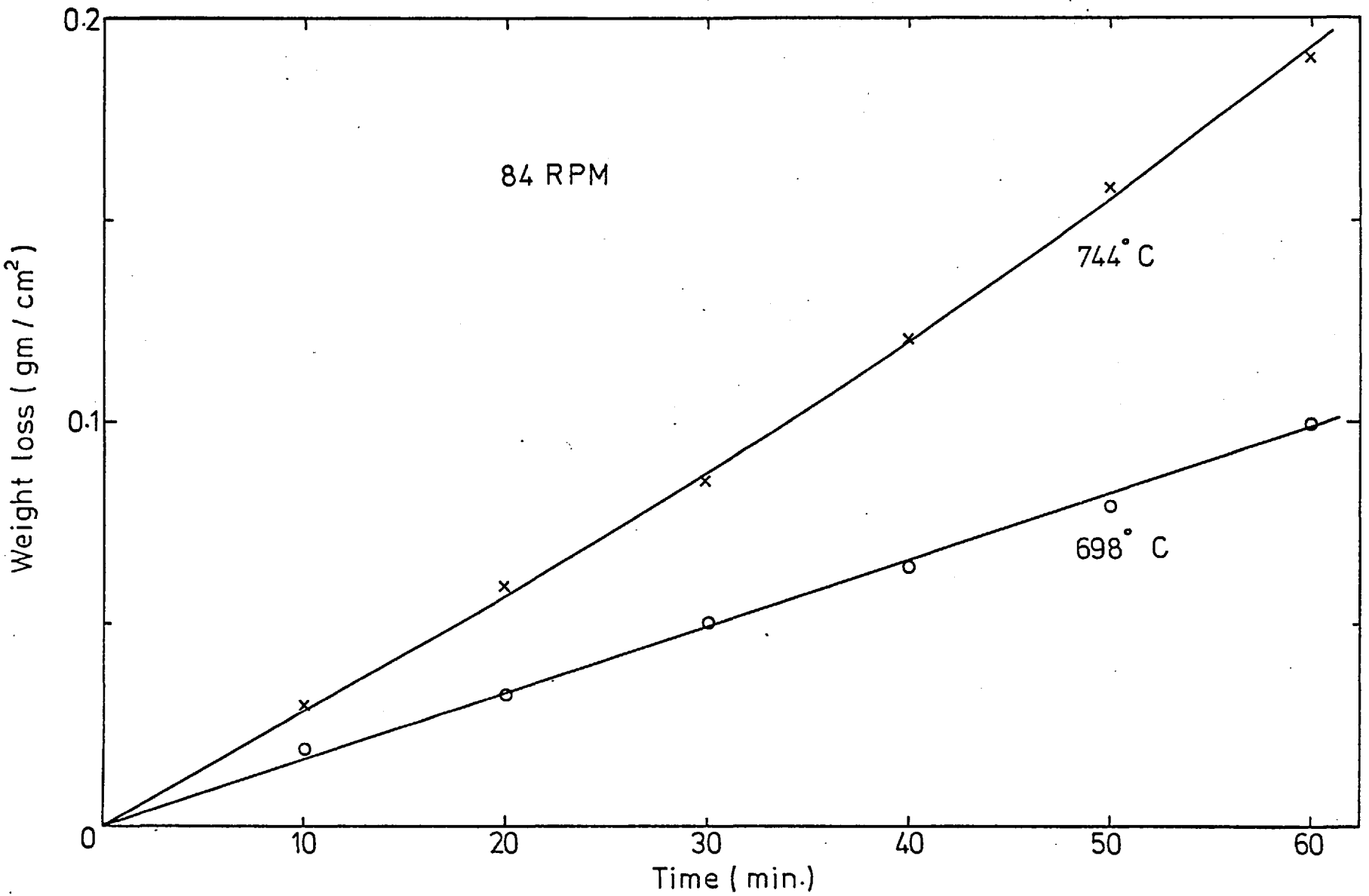

Figure 7.16. Corrosion of 32 % porous magnesia with stirring in sodium metavanadate.

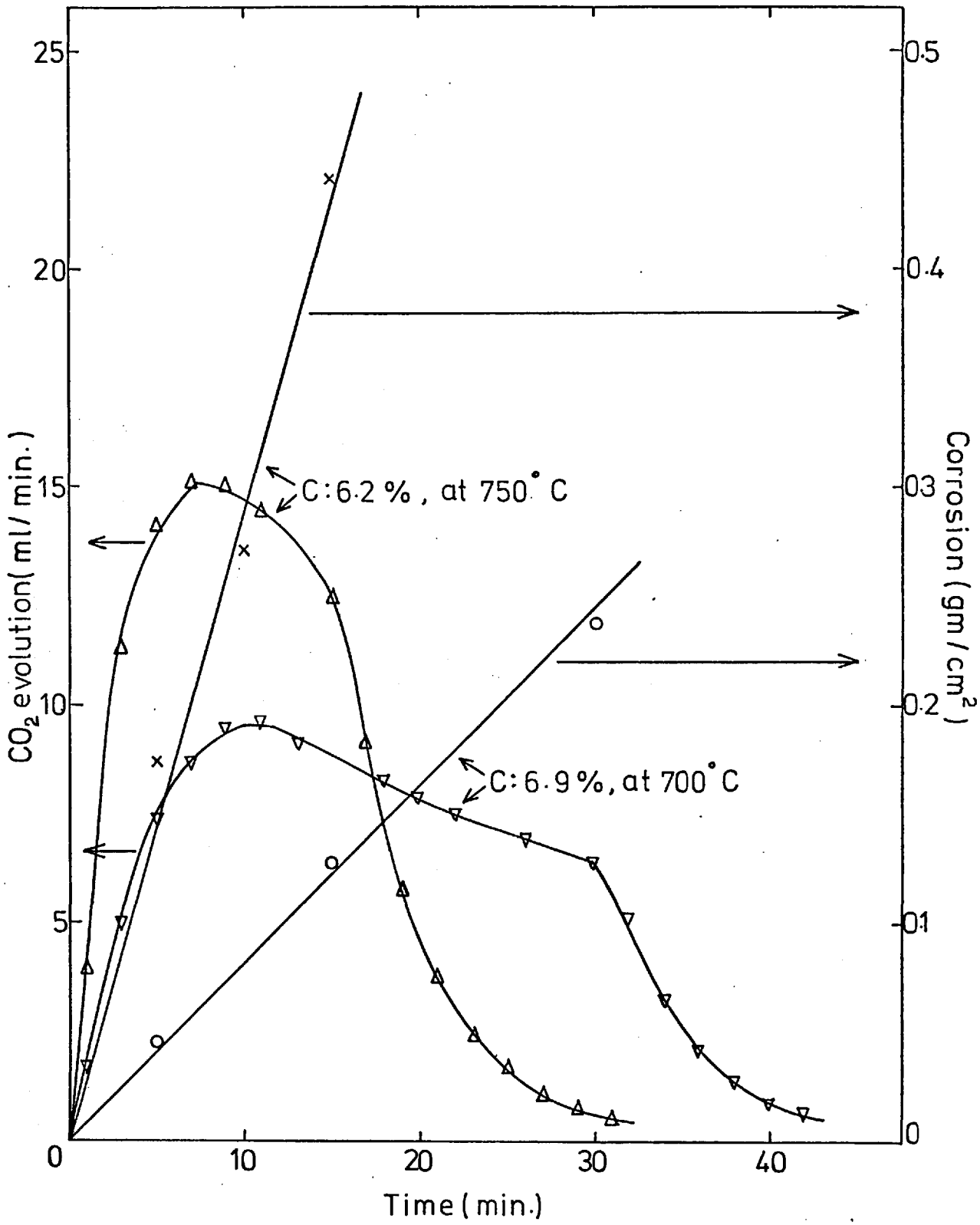

Figure 7.17. Oxidation and corrosion of carbon-containing magnesia in sodium metavanadate at two temperatures.

of magnesia with and without carbon as a function of reciprocal of absolute temperature is shown in figure 7.18. in comparison with those values for single crystal under forced convection (84 RPM).

The plausible reason for enhanced corrosion is considered to be the combination of several factors that will be discussed in turn.

As is well known the reaction $C + O_2 \rightarrow CO_2$ being exothermic ($\Delta H = 94,318$ cal/mol at $1,000^{o}K$) carbon gets hotter than the furnace temperature. Tu, Davies and Hottel (94) reported that the temperature of carbon was $70^{o}C - 110^{o}C$ higher than the ambient furnace temperature when it was being oxidized in air. As figure 7.17. illustrates, the reaction between carbon and $NaVO_3$ produced CO_2 and accordingly was exothermic As a result, the temperature of the specimen and the melt and container would be raised above that of the surrounding furnace with a consequently increased rate of corrosion. To pursue the supposition further, heat balances were made based on the amount of CO_2 produced assuming that the heat liberated heats up either the specimen (ΔT_2) or the melt and container (ΔT_3). It should be noted that the specimen would be to some extent insulated from the melt by the layer of bubbles of CO_2 on it. These values were then compared with the values (ΔT_1) extracted from the figure 7.18., by reading off the temperature for the corrosion of porous magnesia equivalent to the corrosion of carbon - containing magnesia. No account was taken of the heat carried away from the system by gas bubbles or by radiation, convection and conduction to the furnace interior.

As calculations show in Appendix , the enhanced rate of corrosion of magnesia when carbon is present is proportional to the amount of carbon oxidized. It is conceivable that the rises in temperature of $109^{o}C$ and $177^{o}C$, necessary to produce the enhanced rates of dissolution, actually occured in the specimens, but one would expect such large temperature rises in the specimens to result in heat being conveyed to the melt and crucible

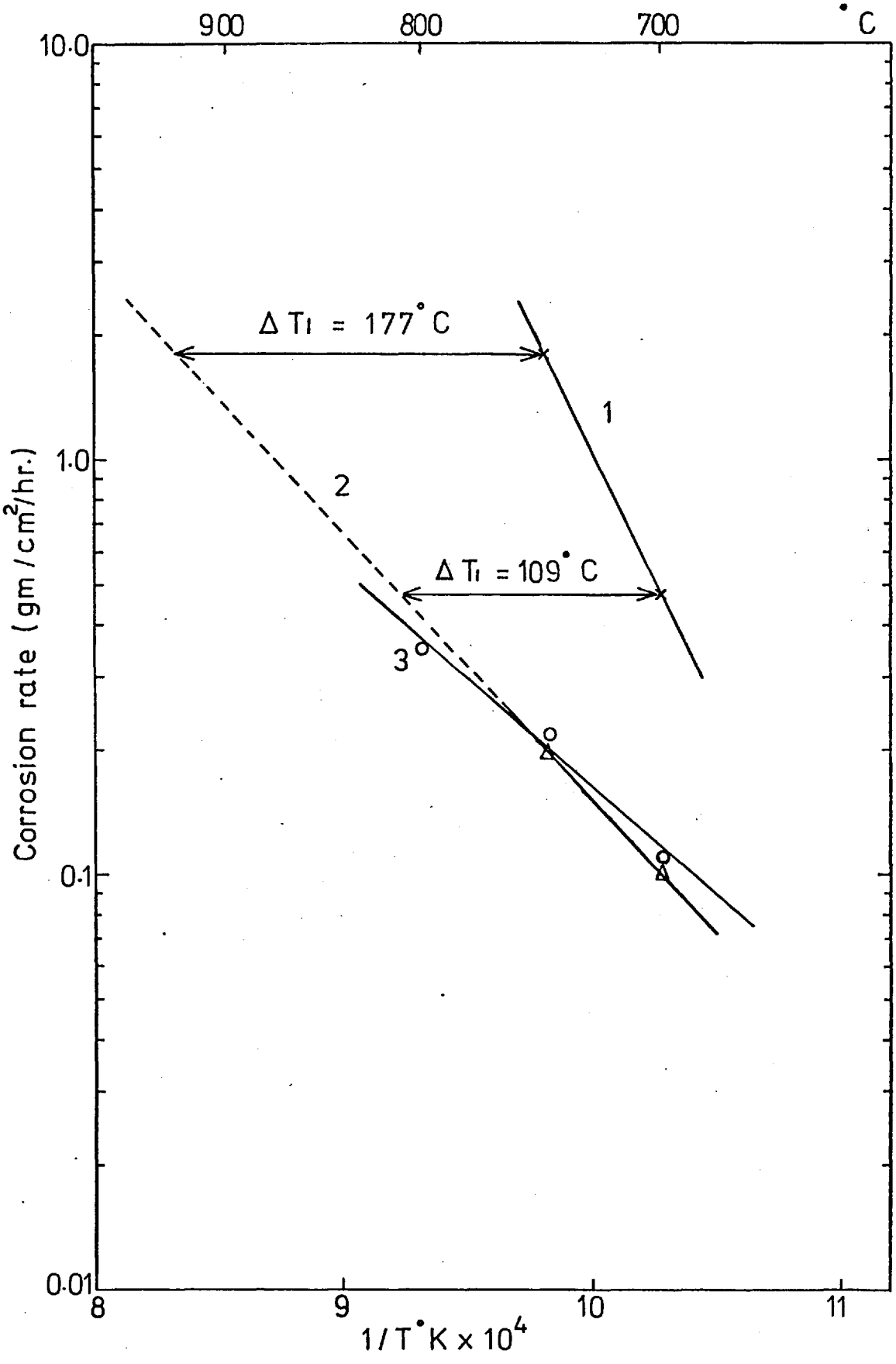

Figure 7.18. Plot of Log corrosion rate against reciprocal of absolute temperature for 1) carbon-containing magnesia 2) corresponding porous magnesia 3) single crystal magnesia.

because stirring was in progress. This is confirmed by small rises observed in the melt of 5 - 7°C when the carbon was oxidized.

As is also well known, release of bubbles introduced extra convection current into the melt. Then one would expect increased corrosion due to thinning effect of the diffusion layer resulted from accelerated convection current. Assuming the dependence of the corrosion rate on the square root of stirring rate (RPM) as discussed in the section 7.2., the increased rates of corrosion were converted to equivalent stirring speed and listed below compared with the rate of CO_2 evolution.

	MgO corrosion rate $gm/cm^2/min$	Estimated RPM	CO_2 ml/15 min
750°C	0.0294	10,609	1.032
700°C	0.0079	2,916	547

Although it could be said that non-direct relationship between the estimated stirring speed and the amount of gas evolved does not support this consideration strongly, the direction of the increase is suggestive of its feasibility.

Previous work (39) has shown that the melt of composition equivalent to sodium - vanadyl - vanadate ($Na_2O\ V_2O_4\ 5V_2O_5$) was more corrosive than sodium metavanadate. This is connected with the ease with which vanadium IV may be oxidized to vanadium V. Since the sodium metavanadate was reduced by carbon in the pores of magnesia, it may be postulated that the oxidation of reduced melt may enhance the rate of corrosion.

Increased corrosion due to hypothetical reaction product discussed in the chapter 5, namely carbonate anion, evolved by the oxidation of carbon in the melt could also be considered as a possible reason. Unfortunately, the corrosion rate of magnesia in sodium carbonate is not available. However, the corrosion of alumina in both melts was studied by Faruqi (32)

who reported that the rate in sodium carbonate melt is far less than the rate in sodium vanadate melt, i.e. 0.00006 gm/cm^2/min for the former process and 0.00028 gm/cm^2/min for the latter process at 1,000^{o}C. If the rate of magnesia corrosion was similar with alumina in both melts, then this supposition would be highly unlikely.

In conclusion, it may be said that carbon in the pores enhances the rate of corrosion of magnesia due to direct oxidation of carbon by the melt, although considerably more work needs to be done to draw definite conclusions for enhanced corrosion.

7.3.3. Corrosion of carbon - containing magnesia in sodium disilicate melt

The plots of weight loss/unit area for porous magnesia containing varying amount of residual carbon against time in sodium disilicate melt are shown in figure 7.19. and 7.20. at 1,300^{o}C and 1,350^{o}C in comparison with the values for single crystal.

As readily seen from the figures, successive additions of residual carbon content reduced the corrosion rate of magnesia indicating the carbon was effective. The importance of residual carbon content had already been reported in the literature. Hubble and Kappmeyer (50) observed refractories containing high residual carbon contents up to about 4% had better slag resistance from their simulative BOF slag test. Later Hubble (49) observed refractories containing more than 4% up to 12% have not given any improvement in slag resistance. Herron, Beechan and Padfield (43) concluded that at least 3% of residual carbon content is required to minimize slag migration from microscopic examination of corroded carbon-bearing magnesite refractories. Although direct comparison between these observations and present results could not be made because of difference in experimental condition, refractory properties and slag compositions, present results largely supports earlier observations. Table 7.6. list the residual carbon content, the rate of magnesia corrosion compared

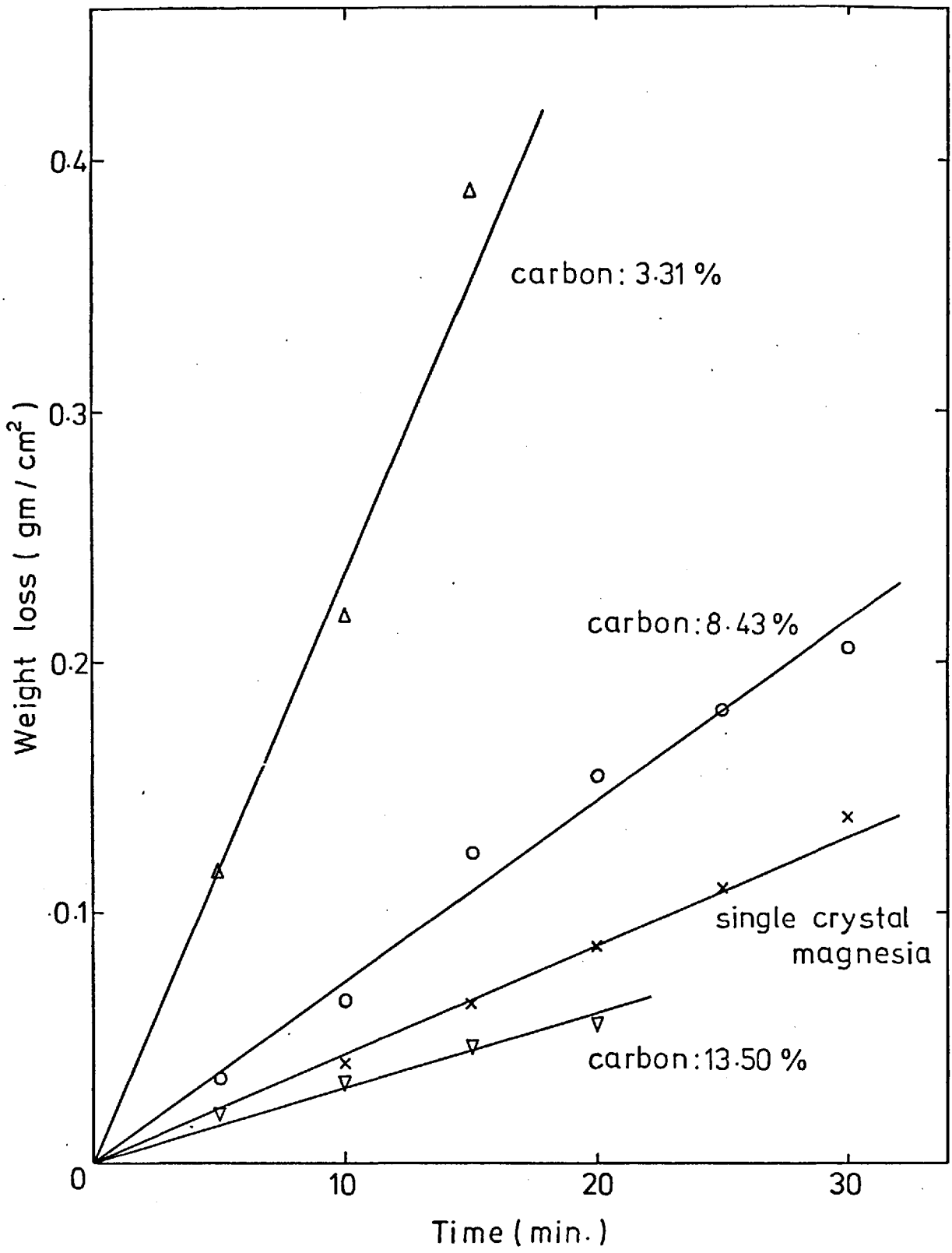

Figure 7·19. Corrosion of carbon-containing magnesia in sodium disilicate at 1·300° C.

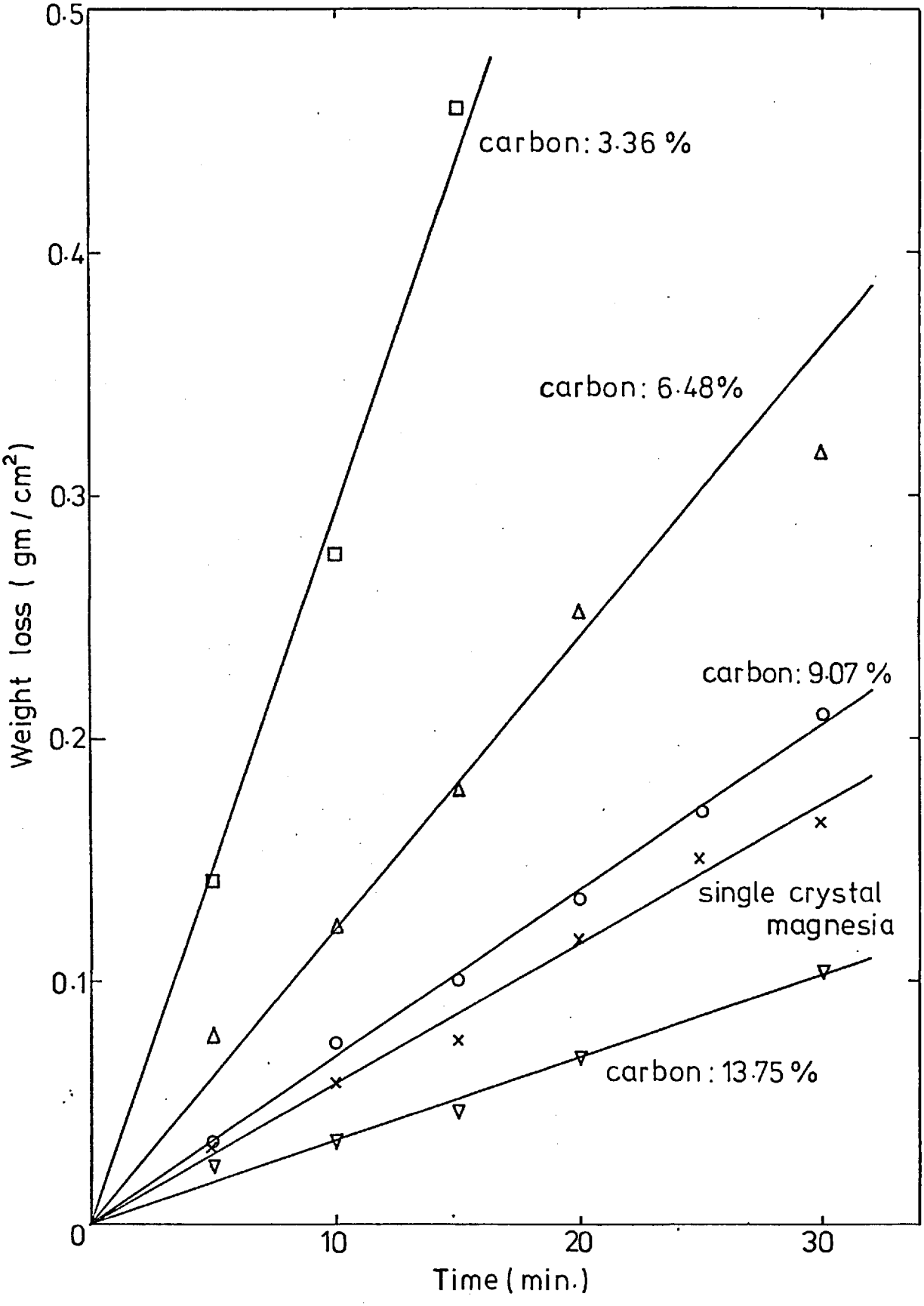

Figure 7·20. Corrosion of carbon-containing magnesia in sodium disilicate at 1·350° C.

with the amount of carbon oxidized per minute. Also compared is the porosity of the residual carbon in the pores of magnesia calculated as follows:

$$B.D. = \frac{M}{V}$$

$$\text{Porosity } (\%) = (1 - \frac{B.D.}{T.D.})100$$

Where B.D. = bulk density of carbon (gm/cm^3)

T.D. = true density of carbon - 2.25 gm/cm^3 (98)

M = mass of carbon (gm)

V = volume of the pores (cm^3).

Table 7.6.

Temperature °C	C content %	Porosity of C %	C oxidation mg/min	MgO corrosion $gm/cm^2/min$
1,300	3.31	88.2	3.91	0.0237
	8.43	68.7	3.29	0.0073
	13.50	51.3	3.28	0.0029
1,350	3.36	88.9	4.19	0.0295
	6.48	77.1	2.90	0.0121
	9.07	66.5	3.50	0.0069
	13.75	50.5	3.03	0.0035

From the table, it can be seen that the more porous the carbon the greater the amount of carbon oxidized. This would mean that porous residual carbon exposed larger surface area than less porous carbon to be oxidized by the melt. In other words, the melt penetration was greater with the specimen containing less residual carbon content, since the residual carbon content (%) is reciprocally related to the porosity of carbon as shown in the table 7.6. This consideration suggests that the more the melt penetrated through the pores, the greater the rate of magnesia corrosion. Comparison of the rate of magnesia corrosion to the

residual carbon content also listed in the table, substantiates this remark.

The oxidation of carbon following is shown in figures 7.21. and 7.22. Although the work of Pickering and Batchelor (72) has shown that the significant internal reaction between carbon and magnesia can occur above 1,400°C, a small amount of carbon removed by this reaction at the experimental temperature range 1,300°C - 1,350°C was anticipated. In order to elucidate how the carbon was removed, a separate identical run was carried out without the melt. These are also included in figures 7.21. and 7.22. As is shown, the amount of carbon removed by the reduction of MgO amounts to about 15% of the total carbon oxidized. It indicates that the majority of carbon was removed by the melt and the carbon removed by the reduction of magnesia is minor.

The effect of temperature rise due to the carbon oxidation in $Na_2Si_2O_5$ melt was also considered. The values of heat liberated and equivalent values of temperature rise of the melt (ΔT) are calculated and tabulated in table 7.7. compared to the values for $NaVO_3$ and $Na_2B_4O_7$. Also listed in the table are the reaction products, CO/CO_2 ratio.

Table 7.7.

Temperature °C	Melt	C content %	Heat liberated cal	ΔT* °C	CO/CO_2
700	$NaVO_3$	6.9	547	∿ 8	0.002
750	$NaVO_3$	6.2	1,031	∿16	0.001
952	$Na_2B_4O_7$	11.50	54	∿ 1	0.13
1,300	$Na_2Si_2O_5$	3.31	246	∿ 3	1.96
1,300	$Na_2Si_2O_5$	8.43	169	∿ 2	3.79
1,300	$Na_2Si_2O_5$	13.50	183	∿ 2	2.95
1,350	$Na_2Si_2O_5$	3.36	212	∿ 3	4.24
1,350	$Na_2Si_2O_5$	6.48	148	∿ 2	4.16
1,350	$Na_2Si_2O_5$	9.07	177	∿ 2	4.03
1,350	$Na_2Si_2O_5$	13.75	165	∿ 2	3.25

* ΔT values were calculated by the method used above and fully explained

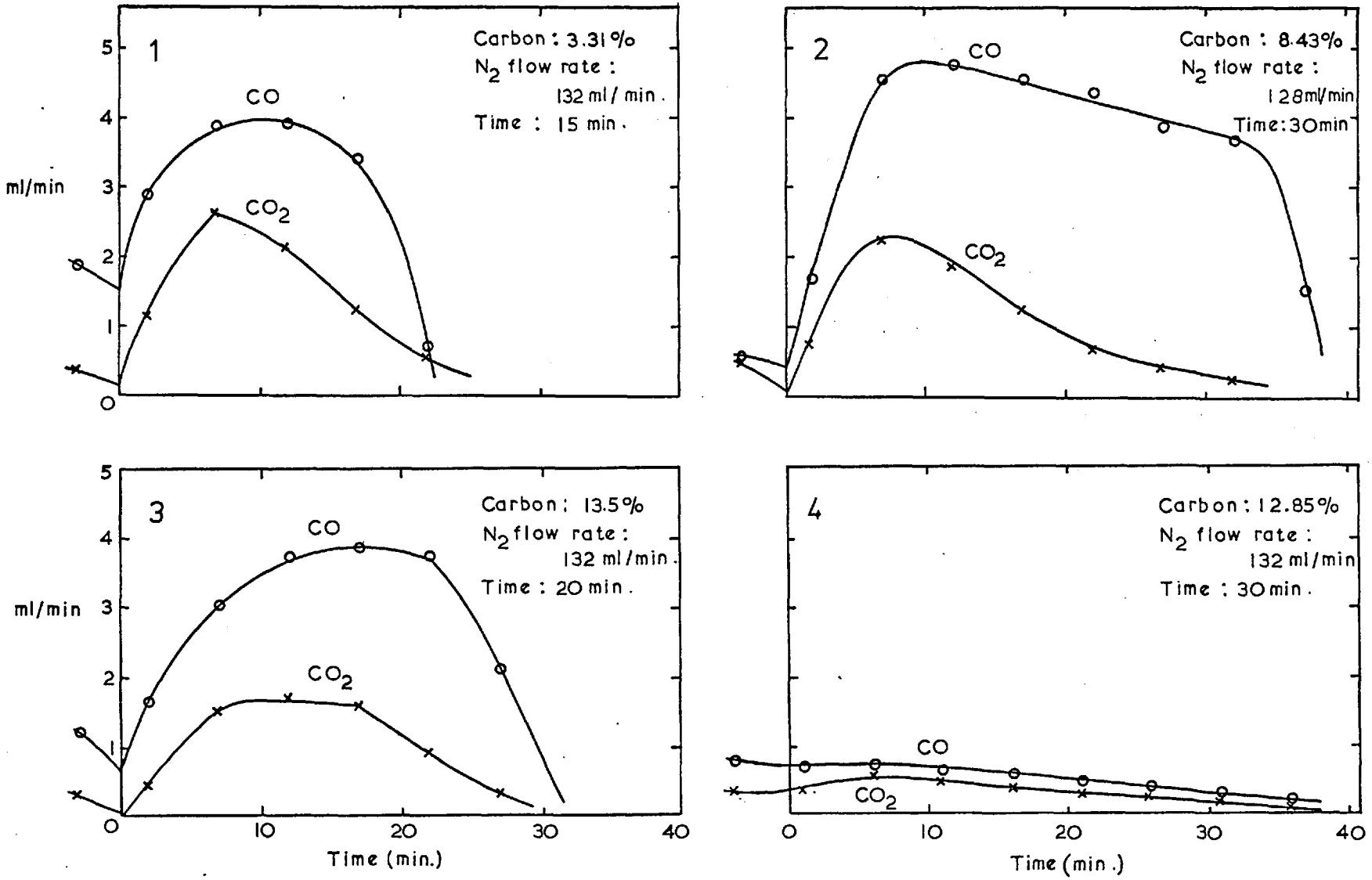

Figure 7.21. Evolution of gases during the corrosion of carbon-containing magnesia in sodium disilicate (1,2,3) and in N_2 without the melt (4) at 1.300° C.

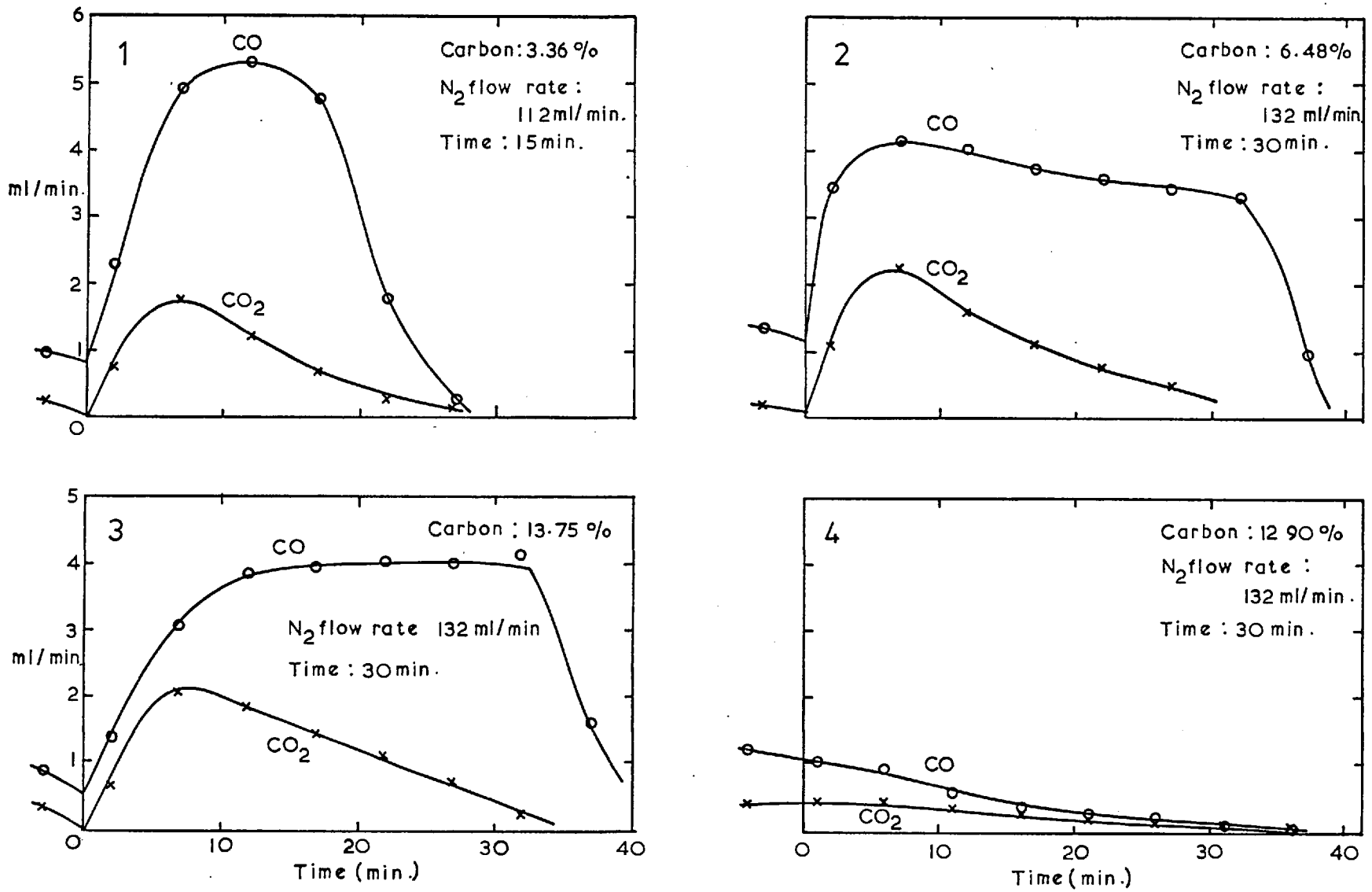

Figure 7.22. Evolution of gases during the corrosion of carbon-containing magnesia in sodium disilicate (1, 2, 3) and in N_2 without the melt (4) at 1.350 °C.

in Appendix. The values of true specific heat (C_p) for $Na_2B_4O_7$ and $Na_2Si_2O_5$ were calculated by the relationship given by Sharp and Ginther (86),

$$C_p = \frac{0.00146at^2 + 2at + C_0}{(0.00146t + 1)^2}$$

where, a and C_0 were factors (given below) for calculation of C_p of glass from the composition.

Oxide	a	C_0
SiO_2	0.000468	0.1657
Na_2O	0.000829	0.2229
B_2O_3	0.000635	0.1980

The table shows that the temperature rise of $Na_2Si_2O_5$ is considerably less than the values for $NaVO_3$. This led the author to speculate about the effect of carbon as follows. If the carbon is inert to the melt, the carbon is most effective and reduces the rate of corrosion due to the effect of reduced surface area, i.e. carbon - containing magnesia in sodium borate melt. If the carbon was oxidized by the melt, there may be competition between temperature rise and disturbance of boundary layer due to the carbon oxidation that would tend to enhance the rate of corrosion, and reduced surface area effect due to inhibited melt penetration that would tend to reduce the rate of corrosion. The deciding factor here would mainly be of the rate of oxidation by a melt. Experimental results seem to indicate that the former effect was operative in $NaVO_3$ melt, whilst the latter effect was operative in $Na_2Si_2O_5$ melt. Such a mechanism involving the oxidation of carbon by the slag as the rate - controlling factor in the corrosion rate of carbon - bearing basic refactories was proposed earlier by Carr, Evans, Leonard and Richardson (14).

The effect of carbon in porous magnesia with respect to the rate of magnesia corrosion in sodium silicate melt is summarized in figure 7.23.

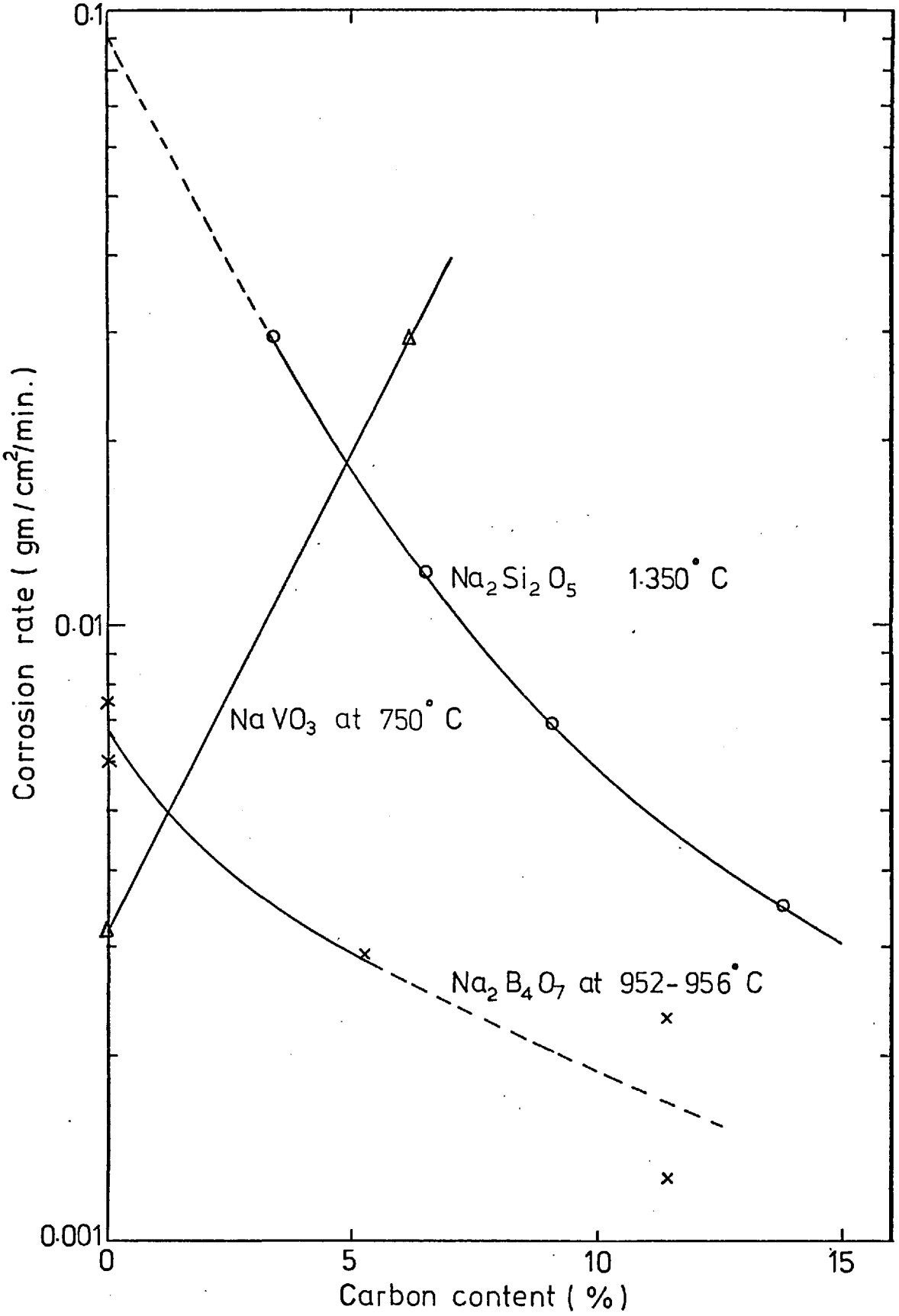

Figure 7·23. Effect of varying carbon content on the rate of corrosion.

compared with figures for sodium borate and sodium vanadate melts. As described previously, it can be noticed that the carbon was effective in both borate and silicate melts, whereas the effect of carbon is otherwise in vanadate melt. Similar treatment of reduced corrosion rate due to reduced surface area effect, as was done for sodium borate melt, show that about 12.5 weight % carbon was required to reduce the rate to the same value as that of single crystal, whilst only about 3.2 weight % of carbon was required for sodium borate melt. The reason for the greater amount of carbon needed for silicate melt is attributed to the greater oxidation rate of carbon in the melt at 1,350^{o}C than in borate melt at 952^{o}C.

SUMMARY

I. Magnesia corrodes in sodium borate, sodium silicate and sodium vanadate by diffusion control. The evidence for this was that the rate of corrosion was increased with the speed of stirring of the melt. Magnesia corrosion in sodium borate melt was studied in detail. This study revealed that,

1) the rate of corrosion was dependent on the square root of the stirring speed;
2) the recession of the face of an immersed slab in the melt under natural convection was proportional to the reciprocal of the fourth root of the distance from the leading edge as predicted by a mass transfer theory;
3) there was enhanced corrosion at the flux line.

II. The effect of carbon in the pores of refractory with respect to the corrosion rate of refractory can be summarized as follows:

Carbon reduces the corrosion rate, as it blocks melt penetration through the pores, of porous refractory in melts. If oxidation of carbon is negligiable, a small amount of carbon is required to reduce the rate of corrosion to as low as that of single crystal. If, however, the carbon is oxidized by a melt, a greater carbon content is required to compensate for the carbon removed. However, if carbon reacts with the melt vigorously carbon enhances the rate of corrosion of porous refractory.

APPENDIX

Calculations of temperature rise of the specimen (ΔT_2) and the melt and container (ΔT_3) due to exothermic reaction of carbon with $NaVO_3$ melt (See section 7.3.2.)

At 700°C

ΔT_1 : Temperature rise extracted from the figure 7.18. by reading off the temperature for the corrosion of porous magnesia equivalent to the corrosion of carbon-containing magnesia = 109°C

ΔT_2 : The amount of CO_2 produced, 130 ml for 15 minutes (see figure 7.17.), is equivalent to 0.0696 gm of carbon which liberates 547 cal*. And if 547 cal heats up 2.5 gm of MgO

$$547 \text{ cal} = 2.5 \times Cp \text{ of MgO} \times \Delta T_2$$

where, Cp of MgO = 0.3 (40)

$$\therefore \Delta T_2 = 729.3^{\circ}C$$

ΔT_3 : If 547 cal heats up 200 gm of melt and container

$$547 \text{ cal} = 200 \times Cp \text{ of } NaVO_3 \times \Delta T_3 + 165 \times 2/3 \times Cp \text{ of Pt.container} \times \Delta T_3$$

where, Cp of $NaVO_3$ = 0.3†

Cp of Pt. = 0.0360 (51)

$$\therefore \Delta T_3 = 8.6^{\circ}C$$

At 750°C

ΔT_1 : Temperature rise obtained as explained above = 177°C

ΔT_2 : The amount of CO_2 produced, 245 ml for 15 minutes (see figure 7.17.), is equivalent to 0.1312 gm of carbon which liberates 1.032 cal*. And if 1.032 heats up 2.5 gm of MgO

$$1.032 = 2.5 \times Cp \text{ of MgO} \times \Delta T_2$$

$$\Delta T_2 = 1376.0^{\circ}C$$

ΔT_3 : If 1.032 cal heats up 200 gm of melt and container

$$1.032 \text{ cal} = 200 \times Cp \text{ of } NaVO_3 \times \Delta T_3 + 165 \times 2/3 \times Cp \text{ of Pt. container} \times \Delta T_3$$

where, Cp of Pt. = 0.0365 (51)

$$\therefore \Delta T_3 = 16.1^{\circ}C$$

* ΔH for CO_2 at 700°C : 94.306 cal/mol
  ΔH for CO_2 at 750°C : 94.320 cal/mol (81)

† As Cp of $NaVO_3$ was not available in literature, the value of 0.3 was evaluated by taking atomic heat of oxy-salts as approximately 7 cal/mol i.e.

	Heat Content	Atomic Heat
$NaNO_3$	31.5 or 37.0	6.3 or 7.4
Na_2CO_3	46.6	7.8
Na_2SO_4	47.2	6.7

This gives a heat content of liquid $NaVO_3$, 7 x 5 = 35 cal/mol. Then a specific heat in the liquid state is approximately 35/122 = 0.3 cal/gm.

REFERENCES

1. Arthur, J.R., Trans.Faraday Soc., 47, 164, 1951
2. Barham, D., Ph.D. Thesis, University of London, 1964
3. Barrett, L.R., Ford, W.F. and Green, A.T., Trans. Inst. Gas Engrs., 93, 222, 1943-4
4. Barthel, H., Ber.Deutch.Keram.Ges., 47, (7), 402, 1970
5. Barthel, H., Stahl und Eisen, 86, 81, 1966
6. Bigg, P.H., J.of Anal.Phys., 15 , 1111, 1964
7. Bircumshaw, L.L. and Riddiford, A.C., Rev.Chem.Soc., 6, 157, 1952
8. Blyholder, G. and Eyring, H., J.Phys.Chem., 61, 682, 1957
9. Bockris, J.O.M., Mackenzie, J.D. and Kitchener, J.A., Trans.Faraday Soc., 51, 1734, 1955
10. Brezny, B. and Landy, R.A., Trans.Brit.Ceram.Soc., 71, 163, 1972
11. Cable, M. and Martlew, D., Glass Technol., 12, (6), 142, 1971
12. Cable, M., The University of Sheffield, Private Communication
13. Carniglia, S.C., Amer.Ceram.Soc.Bull., 52, (2), 160, 1973
14. Carr, K., Evans, J.L., Leonard, L.A. and Richardson, H.M., Trans.Brit.Ceram.Soc., 64, 473, 1965
15. Chesters, J.H., 'Refractories for iron - and steelmaking' The Metal Society, London, 1974
16. Chesters, J.H., Iron and Steel Inst.Spec.Rep., 74, Discussion p.26, 1962
17. Chumarev, V.M. and Okunev, A.I., Dokl.Akad.Nauk.USSR, 170, (5), 1143, 1966
18. Chumarev, V.M. and Vlasova, T.F., 1ZV.Akad.Nauk.USSR, 5, 23, 1969
19. Comeforo, J.E. and Harsh, R.K., J.Amer.Ceram.Soc., 35, (6), 130 and 142, 1952
20. Cooper, A.R. and Kingery, W.D., 'Kinetics of high-temperature processes', Kingery W.D., Ed., John Wiley and Sons, Inc., New York, 1959
21. Cooper, A.R. and Kingery, W.D., J.Amer.Ceram.Soc., 47, 37, 1964
22. Cooper, A.R. and Kingery, W.D., J.Phys.Chem., 66, 665, 1962
23. Dancy, T.E., J.Iron Steel Inst., 169, 17, 1951

24. Davies, M.W., Hazeldean, G.S.F. and Smith, P.N., 'Physical chemistry of process metallurgy': the Richardson conference, Jeffes, J.H.E. and Tait, R.J., Ed., The Institution of Mining and Metallurgy, London, 1974

25. Day, R.J., Ph.D. Thesis, The Pennsylvania State University, 1949: quoted in reference 97

26. Dodd, A.E. and Green, A.T., Iron and Steel Inst.Spec.Rep. 26, 127, 1939

27. Doremus, R.H., 'Modern aspects of the vitreous state', Mackenzie, J.D., Ed., Vol.2, 1, Butterworths, London, 1962

28. Elwell, W.T. and Gidley, J.A.F., 'Atomic - absorption spectrophotometry' Pergamon press, Oxford, 1961

29. English, S., J.Soc.Glass Tech., 8, (31), 205, 1924

30. Ephraim, F., 'Inorganic Chemistry', Thorne, P.C.L. and Roberts, E.R., Ed., p.154, Oliver and Boyd, London, 1954

31. Faktor, M.M., Fiddyment, D.G., Newns, G.R., J.of Electrochem.Soc., 114, (4), p.356, 1967

32. Faruqi, F.A., Ph.D. Thesis, University of London, 1960

33. Fay Fun, Met.Trans., 1, 2537, 1970

34. Field, M.A., Gill, D.W., Morgan, B.B. and Hawksley, P.G.W., 'Combustion of pulverised coal', B.C.U.R.A., Leatherhead, 1967

35. Flood, H. and Seltveit, A., Kgl.Norske.Forth, 28, 150, 1955

36. Fulton, J.C. and Chipman, J., Trans. A.I.M.E., 215, 888, 1959

37. Gilbert, V. and Batchelor, J.D., Amer.Ceram.Soc.Bull., 50, (2), 1971

38. Goldman, M.R., Ph.D. Thesis, University of London, 1963

39. Gravette,N.C.,Ph.D. Thesis, University of London, 1968

40. Green, A.T., Trans.Brit.Ceram.Soc., 22, 393, 1923

41. Haxell, J.P.N., Ph.D. Thesis, University of London, 1972

42. Heidtkamp, G. and Endell, K., Glastech.Ber., 14, 89, 1936 : quoted in Morey, G.W., 'The properties of glass', p.261, Reinhold Publishing Corporation, New York, 1938

43. Herron, R.H., Beechan, C.R., and Padfield, R.C., Amer.Ceram.Soc.Bull., 46, (12), 1163, 1967

44. Herron, R.H. and Runk, E.J., Amer.Ceram.Soc.Bull,, 48, (11), 1049, 1969

45. Heuchamps, C. and Duval, X., Carbon 4, 243, 1966

46. Hill, B., Ph.D. Thesis, University of London, 1963

47. Hlavac, J. and Strnad, P., Silikaty, 5, 302, 1961

48. Hrma, P., Chem.Eng.Sci., 25, 1679, 1970

49. Hubble, D.H., Amer.Ceram.Soc.Bull., 47, (2), 170, 1968

50. Hubble, D.H. and Kappmeyer, K.K., Amer.Ceram.Soc.Bull., 45, (7), 646, 1966

51. Jaeger, F.M., 'Optical Activity and high tempearture measurements', p.367, McGraw-Hill Book Company Inc., New York, 1930

52. Janz, G.J. Molten Salts Handbook, p.55, Academic Press, New York, 1967

53. Kappmeyer, K.K. and Hubble, D.H., 'High-temperature oxides', part 1, Alper, A.M., Ed., Academic Press, 1970

54. Khundkar, M.H., Ph.D. Thesis, University of Durham, 1949

55. Komarek, K.L., Coucoulas, A. and Klinger, N., J.Electrochem.Soc., 110, (7), 783, 1963

56. Lambertson, W.A., Amer.Ceram.Soc.Bull., 28, (7), 260, 1949

57. Leonard, R.J. and Herron, R.H., J.Amer.Ceram.Soc., 55, (1), 1, 1972

58. Lester, M. and Cooper, S.C., Trans.Brit.Ceram.Soc., 75, 12, 1976

59. Levich, V.G., 'Physiocochemical Hydrodynamics', Prentice-Hall, New Jersy, 1962

60. Levin, E.M., Robbins, C.R. and McMurdie, H.F., 'Phase diagrams for ceramists', Reser, M.K., Ed., p.181, The Amer.Ceram.Soc., 1964

61. Lewis, J.B., 'Modern aspects of graphite technology', Blackman, L.C.F., Ed., Academic Press, London, 1970

62. Mackenzie, J.D., Chem.Rev., 56, 455, 1956

63. Mackenzie, J.D., 'Modern aspects of the vitreous state', Mackenzie, J.D., Ed., Vol.1, 188, Butterworths, London, 1960

64. McCallum, N., Ph.D. Thesis, University of London, 1950

65. Moroney, M.J., 'Facts from figures', p.64, Penguin books, 1951

66. Nacamu, R.L. and Batchelor, J.D., Amer.Ceram.Soc.Bull., 54, (7), 1975

67. Ohba, H., Ikenoue, T. and Nishikawa, Y., Iron and Steel Inst.Spec.Rep., 74, p.55, 1962

68. Palin, F.T. and Richardson, H.M., Trans.Brit.Ceram.Soc., 71, 37, 1972

69. Park, H.K., M.Phil. Thesis, University of London, 1972

70. Pask, J.A. and Parmelee, C.W., J.Amer.Ceram.Soc., 26, (8), 267, 1943

71. Perron, P.O. and Bell, H.B., Trans.Brit.Ceram.Soc., 66, 347, 1967

72. Pickering, G.D. and Batchelor, J.D., Amer.Ceram.Soc.Bull., 50, (7), 611, 1971

73. Price, W.J., 'Analytical atomic absorption spectrometry', p.201, Heyden and sons Ltd., London, 1972

74. Reed, L., Ph.D. Thesis, University of London, 1952

75. Reed, L. and Barrett, L.R., Trans.Brit.Ceram.Soc., 54, 671, 1955

76. Reed, L. and Barrett, L.R., Trans.Brit.Ceram.Soc., 63, 509, 1964

77. Richardson, F.D.,'Physical chemistry of melts in metallurgy' Vol.1, Chapter 3, Academic Press, London, 1974

78. Richardson, F.D.,'Physical chemistry of melts in metallurgy' Vol.2, Chapter 11, Academic Press, London, 1974

79. Riley, W.C., 'High-temperature materials and technology', Campbell, I.E. and Sherwood, E.M., Ed., p.206, John Wiley and Sons, Inc., New York, 1967

80. Robinson, P.C., Refractories J., 42, (6), 218, 1966

81. Rossini, F.D., Pitzer, K.S., Arnett, R.L., Braun, R.M. and Pimentel, G.C., 'Selected values of physical and thermodynamic properties of hydrocarbons and related compounds', p.204, Carnegie Press, Pittsburgh, 1953

82. Ruddlesden, S.N., Trans.Brit.Ceram.Soc., 66, 587, 1967

83. Safdar, M., Ph.D. Thesis, University of London, 1961

84. Safdar, M., Barham, D. and Barrett, L.R., Proceedings of Fourth International conference on thermal analysis,Budapest, 3, 905, 1974

85. Samaddar, B.N., Kingery, W.D. and Cooper, A.R., J.Amer.Ceram.Soc., 47, 249, 1964

86. Sharp, D.E. and Ginther, L.B., J. Amer.Ceram.Soc., 34, (9), 260, 1951

87. Shartsis, L., Capps, W. and Spinner, S., J.Amer.Ceram.Soc., 36, (10), 319, 1953

88. Shurygin, P.M., Boronenkov, V.N., Kryuk, V.I. and Revebtsov, Izv. Vysshykh Uchebn.Zavedenii, 8, (2), 23, 1965

89. Souquet, J.L., Deporles, C. and Besson, J.Silicates Industriels, 33, No.2 + 3, 39 and 75, 1968 :quoted in 'Diffusion data', 3, p.194, Diffusion Information Centre, Ohio, 1969

90. Spencer, D.R.F., Refractories J., 51, 8, 1975

91. Towers, H., Trans.Brit.Ceram.Soc., 53, 180, 1954

92. Truhlarova, M., Silikaty, 4, 267, 1972

93. Truhlarova, M. and Veprek, O., Silikaty, 14, 1, 1970

94. Tu, C.M., Davis, H. and Hottel, H.C., Ind.Eng.Chem., 26, (7), 749, 1934

95. Vago, E. and Smith, C.E., Proceedings of Seventh International Congress on Glass, Paper No.62, Brussels, 1965

96. Wagner, C., J.Phys.Colloid.Chem., 53, 1030, 1949

97. Walker, P.L., Rusinko, F. and Austin, L.G., 'Advances in Catalysis', Academic Press, 1959

98. Washburn, E.W. (Ed.), 'International Critical Tables', Vol.1, p.103, McGraw-Hill Book Company Inc., New York, 1926

99. Webster, R. and Jackson, B., Trans.Brit.Ceram.Soc., 74, 233, 1975

100. White, J., Bull.Inst.Fuel, 20, 117, 1947

101. White, J., Iron and Steel Inst.Spec.Rep.74, Discussion, p.26, 1962

102. Wicke, E., 'Proceedings 5th Symp.Combustion', Pittsburgh, p.245, 1955

103. Zoglemeyr, G., Osterreichisch - Amerikanische MagnesitAktiengesellschaft, Private communication.